STORAGE AND CONTROL OF A SINGLE PHOTON WAVE PACKET

A Dissertation

by

XIWEN ZHANG

Submitted to the Office of Graduate and Professional Studies of
Texas A&M University
in partial fulfillment of the requirement for the degree of

DOCTOR OF PHILOSOPHY

Chair of Committee,	Olga Kocharovskaya
Committee Members,	Alexey A. Belyanin
	Alexei V. Sokolov
	George R. Welch
	Philip R. Hemmer
Head of Department,	Peter McIntyre

December 2016

Major Subject: Physics

ABSTRACT

Quantum optical memory implies the storage of quantum state of light in an atomic ensemble and its retrieval at the later moment of time on demand. It is one of the key elements of both quantum communication and quantum computing. Two types of quantum optical memory techniques have been developed in the last decade. The first one is based on an optimal temporal shaping of the amplitude of a strong coherent control field, forming along with the quantum field a three-level configuration in atomic medium (such as EIT and Raman quantum memories). The second one is based on photon echo mechanism [such as atomic frequency comb (AFC) and gradient echo memory (GEM)]. Each method has its advantages and disadvantages, but in general, an experiment-friendly, reliable, high speed, low loss, broad band quantum storage of a single-photon wave packet with large efficiency and fidelity remains a very challenging task.

Here we propose two new quantum optical storage techniques to resolve some of the difficulties and to introduce more controllability over the single-photon processing. The first method is based on phase matching control in Raman configuration (via the modulation in time of the control field's refractive index, propagation direction, and/or carrier frequency chirp). The second method is based on (continues or discrete) spatial frequency chirp of a control field. In order to overcome some general problems inherent to light-atoms interfaces, we propose also a new quantum interface based on γ-ray-nuclear transitions, which looks promising for quantum information processing.

To

My parents Zhenqing Ma, Falai Zhang

And my grandparents Shiying Zhang, Yunfeng Ma, Hongying Qin, Yuanhou Zhang

With love

ACKNOWLEDGMENTS

I would like to express my immense gratitude to my advisor Olga Kocharovskaya for her strong support and patient guidance in every step of my Ph.D study. I sincerely appreciate her professional instructions and generous help throughout my scientific research. The essence of her academic thoughts gives me a lifetime benefit. Without her encouragement, motivation, profound insight and extensive knowledge, this dissertation would not have been possible.

It is with vast gratitude that I acknowledge the continuous support and plentiful help of Marlan O. Scully, who has always been my scientific mentor. I am deeply thankful for the various opportunities and profound advices he gave me to develop my scientific experience. I consider it an honor to do research in his projects, where I benefited enormously from his guidance and inspiration, and learned immensely from his scholarship and erudition.

I owe my great gratitude to Anatoly Svidzinsky and Alexey Kalachev, who are my scientific teachers, research collaborators and close friends. They have been providing me with endless support in all aspects during my Ph.D work. I learned from them a tremendous amount of skills and knowledge, as well as the joy and enthusiasm they have for science and for life.

My sincere thanks also goes to the committee members Alexei V. Sokolov, Philip R. Hemmer, Alexey A. Belyanin, and George R. Welch for their insightful comments and intellectual support both in their classes and in many discussions.

It gives me great pleasure in acknowledging my collaborators Peter Valkó, Hans Schuessler, Wen-Te Liao, Rustem Shakhmuratov, Luojia Wang, Gavriil Shchedrin, Yuri Rostovtsev, Raymond Ooi, Fu Li, Jizhou Wang and Hongyuan Li. It was truly fruitful and delightful in cooperating with them. I would like to also thank my colleagues Timur Akhmedzhanov, Kimberly Chapin, Goong Chen, Hui Dong, Xia Hua, Wayne Huang, Pankaj Jha, Moochan Kim, Shengwen Li, Zeyang Liao, Christopher O'Brien, Tao Peng, Dmitri Voronine, Da-Wei Wang, Kai Wang, Yongrui Wang, Zhenhuan Yi, and many others for lots of useful discussions.

Last but not least, I must thank my family for the immense spiritual support on my work.

NOMENCLATURE

AFC   Atomic Frequency Comb

CRIB   Controlled Reversible Inhomogeneous Broadening

EIT   Electromagnetic Induced Transparency

FWHM   Full-width-half-maximum

GEM   Gradient Echo Memory

NV   Nitrogen-vacancy

NVD   Nitrogen-vacancy Centers in Diamond

PMC   Phase Matching Control

SiV   Silicon-vacancy

SNR   Signal-to-noise Ratio

TABLE OF CONTENTS

LIST OF FIGURES

CHAPTER I

INTRODUCTION

Quantum information processing [1], suggested by Feynman and other pioneers [2, 3] in 1980s, has been one of the primary driving forces for a wide scope of studies in quantum physics. This is not only because of its close connection to the fundamental test of the quantum mechanics theory [4, 5], but also due to its revolutionary change of the real-world application of information science (e.g., Refs. [6--8]). One essential element of quantum information processing is quantum memory [9--14]. It lies in the heart of quantum communications [15] and quantum computations [16], and provides a way to realize the linear logic gates [17], on demand single-photon sources and single-photon detectors [18, 19], precision measurements [20--22], etc. The quantum memory techniques being developed in the course can also be transferred to other applications, such as, ultrasound detection [23], etc.

A quantum bit, or qubit, is en elementary unit of quantum information, which is essentially a two-state quantum mechanical system possessing superposition principle. At a very basic level of architecture, qubit can be classified by its functionality into stationary qubit which is used for local quantum gate operation, and "flying qubit" that is used for long-distance information transmission [1, 16, 24]. Single photon is considered to be the ideal "flying qubit" for quantum information processing because of its fast propagation speed. An immediate choice of the realization of a photonic qubit is its two independent polarization states. Unfortunately, such natural internal degree of freedom is quite un-

stable in an actual environment such as optical fiber, where inevitable birefringence and random polarization-mode coupling [25] constantly deteriorate the fidelity of the qubit. A much better choice of the encoding scheme in this regard is a time-bin qubit [26], which is produced easily by passing a single photon through an unbalanced Mach-Zehnder interferometer. The resulted state of the single photon then becomes $|\psi\rangle = \alpha|e\rangle + \beta e^{i\varphi}|l\rangle$, where $|e\rangle$ ($|l\rangle$) is the state of the photon taking the short (long) arm of the interferometer, thus arriving early (late) in time. Such time-bin qubit encodes information using the waveform of a single photon, which is much more robust against the environmental fluctuations during a long-distance propagation. Further investigation of time-bin qubit shows that it is not only a promising stable flying qubit, but also an important candidate for operational qubit without resorting to spatial mode multiplexing [27]. Thus, it is crucially important to store, manipulate, and retrieve the waveform of a single photon with high efficiency and fidelity. In this dissertation, by quantum memory or quantum storage of a single photon, we always refer to the capability of recovering not only its quantum state in Fock space, but also its wave packet shape in time domain.

Since photons practically do not interact with each other, their storage and manipulation have to be based on the light-matter interaction on various quantum interfaces. Single atom is naturally considered to deal with single photon due to its conceptual simplicity. However, because of the rather weak interaction strength, the probability of successful operation in such a system is too small. In order to increase the light-matter interaction, one resorts to either cavity-assisted or ensemble-assisted enhancements. The former approach

2

is proposed [28] in late 90's and realized thereafter [29, 30]. But generally speaking, the use of cavity greatly complicates the experimental setup. The latter one [31], on the other hand, is much easier to be implemented in free space.

In free space, quantum memory of a single photon can be achieved in a number of ways. The major techniques can be divided into two groups. The first one uses an optimized shaped-in-time control field to convert a single photon into collective spin waves. This includes electromagnetically induced transparency (EIT) [32--37] and off-resonant Raman scheme [38--42]. Quantum memory based on EIT can be understood in a simple way via a concept of "slow light". That is to say, the group velocity of the coupled signal field-spin excitation (so called dark state polariton) as well as the ratio of the two components of the polariton strongly depends on the intensity of the control field. By adiabatically tuning off (on) the control beam, it is possible to freeze (release) the signal photon into (out from) the collective spin excitation in the medium. But this immediately brings a problem. In order to reach the synchronization between the control and signal fields and the optimization of the control field temporal shape, a prior knowledge of the exact arrival time and waveform of the single photon is required. Sometimes this is inconvenient, or even impossible, especially in the case when the information is encoded in a very complicated temporal wave packet [43]. The same problem is inherent to quantum memory based on off-resonant Raman interaction.

The second category of free-space quantum memory schemes, such as gradient echo memory (GEM) [44--46] and atomic frequency comb (AFC) [47], are free of this problem.

3

They take advantage of photon-echo mechanism, and do not require a modulated control field amplitude to match an input signal field. Specifically, GEM uses a gradient of external electric or magnetic field along the propagation direction to produce an artificial controllable inhomogeneous broadening during the photon storage process, which can be reversed by switching the sign of that gradient to implement a retrieval process. This technique relies on the existence of Stark or Zeeman effect in the storage medium, and often implies also a selection of an initially homogenous subensemble from the originally naturally inhomogenously broadened transition via the process of optical pumping, which, in its turn, implies a presence of the appropriate hyperfine structure in the ground atomic state. It has been realized in rare-earth-doped crystals [48--50], warm [51--55] and cold [56] atoms. While AFC uses a discrete, isotropic absorption structure, its preparation requires delicate spectral tailoring on a very broad inhomogeneous broadening via optical pumping with a sequence of pulses. Up to now, it has been implemented in only rare-earth-doped crystals under cryogenic temperature [57--84]. Such requirements on photon-echo-based quantum memory schemes can become limiting factors for the actual implementation in different light-atom interfaces under various scenarios. So it is important to design new schemes to overcome the above disadvantages.

Therefore, after almost two decades of development, optical quantum memory is still challenging researchers with a lot of practical problems that has yet to be resolved by designing novel schemes. We want these new schemes to demonstrate the ability of (including but not limited to):

4

- Recovering not only the Fock state of a single photon but also its temporal waveform with high efficiency and fidelity;

- On-demand retrieval, and other single-photon processing functionalities, such as time sequencing, waveform shaping, etc;

- Standby operation that requires no synchronization, nor any prior knowledge of the signal photon;

- Being implementable in as many physical systems as possible, including atomic gases, rare-earth-doped-crystals, color centers, molecular ensembles, etc;

- Being realized easily, preferably at room temperature, without resorting to complicated spectral tailoring techniques, etc.

The current techniques, as discussed above, only satisfy either some of these requirements or other. In this dissertation, we propose several schemes demonstrating the above advantages.

The first new scheme we suggest is quantum storage based on phase matching control (PMC). It maps different temporal parts of the single-photon wave packet into the spin coherence waves by controlling the phase matching condition. In doing so, quantum storage and retrieval can be realized without using inhomogeneous broadening of the atomic transitions nor manipulating the amplitude of the control field. The second new scheme we suggest is quantum storage based on control field spatial chirp. In this method, the frequency chirp across the control beam propagating in the direction orthogonal to the signal photon propagation direction provides a direct all-optical analogue of the frequency gra-

dient in GEM scheme. However, it dose not require either linear Stark or Zeeman effect, thus can be implemented in materials demonstrating no such effect and/or placed in specific external fields. Both the above two schemes are proven to be mathematically equivalent to GEM scheme, which promises high efficiency and fidelity without backward retrieval. The exact analytical solution describing the processes of storage and retrieval in GEM is also found, which is important for understanding the dynamics of the field-atom evolution in all these schemes. The third scheme we suggest is a discrete spatial chirp memory, which uses a set of control beams with fixed different frequencies propagating across the signal photon propagation direction. This scheme possesses some properties of both AFC and GEM as well as some new favorable features. It not only allows high efficiency quantum storage, but also can be used for temporal sequencing of a single photon. Finally, the extension of the last scheme operating in the γ-ray regime is suggested to be implemented in nuclear transitions via Doppler frequency comb. This scheme aims at the control of a single photon's temporal mode. We also proposed a fast switch of a γ-ray photon's Bragg mode. These methods help to broaden the concept of quantum information processing to more energetic photons, therefore may benefit relative subjects in various aspects.

I.1 Quantum storage based on phase matching control

It is usually assumed that to store and recall optical photon waveform one needs either an inhomogeneous broadened atomic transition (tailored or controlled) or a modulated control field amplitude matched an input pulse. In Chap. II we propose another approach

6

which requires neither inhomogeneous broadening nor temporal modulation of the control field amplitude, but takes advantages of continuous phase matching control (PMC) in an extended three-level resonant Raman medium. The basic idea of PMC is to regulate the excited spin wave vectors (i.e., spatial mode of the spin wave) in time by manipulating the control field wave vector. The one-to-one mapping between the temporal mode of the signal field and the spatial mode of the spin wave then allows the storage of the information encoded into the input photon's waveform.

Depending on the concrete way how the control field wave vector is manipulated with time, PMC memory may be implemented via three different schemes, namely, the refractive index control [85--87], the control field propagation direction angular scanning [88, 89], and the control field frequency chirp [90]. The angular manipulation of the control field is more simple and promising for experimental implementation than the other two. PMC via control field angular scanning can be realized in color centers in diamond, rare-earth-doped crystals and cold atoms. The mathematical description of PMC is equivalent to the GEM scheme and hence it possesses all its advantages, including high efficiency and high fidelity. But contrary to GEM, the angular scanning PMC is an all-optical scheme, which does not use external dc electric or magnetic field. In particular, it can be realized even in the materials for which the using of external dc field is difficult or impossible. For example, in nitrogen-vacancy centers in diamond, the external dc field strongly affects the Λ-level structure, so that traditional GEM scheme is not feasible. But with the angular scan of the control field, one can achieve the same storage performance

as GEM without using gradient dc field.

I.2   Quantum storage based on spatial chirp of the control field

PMC quantum memory schemes typically use the Raman configuration, but unlike EIT or Raman scheme they do not require exact synchronization of the control and signal fields, and can operate with control field of a constant amplitude. However they still imply a manipulation with time of the refractive index or control field propagation direction.

In order to remove all the time-dependent manipulations, in Chap. III we propose an all-optical quantum storage based on spatial chirp of the control field [91]. It does not require any inhomogeneous broadening of the resonant medium, and in principle, is free of any temporal modulation of the control field. In a transverse excitation setup, the signal field experiences a longitudinal inhomogeneity of the Raman interaction with the control field that is spatially chirped along the z axis. The spatial chirp leads to a varying two-photon detuning across the beam, which exactly mimics the role of gradient absorption structure in GEM. However, contrary to GEM and similar to PMC angular scanning, the spatial chirp scheme can be realized without additional electric or magnetic field. More-over, a phase modulation of the control field will allow the output pulses to be shifted in time without their temporal squeezing or stretching.

I.3   The exact analytical solution for gradient echo memory scheme

Both PMC and control field spatial chirp quantum memory schemes demonstrate the same performance as GEM scheme. In GEM scheme, an external electric or magnetic

8

field with gradient along the longitudinal direction is applied to the medium of very narrow linewidth. This produces a position dependent resonant absorption condition for different frequency components of the input photon. After absorption, the field gradient is reversed to the opposite. The polarizations in the medium then evolve backward until reaching their original status, upon which a photon echo emerges. While most of the forward photon-echo quantum memory schemes demonstrate a maximally 54% efficiency, GEM can recall almost 100% of the input field energy. This rather peculiar property results from its highly non-trivial field-atomic evolution, which is described by the equations as follows:

$$\frac{\partial}{\partial z}a(z,t) = g^*NS(z,t), \tag{I.1}$$

$$\frac{\partial}{\partial t}S(z,t) = -(\gamma - i\beta z)S(z,t) - ga(z,t), \tag{I.2}$$

where $a(z,t)$ is the slowly varying amplitude of the single-photon annihilation operator and $S(z,t)$ is the slowly varying part of the atomic coherence operator, g is the field-atom coupling constant, N is the atomic density, γ is the decoherence rate and β is the frequency gradient.

In Chap. IV we derive the exact solution of GEM Eqs. (I.1) and (I.2) for storage and retrieval for arbitrary linear gradient without any additional approximations. The response of storage process is proportional to the Kummer confluent hypergeometric function $_1F_1$, and the kernel of the gradient echo solution after retrieval is proportional to the Humbert double hypergeometric series Φ_2. The solution is written in its final form, i.e., in terms of a response to the input signal. In such a way, how the medium subjecting to the a switchable frequency gradient manage to generate the gradient echo becomes clear. Moreover, the

gradient absorption of a single photon is closely related to the single-photon superradiance process [92--97]. So the solution and mathematical treatment presented in this paper can also provide insights, for example, into the problem of the preparation and control of the timed Dicke state [98, 99].

I.4   Quantum storage based on discrete spatial chirp: gradient frequency comb and stepwise gradient echo memories

A much easier, and also more interesting, realization of spatial-chirp-based quantum memory is to use, instead of one beam with a spatially varied frequency, a set of coherent control beams propagating across the signal field, each having different fixed frequency with the same frequency spacing between the neighboring beams. This is discussed in Chap. V.

Such discrete spatial chirp quantum memory presents itself a hybrid of AFC and GEM memories, possessing some unique properties. Indeed, the presence of the discrete equidistant spectral components in the control field leads to a comb structure in resonant absorption profile of the incoming signal photon, similar to AFC memory. However, contrary to the usual AFC, where the whole structure is formed at any point in space, here each comb tooth is present in different layer of the medium, forming a frequency gradient along the propagation direction of signal field. For this reason it can be called a gradient frequency comb (GFC). On the other hand, presence of the frequency gradient along the propagation direction leads to some similarities of our scheme to the GEM scheme. But

unlike the usual GEM, where frequency of an atomic transition is continuously changed along the propagation direction, in our scheme it is changed in a stepwise manner. For this reason it may be called stepwise gradient echo memory (SGEM). So, if the frequency gradient is not changed, the scheme operates in the regime similar to AFC. If it is reversed before the appearance of the fist GFC echo, it operates in the regime similar to GEM.

A unique combination of two different memory mechanisms within one all-optical scheme along with the possibility of independent control over the phases of the control beams leads not only to a high performance of this scheme for quantum storage, but also to a wide spectrum of single photon operations, including an arbitrary time sequencing of peaks in the waveform of a single photon (time reversing of a time-bin qubit, permutation of qutrit, etc.).

I.5   Nuclear quantum memory and time sequencing of a single γ-ray photon

In the last decade optical-atomic interfaces [31] have been developed as one of the basic building blocks for quantum information processing [1]. However, optical photons (~ 1 eV) have both some practical and fundamental limitations, such as a lack of reliable, economical single-photon sources, low efficiency and high dark-count rate of single-photon detectors, and diffraction limit set by a wavelength ~ 1 μm on the size of information processing devices. These problems can be resolved in the γ-ray range (10 - 100 keV), where single-photon detectors have nearly 100% efficiency with almost no false detection, radioactive decay in a cascade scheme produces heralded single γ photon, and the sub-

11

angstrom wavelength does not impose any practical limit on the size of a photonic circuit. In this frequency regime, the nuclear transitions in Mösbauer solid may naturally provide almost perfect platform with its extremely high Q factor and strong coupling between a single γ photon and nuclear ensemble. For example, the 14.4 keV transition in ^{57}Fe has a room temperature recoilless fraction 75% and linewidth 1.1 MHz, with an absorption coefficient as high as 10 μm^{-1} for 98%-enriched stainless-steel film.

However, up to now there is not yet a feasible scheme to faithfully store and retrieve a γ photon. All the existing techniques have different kinds of difficulties in the γ-ray range. In Chap. VI we propose a method for the implementation of γ-ray quantum memory via a Doppler frequency comb, produced by a set of resonantly absorbing nuclear Mössbauer targets each moving at different velocities. The upper bound of the efficiency is 54%. However, much higher efficiency can be achieved by reversing the moving directions of all the targets. Moreover, the single γ-photon processing, such as holding, delaying and/or advancing, and permuting the time bins of a γ photon, can be realized simply by modulating the speed of the Mössbauer targets.

The Doppler frequency comb scheme manipulates the temporal mode of a single γ-ray wave packet. Meanwhile, the control of the spatial mode of a γ photon is as well important. In order to do this, we suggest a picosecond switch of the propagation direction of γ-ray wave using optically controlled vibrating nuclear lattice. Namely, if the incident γ wave is detuned from the nuclear transition, it passes through a static nuclear array. However, if the nuclei vibrate with frequency matching the γ-ray detuning, parametric

12

resonance can yield energy transfer into a Bragg deflected beam on the superradiant time scale.

The combination of γ-ray optics, quantum memory, and superradiant control of propagation direction may provide novel solutions for advancing information technology on an unexplored level.

CHAPTER II

QUANTUM STORAGE BASED ON PHASE MATCHING

CONTROL[*]

II.1 Introduction

Developing optical quantum memory [9--14, 31] is considered to be one of the essential steps to build quantum repeaters that provide a way of implementing long distance fiber-based quantum communication. Quantum repeater protocols involve creating entangled photons, storing them in quantum memories, and swapping their entangled states [12]. Thus it is important to develop effective methods of storage and retrieval of single-photon wave packets. Several promising schemes for efficient quantum storage have been experimentally demonstrated, including electromagnetically induced transparency (EIT) [32--37], Raman interaction [38--42], controlled reversible inhomogeneous broadening (CRIB) or gradient echo memory (GEM) in rare-earth-doped crystals [48--50] and warm and/or cold atomic gases [51--56], and atomic frequency comb (AFC) [57--84].

In EIT and Raman schemes, the storage is based on temporal variation of the control field amplitude. An optimal temporal shape of the control field and a control-signal fields synchronization are needed to efficiently store and recall the signal pulse. Consequently, before the storage one needs to know the shape and arrival time of the signal field, which

---

inevitably limits the real applications of quantum memory. In GEM scheme, the storage of the signal relies on the creation of a resonance absorption frequency gradient by Stark or Zeeman effect. This confines the materials for implementation to those demonstrating these effects. In AFC scheme, a tailored inhomogeneous broadening (frequency comb) is created before storing the signal. In order to achieve good memory efficiency, a high quality frequency comb should be prepared via optical pumping. Such preparation requires a presence of the fine structure in the ground state and usually takes long time.

Bearing in mind the above limitations, we study the possibility of a quantum storage scheme based on phase matching control (PMC), which does not require manipulation with the inhomogeneous broadening or amplitude variation in time of the control field and its synchronization with the signal field. Specifically we consider the PMC quantum memory protocol based on Raman interaction of the quantum signal field and classical control field with the medium, i.e. under two-photon resonance condition, when the frequency difference of these fields coincides with the spin transition frequency. The benefit of using the Raman interaction is the possibility to achieve wide-bandwidth, low-noise and inhomogeneous-broadening-insensitive storage [38]. The pay-off is a relatively low coupling constant, which however can be overcome by using a strong transition, large driving power, and/or placing the medium into a cavity.

Phase matching is a widely used concept in optics, especially in nonlinear optics. It stems from the conservation of momentum, meaning that the optical process is most efficient when the wave vectors match each other. In the context of quantum memory

protocol, the phase matching condition in the case of Raman interaction means that the established spin coherence wave should have the wave vector matching the combination of the wave vectors of the signal and control fields. As a result, a manipulation on the control field wave vector eventually acts as a modulation of the spin wave vector. The idea of quantum storage scheme based on PMC is to map the different temporal parts of the signal field into the spin coherence waves with different wave vectors by exciting them selectively and subsequently via continues temporal variation of the wave vector of the control field. By the end of this mapping process the coherence grating is formed in the medium which stores the information about the signal field within the life time of the spin coherence. During the read out process, the control field wave vector is manipulated as a time reversal of the storage one. This allows the control field to pick up the wave-vector-matched spin wave in time ordered manner and to retrieve the signal field from the spin grating.

Depending on how the control field wave vector is manipulated with time, there are three different schemes of the Raman PMC quantum memory, namely, quantum storage based on (i) the refractive index control [85--87], (ii) the control field propagation direction angular scanning [88, 89], and (iii) the control field frequency chirp [90].

In this chapter, we develop the general model of the Raman PMC quantum memory, discuss and compare the basic conditions and requirements for all three PMC quantum memory schemes. Specifically, we propose the experimental realization of PMC quantum storage based on control field angular scanning in nitrogen vacancy centers in diamond

and in rare-earth-doped crystals.

II.2 The general model and basic equations for the Raman PMC quantum memory

In this section we introduce the general model of the quantum memory scheme based on PMC. As shown in Fig. 2.1 (a), we consider the interaction of a single-photon wave packet $E_s(\mathbf{r},t)$ of duration Δt through Raman interaction with a strong classical field $E_c(\mathbf{r},t)$ in a three-level atomic medium with a Λ-type level structure. The signal (control) field has a carrier angular frequency ω_s (ω_c), a wavelength λ_s (λ_c) and a wave vector $\mathbf{k}_s$ ($\mathbf{k}_c$). The atoms are assumed to be distributed uniformly in a cylindrical geometry of length L, and remain mostly on their ground states. The coordinate system is originated at the center of the sample. The time windows of storage and retrieval processes are both equal to T. During the storage, $t \in [-T,0]$, the signal field (single photon) and the wave-vector-modulated control field together create spin-wave excitations in the medium, as shown in Fig. 2.1 (b, c). During retrieval, $t \in [0,T]$, the spin-wave excitations and the anti-modulated control field together produce (recall) the signal field of the same (or temporally reversed) wave-form as the input. Since the two ground states on which the spin wave lives are usually very long-lived (e.g., longer than $\sim$ microseconds), for the sake of simplicity, unless otherwise indicated, we will neglect the natural decoherence of the spin wave between the end of the storage and the beginning of the retrieval in this dissertation. Such decoherence can be taken into account simply by multiplying an exponential decay factor onto the efficiency.

The signal field (single-photon wave packet) propagating along the $\hat{z}$ direction can
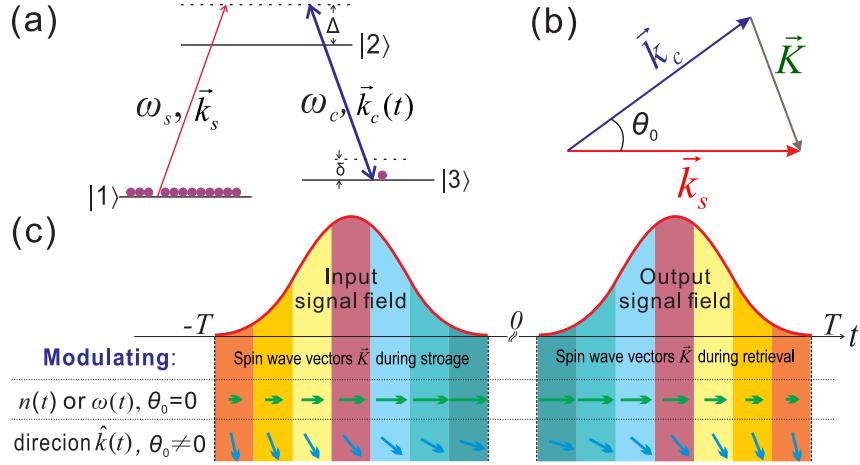
Figure 2.1: (a) Energy diagram of the Raman interaction in a three-level Λ system, where $\omega_{s,c}$ ($\mathbf{k}_{s,c}$) is the angular frequencies (wave vectors) of the signal and control fields, respectively, and Δ (δ) is the one-photon (two-photon) frequency detuning. (b) Phase matching diagram among the signal, control, and spin wave vectors. (c) Schematic illustration of the principle of quantum storage based on off-resonant Raman phase matching control. By manipulating the control field wave vector as a function of time, the temporal profile of the signal field is mapped into (storage) or out from (retrieval) the spin waves with different wave vectors. For illustration purpose, discrete spin wave vectors are sketched.

be written as

$$E_s(\mathbf{r},t) = i\sqrt{\frac{\hbar\omega_s}{2\varepsilon_0 n_s c}} a(\mathbf{r},t) e^{i(k_s z - \omega_s t)} + \text{H.c.}, \qquad (\text{II.1})$$

where n_s is the refractive index on the frequency of the signal field taking into account the contributions from the host material and the resonant atoms, and c is the speed of light in vacuum, $a(z,t)$ is the slowly varying part of the photon annihilation operator.

The classical control field contains a wave vector modulation, which is described by the phase factor $\phi(\mathbf{r},t)$:

$$E_c(\mathbf{r},t) = E_0 e^{i[\bar{\mathbf{k}}_c \mathbf{r} - \omega_c t + \phi(\mathbf{r},t)]} + \text{c.c.}, \qquad (\text{II.2})$$

where E_0 is a constant amplitude, and $\bar{\mathbf{k}}_c$ is the average wave vector of the control field.

The collective atomic operators are defined as the mean values of the single-atom

18

operators

$$\sigma_{mn}(\mathbf{r},t) = \frac{1}{N} \sum_j |m_j\rangle\langle n_j| \, \delta^{(3)}(\mathbf{r}-\mathbf{r}_j), \qquad (\text{II.3})$$

where N is the constant atomic number density, and $|n_j\rangle$ is the nth state ($n = 1, 2, 3$) of jth atom with the energy $\hbar\omega_n$ (set $\omega_1 = 0$). The collective spin coherence operator can be expressed into a slowly varying amplitude of coherence on the Raman transition $s(z,t)$ multiplied by a fast oscillating factor:

$$\sigma_{13}(\mathbf{r},t) = s(\mathbf{r},t) \, e^{-i[(\omega_s-\omega_c)t-(\mathbf{k}_s-\bar{\mathbf{k}}_c)\mathbf{r}]}. \qquad (\text{II.4})$$

We assume here and thereafter a large Fresnel number $F = A/(L\lambda)$ of the signal field in the medium to neglect the transverse diffraction, where A and λ are the characteristic transverse size and wavelength of the field, respectively. We consider all the atoms initially in the ground state $|1\rangle$ so that Langevin noise atomic operators are not present [100, 101], then the off-resonant Raman interaction can be described by the following equations (see Appendix A):

$$\left(\frac{\partial}{\partial z} + \frac{1}{v_{\text{sg}}}\frac{\partial}{\partial t}\right) a(\mathbf{r},t) = -g^* N s(\mathbf{r},t) e^{i\phi(\mathbf{r},t)}, \qquad (\text{II.5})$$

$$\frac{\partial}{\partial t} s(\mathbf{r},t) = (-\gamma + i\delta) s(\mathbf{r},t) + g a(\mathbf{r},t) e^{-i\phi(\mathbf{r},t)}, \qquad (\text{II.6})$$

where the decoherence rate between level $|2\rangle$ and $|1\rangle$ is neglected comparing with one-photon detuning $\Delta = \omega_s - \omega_2$, v_{sg} is the group velocity of the signal field inside the medium, $g = (d_{21}\Omega^*/\Delta)\sqrt{\omega_s/(2\hbar\varepsilon_0 n_s c)}$ is the coupling constant between the atoms and the weak quantized field, and $\Omega = d_{23}E_0/\hbar$ is the Rabi frequency of the classical control field, d_{ij} is the dipole matrix element of the transition between $|i\rangle$ and $|j\rangle$, γ is the decoherence rate

the spin wave excitation, and $\delta = \omega_s - \omega_c - \omega_3$ is the two-photon detuning. For the sake

of simplicity, the Raman transition frequency shift $|\Omega|^2/\Delta$ is included in the control field

frequency ω_c. Equation (II.5) and (II.6) can be reduced to the equations describing the

GEM scheme[1] if the incoming signal pulse duration is much longer than the propagation

time inside the medium and the phase factor $\phi(z,t)$ is linearly dependent on time and space.

Such equivalence can be understood by regarding the phase factor $\phi(z,t)$ as a result of either

a time dependent wave vector or a spatial dependent frequency of the control field. This

analogy provides a useful interpretation of the considered approach in frequency domain.

The two major figures of merit we consider for the quantum storage are total effi-

ciency η and fidelity $\mathscr{F}$. The total efficiency characterizes how much photon energy is

retrieved from the medium out of the input field, which can be defined as

$$\eta = \frac{N_{\text{out}}}{N_{\text{in}}}, \tag{II.7}$$

where

$$N_{\text{in}} = \int_{-\infty}^{0} dt \langle a_{\text{in}}^{\dagger}(t) a_{\text{in}}(t) \rangle, \tag{II.8}$$

$$N_{\text{out}} \int_{0}^{\infty} dt \langle a_{\text{out}}^{\dagger}(t) a_{\text{out}}(t) \rangle, \tag{II.9}$$

since we assume that the storage process terminates at the moment $t = 0$, while retrieval

process begins at this moment of time (by neglecting the decoherence in between). Here

we use $a_{\text{in,out}}$ to denote the slowly varying part of the input or output field.

The fidelity, on the other hand, indicates the waveform preservability of a memory

---

[1]For the analytical discussion of GEM system, please refer to Chap. IV of this dissertation.

scheme by comparing the output field with the input, which is defined as

$$\mathscr{F} = \frac{\left| \int_0^\infty dt \langle a_{\text{out}}^\dagger(t) a_{\text{in}}(\bar{t} \pm t) \rangle \right|^2}{N_{\text{in}} N_{\text{out}}}. \tag{II.10}$$

Here $\bar{t}$ is the delay that maximizes the fidelity $\mathscr{F}$, and "$\pm$" takes into account the fact that the retrieved field may or may not be a time-reversal (or quasi time-reversal) of the input field, depending on the scheme. The definitions of η and $\mathscr{F}$ can also be done in a similar way in terms of the spatial variables $a_{\text{in}}(\mathbf{r}, t)$ and $a_{\text{out}}(\mathbf{r}, t)$. In real space $N_{\text{in}} = \int d^2\rho \int_{-\infty}^0 dt \langle a_{\text{in}}^\dagger(\boldsymbol{\rho}, t) a_{\text{in}}(\boldsymbol{\rho}, t) \rangle$, and $N_{\text{out}} = \int_0^\infty dt \int d^2\rho \langle a_{\text{out}}^\dagger(\boldsymbol{\rho}, t) a_{\text{out}}(\boldsymbol{\rho}, t) \rangle$, while $\mathscr{F} = \left| \int_0^\infty dt \int d^2\rho \langle a_{\text{in}}^\dagger(\boldsymbol{\rho}, \bar{t} - t) a_{\text{out}}(\boldsymbol{\rho}, t) \rangle \right|^2 \big/ (N_{\text{in}} N_{\text{out}})$. For the sake of simplicity, in this dissertation we will consider (most of the time) only a single spatial mode, thus the definitions (II.7) and (II.10) are enough. The detailed discussion of the spatial multiplexing of our scheme can be found in Ref. [89].

It is sometimes also very useful, especially for forward GEM scheme, to introduce a parameter characterizing the retrieval field amplitude preservation, which is defined as

$$\mathscr{A} = \frac{\int_0^\infty dt \left| \langle a_{\text{out}}^\dagger(t) a_{\text{in}}(\bar{t} \pm t) \rangle \right|^2}{N_{\text{in}} N_{\text{out}}}. \tag{II.11}$$

The amplitude preservation $\mathscr{A}$ completely neglects the phase distortion of the input photon due to complicated field-atom evolution in the medium. It is the accessible parameter in an experiment of photon energy measurement. A theoretical benefit of introducing $\mathscr{A}$ lies in the quantification of the additional phase modulation on the retrieved signal by comparing $\mathscr{A}$ with $\mathscr{F}$. This is especially important for the GEM-like scheme, where such phase modulation commonly exists (see discussions in Chap. IV).

21

In our scheme, the essential idea is to manipulate the wave vector of the control field such that its phase factor $\phi(\mathbf{r},t)$ in Eq. (II.2) becomes a time-dependent externally controllable parameter that provides accessibility to the internal field-atom evolution. In such a case, we will be able to enforce a time reversal of the in-medium dynamics by switching the controllable parameter. Since a wave vector is $\mathbf{k} = \hat{k}n\omega/c$, it immediately becomes obvious that there are three different ways to manipulate the control field wave vector, each corresponding to the modulation of n, $\hat{k}$, and ω. Accordingly, there are three different methods to realize the Raman PMC quantum memory scheme: by modulating (i) the refractive index[2], (ii) the propagation direction, and (iii) the control field frequency. These schemes are discussed below.

II.3 Quantum storage via variation of refractive index

Let us consider a linearly changed-in-time refractive index $n = n(t) = \dot{n}(t)t$ of the material in an off-resonant Raman interaction between the collinear signal and control fields. Generally speaking, this refractive index can be different for the two fields in the presence of a weak dispersion such that $k_s - k_c \neq 0$. Otherwise we arrange a counter-propagating setup to make sure the created spin wave vector $\mathbf{K} = \mathbf{k_s} - \mathbf{k}_c$ does not constantly vanish. Then the magnitude of the wave vector $\mathbf{K}$ also becomes a linear function of time so that during storage the single-photon wave packet is mapped into a superposition of spin waves

---

[2]It is worth noting that PMC quantum memory in general and, it's particular scheme based on refractive index modulation, does not necessary require a three-level system or additional control laser. A two-level version of PMC quantum memory based on refractive index change was developed in $LiNbO_3$ doped by Tm^{3+} ions [87].

with different magnitudes of the wave vector [see Fig. 2.1 (c)]. In doing so the amplitude of the signal pulse as a function of time, $E_{\text{in}}(t)$, is imprinted in the amplitude of the spin wave as a function of the wave vector $S(K)$. Retrieval is achieved by interaction of the atomic system with the control field as the same values of refractive index are scanned back. If they are scanned in the reversed order as that during storage, the output pulse $E_{\text{out}}(t)$ becomes a time-reversed replica of the input one, while in the case of scanning in the same order, the output pulse reconstructs the input signal [85]. Such retrieval without reversal is possible in a cavity with an optically thin medium.

The number of the spin wave mode in the medium is simply equal to KL, where L is the medium length. For a single pulse to be stored or retrieved, the spin wave mode has to be swept over by several number, i.e., $\Delta K = \Delta n 2\pi/\lambda \gtrsim 1$. Suppose we only manipulate the control field refractive index, then the total change of such refractive index modulation needs to be on the order of λ_c/L, where λ_c is the control field wavelength [85], which gives $\Delta n_{\text{min}} \sim 10^{-5}$ under typical experimental conditions. The ratio between the total accessible range Δn and this minimum value determines the number of pulses that can be stored in a series.

While the underlying principle is easy for the quantum storage via variation of refractive index, its experimental realization still remains challenging because, in general, it is rather difficult to achieve a modulation of refractive index without modulations of atomic levels. For example, in a doped nonlinear crystal, the refractive index can be conveniently modulated by the linear electro-optic effect. However, the linear Stark effect on

all energy levels imposes a serious constraint on such system, because one needs to select a specific class of impurity ions with a definite relative orientation between the ground and excited states' permanent dipole moments. A possible candidate is $LiNbO_3$ crystal doped by rare-earth ions, which provides maximum value of index change $\sim 10^{-3}$ [86, 102].

II.4   Quantum storage via angular scanning of the control field

As mentioned above, the realization of quantum storage via refractive index control requires rather special properties of the material. This departs from our original requirement on the new-designed schemes about their implementations in different systems. In the last section, by continuously changing refractive index we project the input pulse shape onto a subsystem of modes which differ in magnitudes of their wave vectors. In this section we store the input pulse in the modes with different directions of the wave vectors [Fig. 2.1 (c)] by changing the direction of propagation of the control field. However, in order to maintain the single spatial-mode property, we deliberately avoid the usage of the transverse spin-wave mode and project the two-dimensional spin-wave vector onto the longitudinal direction for storage in a first-order approximation. This is exactly what happens in the quantum storage via refractive index modulation in the last section. So we expect this scheme to perform the same as the previous one in terms of efficiency and fidelity, but to be more easily implemented experimentally.

Let us suppose that the control field propagates at a non-vanishing angle θ_0 with respect to the signal field (of duration Δt), and the wave vector of the control field is rotated

24
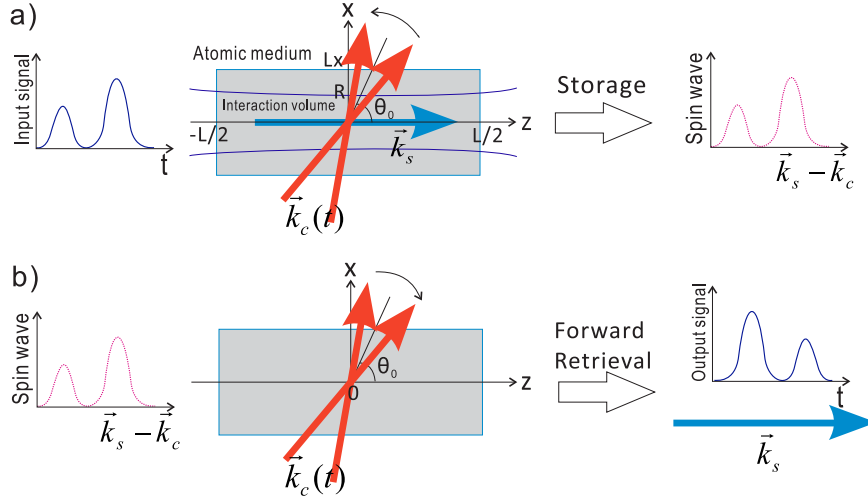
Figure 2.2: Illustration of quantum storage via angular scanning of the control field. (a) During storage, the temporal profile of the signal field is mapped into the spin wave distributed over different spin wave vectors; (b) During forward retrieval, the spin wave profile is mapped back into the output signal field.

continuously around this average direction θ_0 in a small angular range $2\Delta\theta$ (see Fig. 2.2). As a result, the projection of the spin wave vectors along the signal field propagation direction changes its length as a function of time [Fig. 2.1 (c)], thereby mapping the signal pulse shape at different moment of time into different longitudinal modes of the spin wave.

In order to write down the evolution equations, the phase factor $\phi(\mathbf{r},t)$ in Eq. (II.2) needs to be specified. This induced phase shift due to the control field sweeping may be considered as a linear function of the rotation angle. In such linear regime we have

$$\phi(\mathbf{r},t) = \beta_x(x-x_0)t + \beta_y(y-y_0)t + \beta_z(z-z_0)t + \phi_0(\mathbf{r}), \tag{II.12}$$

where β_i is the rate of change of the component $\mathbf{k}_c$ along the i axis ($i = x, y, z$), and the coordinate (x_0, y_0, z_0) corresponds to a phase stationary point where the phase $\phi(t)$ of the control field remains constant during the rotation. $\phi_0(\mathbf{r})$ is a time-independent phase factor which can be incorporated into $s(\mathbf{r},t)$. For the sake of simplicity, we assume in the

following that the wave vector of the control field is rotated in (x, z)-plane around the average polar angle θ_0, as shown in Fig. 2.2, so that the average control wave vector $\bar{\mathbf{k}}_c = k_c \sin\theta_0 \hat{x} + k_c \cos\theta_0 \hat{z}$, where $k_c = \omega_c/c$. Such a configuration also ensures that the control field polarization is unchanged during the interaction. This is particularly important if different polarization selection rules are involved in the two optical transitions of Raman interaction for the purpose of noise suppression. In this case, we have $\beta_x = \beta \cos\theta_0$, $\beta_y = 0$ and $\beta_z = -\beta \sin\theta_0$. The total angle of rotation $2\Delta\theta$ during the storage or retrieval process is $2\Delta\theta = \beta T/k_c = \beta T \lambda_c/2\pi \ll 1$.

II.4.1   Transverse excitation

The simplest scenario of the setup is a transverse excitation, where the control field propagates perpendicular to the signal field, i.e., $\theta_0 = \pi/2$. Generally speaking, the signal field has lots of transverse spatial modes which are inherently coupled to each other through diffraction as well as scattering on a spin wave grating. This corresponds to a cross talk when the spatial mode of a quantum storage is of concern. In order to stay within a single transverse mode, the mode sweeping along $\hat{x}$ direction $k_c - k_c \sin(\pi/2 + \Delta t \Delta\theta/T)$ should be much smaller than $2\pi/L_x$, where L_x is the x-dimension of the medium and Δt is the duration of the signal field. Since $\Delta\theta \ll 1$, the Taylor expansion of the above relation gives the condition $\Delta\theta \ll T/(\Delta t)\sqrt{2\lambda_c/L_x}$. In this single transverse mode regime, after defining

$$S(z, t) = s(z, t)e^{i\beta_z(z-z_0)t}, \tag{II.13}$$

26

we obtain the evolution equations:

$$\frac{\partial}{\partial z}a(z,t) = -g^*NS(z,t)\,, \tag{II.14}$$

$$\frac{\partial}{\partial t}S(z,t) = [-\gamma + i\delta - i\beta(z-z_0)]S(z,t) + ga(z,t)\,. \tag{II.15}$$

In Eq. (II.14), the time derivative on the left hand side is neglected because we consider only a long pulse with its duration $\Delta t \gg L/c$. In such regime, the retardation effect is vanishingly small since the whole medium feels almost a uniform field at all time.

Equations (II.14) and (II.15) are exactly the evolution equations (I.1) and (I.2) describing the GEM system. In GEM scheme, a space dependent absorption line along the medium is created by an external dc electric or magnetic longitudinal gradient field. While the signal field propagates through the medium, different frequency components get absorbed at different positions, resulting in a space-dependent coherence in the sample. Such coherence or medium polarization can be read out into reemitted field by reversing the external gradient field during retrieval. The reason why our scheme is mathematically equivalent to the GEM scheme can be understood as follows: The angular scanning of the control field yields an additional phase factor $e^{i\phi(\mathbf{r},t)} = e^{i\beta_z t(z-z_0)}$ of the field. This phase factor will be imposed onto the spin wave created by the Raman interaction. This spin wave excitation in an off-resonant Raman interaction is essentially playing the role of the optical polarization in a two-level system. So this time dependent wave vector βt multiplied by spacial variable z can be viewed as a space dependent resonant absorption frequency βz multiplied by temporal variable t, which in a two-level system is nothing else but a longitudinal distributed absorption line. The total bandwidth of the absorption

window is $|\beta|L$.

From the above analysis, the absorption of the central frequency of the signal field happens at a place z_p where the frequency offset in Eq. (II.15) equal to zero: $\delta - \beta(z_p - z_0) = 0$, which gives $z_p = z_0 + \delta/\beta$. For a good quantum memory, it is necessary for z_p to be inside the medium ($-L/2 < z_p < L/2$), and better at the middle of the sample[3]. This means that if $z_0 = 0$, i.e. the longitudinal position of the phase stationary point of the control field corresponds to the center of the interaction volume, the two-photon detuning δ should be equal to zero. Otherwise, one can take advantage of the two-photon detuning to shift the phase stationary point longitudinally to the medium center.

II.4.2 Oblique excitation

In a more general scenario, the control field makes an average polar angle $\theta_0 \neq \pi/2$ with respect to the input signal field, as shown in Fig. 2.2. Actually, the transverse excitation discussed above is a special case which experimentally requires more control power because of the large control beam cross section. So now we consider a control field propagating at an arbitrary angle with respect to the z axis. Throughout our discussion we assume the Fresnel number F of the signal field to be much bigger than unity. This approximation ensures a neglect of the second order transverse derivative in Maxwell equations, i.e., the spatial diffraction of the signal field in the medium. Indeed, the transverse derivative term in the reciprocal space is of the form $-i[k_\perp^2/(2k_s)]a(z,t)$, which

---

[3]A z_p deviating from the center of the medium simply introduces additional phase and frequency shift onto the retrieval field. This maybe useful for frequency multiplexing information processing. The analytical treatment of this situation is discussed in Chap. IV.

describes a phase shift due to the transverse momentum. This term can be omitted if $[(2\pi)^2/(L_xL_y)]/[(2\pi)/\lambda_s] \ll 2\pi/L$, which reduces to the condition $F = A/(L\lambda_s) \gg 1$. This means a one-dimensional model of Maxwell equation can be adopted, so that each point in the transverse plane (x,y) can be considered independently. In addition, the transverse profile of the signal field is assumed to be smooth enough and treated as featurelessness within each Fresnel zone.

Although the transverse evolution is neglected for large Fresnel interaction volume, when the control field is rotated and different spin waves are created in the medium during the Raman interaction, the signal beam can be subject to spreading in transverse direction due to the scattering of the control field on the spin waves with different wave vectors. Therefore, we need not only $F \gg 1$, but also sufficiently small angle of control field rotation $\Delta\theta$. The upper limit of $\Delta\theta$ can be estimated in the following way: While $\mathbf{k}_c(t)$ changes from $\mathbf{k}_c(t_1)$ (at an angle $\theta_0 - \Delta\theta$) to $\mathbf{k}_c(t_2)$ (at an angle $\theta_0 + \Delta\theta$), it continuously creates a set of spin wave vectors $\mathbf{k}_s - \mathbf{k}_c(t)$. As a result the signal wave vector can spread over an angle φ. We require the additional phase on the longitudinal dimension due to this signal spreading to be smaller than π, i.e., $\left(\Delta q_x^2 + \Delta q_y^2\right) L/(2k_s) \ll \pi$. Since $\Delta q_x \sim k_s \sin\varphi \leqslant 2\Delta\theta k_s$, $\Delta q_y = 0$, we obtain the limit of the rotation angle: $\Delta\theta \ll \Delta\theta_{\max} = \sqrt{\lambda_s/L}/2 \approx \sqrt{F}\theta_d/2$, where θ_d is the diffraction angle satisfying $\sin\theta_d = 1.22\lambda/D$, D is the diameter of the aperture. It should be noticed that this inequality is a sufficient condition for neglecting the transverse derivatives in Maxwell equation in our theoretical treatment, but not necessarily required for the general Raman PMC quantum storage protocol.

Now, by defining a new variable $S'(\mathbf{r},t) = s(\mathbf{r},t)e^{i[\beta_x(x-x_0)t+\beta_z(z-z_0)t]}$, we have the following equations in the long-pulse regime:

$$\frac{\partial}{\partial z}a(\mathbf{r},t) = -g^*NS'(\mathbf{r},t), \qquad (\text{II.16})$$

$$\frac{\partial}{\partial t}S'(\mathbf{r},t) = \{-\gamma+i\delta+i[\beta\cos\theta_0(x-x_0)-\beta\sin\theta_0(z-z_0)]\}S'(\mathbf{r},t)+ga(\mathbf{r},t). \quad (\text{II.17})$$

Since the proposed scheme is mathematically similar to GEM, the condition for good efficiency and fidelity can be analyzed in the same way as for GEM. On the one hand, the absorption window width $|\beta_z|L$ should cover the input pulse spectrum width: $|\beta_z|L > 2\pi/\Delta t$. Since $\beta_z = -\beta\sin\theta_0$, $\beta = (2\Delta\theta/T)(2\pi/\lambda_c)$, we have $2\Delta\theta\sin\theta_0 > T\lambda_c/(\Delta tL)$. This condition is the same as that resulted from switching between different longitudinal modes during the storage of the signal pulse. On the other hand, it is known that the "optical thickness" for each spectral component of the signal field in Fourier space for GEM [103] is $2\pi|g|^2N/|\beta_z|$. This quantity needs to be larger than unity, so $2\Delta\theta\sin\theta_0 < T\lambda_c|g|^2N$. Combining these two conditions, we have the optimal condition of the quantum storage based on control field angular scanning:

$$\frac{T}{\Delta t}\frac{\lambda_c}{L} \lesssim 2\Delta\theta\sin\theta_0 \lesssim T\lambda_c|g|^2N. \qquad (\text{II.18})$$

The optimization of the parameter is achieved by keeping a balance between the absorption window width and the "optical thickness". The bigger β is, the wider the absorption window opens while the smaller the "optical thickness" becomes, and vice versa.

Apart from the optimization condition (II.18) and the above mentioned $F \gg 1$ and $\Delta\theta \ll \Delta\theta_{\max} = \sqrt{\lambda_s/L}/2 \approx \sqrt{F}\theta_d/2$, we also derive the requirement on the the average polar angle θ_0. The central frequency component of the input signal field gets absorbed

at the position $z_p = \delta/(\beta \sin \theta_0) + z_0 + \cot \theta_0 (x - x_0)$, which should be inside the medium

$(-L/2 < z_p < L/2)$. Again, one can engineer the control field to make the location of

the phase stationary point $(x_0, z_0) = (0,0)$ and set two-photon detuning $\delta = 0$. But more

generally, the frequency shift introduced by z_0 can be canceled by the shift introduced by

x_0 and δ, namely, $z_0 - x_0 \cot \theta_0 + \delta/(\beta \sin \theta_0) = 0$. So the phase stationary point does not

need to be exactly at the center of the sample, but may be situated anywhere on the line

$$x_0 = z_0 \tan \theta_0 + \delta/(\beta \cos \theta_0) . \tag{II.19}$$

When $\delta = 0$, this is just the bisector of the rotation. Experimentally a nonvanishing δ can

be used to move the phase stationary point (x_0, z_0) around according to Eq. (II.19). In the

following we will assume Eq. (II.19) is fulfilled. Then the requirement of $-L/2 < z_p < L/2$

gives $-L/2 < x \cot \theta_0 < L/2$. Replacing x by the radius of the excitation volume R, we

have $|\cot \theta_0| < L/(2R)$. So the condition on the average polar angle θ_0 can be written as

$$\theta_0 > \theta_g = \arctan \frac{2R}{L}, \tag{II.20}$$

where θ_g is a geometry angle of the interaction volume. If Eq. (II.19) is not fulfilled, the

angle θ_0 needs to be even bigger. It is worth noting that, since $\theta_g \approx F\theta_d$ and $\Delta\theta_{\max} \approx$

$\sqrt{F}\theta_d/2$, for Fresnel number $F \gg 1$ condition (II.20) automatically ensures that $\theta_0 \gg \Delta\theta$,

which is an assumption we have made throughout this section.

Under the condition (II.19), Eqs. (II.16) and (II.17) become

$$\frac{\partial}{\partial z} a(\mathbf{r}, t) = -g^* N S'(\mathbf{r}, t), \tag{II.21}$$

$$\frac{\partial}{\partial t} S'(\mathbf{r}, t) = [-\gamma + i\beta (x \cos \theta_0 - z \sin \theta_0)] S'(\mathbf{r}, t) + g a(\mathbf{r}, t). \tag{II.22}$$

The retrieval of the signal is done by switching the sign of wave vector rotational rate β, corresponding to a reversal scan of the control field. As in GEM scheme, the retrieval field demonstrate high efficiency, but may experience a phase modulation [104], which could significantly decrease the fidelity defined as in Eq. (II.10). Generally speaking, the higher the optical thickness is, the stronger the phase modulation becomes. The amplitude preservation $\mathscr{A}$ defined in Eq. (II.11), on the other hand, does not decrease as quick as the fidelity $\mathscr{F}$. Discussions about this phase modulation can be found in Sec. III.2, and in Chap. IV with more detail. In Fig. 2.3 we plot the amplitudes of the retrieval fields for an input single-photon wave packet of Gaussian temporal waveform under both transverse excitation and oblique excitation.

In order to minimize the transverse scattering of the signal field by the spin grating, we store the information by the longitudinal component of the spin wave. So the term $\beta x \cos \theta_0 s'(\mathbf{r},t)$ in Eq. (II.22) appears as a side effect due to the change of $\mathbf{k}_c$ on $\hat{x}$ direction. For forward retrieval, this term could introduce some transversal space dependent time shift (ahead or behind) of the forward retrieved signal, as seen in Fig. 2.3 (b, d).

The reason of the time delay can be explained as follows: the signal field in the medium excites spin wave and evolves in the form of polariton, which is the combination of the signal field and the excited spin wave [44]. During storage, the control field transforms the signal field into the polariton which stays inside the medium at the location of central absorption position $z_p = x \cot \theta_0$. During forward retrieval, the control field picks up the polariton at z_p which then turns into retrieval signal at $z = L/2$. So the
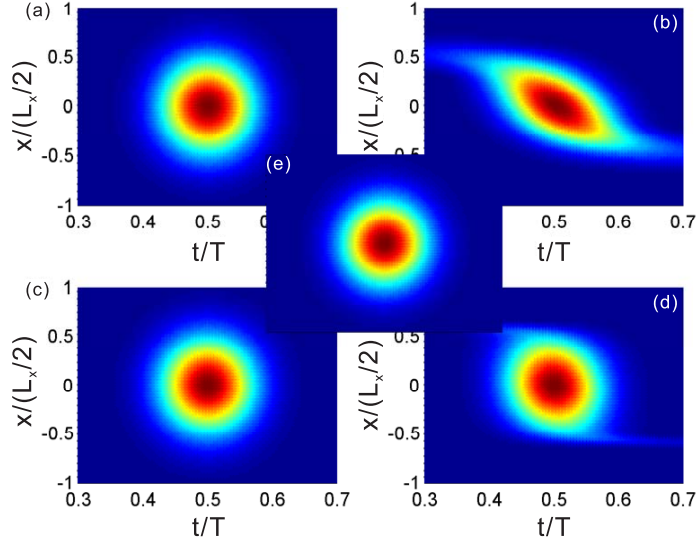
Figure 2.3: Forward retrieval fields of (e) a single-photon wave packet of Gaussian temporal waveform based on control field angular scanning using (a, c) transverse excitation ($\theta_0 = \pi/2$) and (b, d) oblique excitation ($\theta_0 = \pi/9$). (a, b) Retrieval fields for constant $\Delta\theta$. The field is distorted for small θ_0 because (i): the absolute value of $\beta_z = -\beta \sin\theta_0$ becomes smaller such that it approaches the lower limit of Eq. (II.18); (ii): $\beta_x = \beta \cos\theta_0$ becomes large enough to lead a spacial-temporal distortion; (c, d) Retrieval fields for constant $\Delta\theta \sin\theta_0$. There is transverse distortion of the retrieval field due to the non-vanishing β_x. The figures are generated under the following parameters: $\lambda_s \approx \lambda_c = 1550$ nm (fiber-optic communication band), $|g|^2 N = 8.3 \times 10^{10}$ s^{-1}m^{-1}, $\Delta t/T = 1/20$, $T = 1000$ ns, $2R/L_x = 1/6$, where R is considered to be the transverse spatial half width of the input signal and L_x is its normalization factor (which can be taken as the total medium transverse size), $L_x = 0.6$ cm, $L = 1$ cm, $\Delta\theta = 8 \times 10^{-3}$ rad in (a) and (b), $= 8 \times 10^{-3}/\sin\theta_0$ rad in (c) and (d).

group velocity of the signal field reduces from c to 0 while $z = -L/2 \rightarrow z_p$, and recovers from 0 to c while $z = z_p \rightarrow L/2$. As a result, if $z_p \neq 0$, the storage-retrieval dynamics will introduce a time shift onto the forward recalled signal. This time shift can be eliminated in the transverse excitation ($\theta_0 = \pi/2$) because there z_p is independent on x (transversely homogeneous). However, for oblique excitation ($\theta_0 \neq \pi/2$), at $x \neq 0$ this time shift is unavoidable for forward retrieval. Moreover, since it is transversely inhomogeneous, there must be a transverse distortion of the signal. For z_p not deviating much from 0 and $4c|g|^2 N/(\beta^2 L^2 \sin^2 \theta_0) \gg 1$, the group velocity of the signal field near the ends of the medium is calculated in Ref. [104], which is $v_g(z)|_{|z \pm L/2| \ll L/2} \sim \beta^2 (z - z_p)^2 /(|g|^2 N)$. Since the delay is due to the propagation between $z = L/2 + 2z_p$ and $z = L/2$, from $dz = v_g(z)dt$, the delay time can be estimated as

$$t_d \sim \frac{|g|^2 N}{\beta^2 \sin^2 \theta_0} \left(\frac{1}{L/2 + z_p} - \frac{1}{L/2 - z_p} \right). \tag{II.23}$$

Taking $z_p = \pm R \cot \theta_0$, one can estimate the temporal broadening of the forward retrieved signal with respect to the input signal:

$$\Delta t_{br} \sim \frac{|g|^2 N}{\beta^2 \sin^2 \theta_0} \frac{4R \cot \theta_0}{(L/2)^2 - R^2 \cot^2 \theta_0}, \tag{II.24}$$

which is finite and positive under the condition (II.20).

In Fig. 2.4 we show the efficiency and fidelity dependence on θ_0. As can be seen, although a smaller θ_0 requires less control field power (because of the reduce of the cross section of the control beam on the interaction volume), it gives less fidelity due to the transversal distortion for a given $\Delta\theta$. Alteratively, it is necessary to increase $\Delta\theta$ when θ_0 approaches θ_g from above, in order to maintain high fidelity of quantum storage, as shown

34
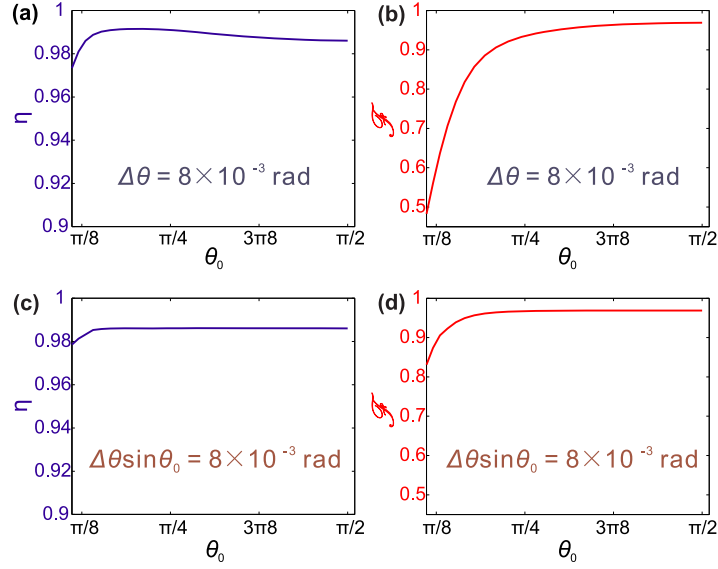
Figure 2.4: Forward retrieval efficiency η and fidelity $\mathcal{F}$ as functions of the average polar angle θ_0 for quantum memory based on control field angular scanning. (a, b) Efficiency (a) and fidelity (b) for forward retrieval with $\Delta\theta$ kept as constant; (c, d) Efficiency (c) and fidelity (d) for forward retrieval with $\Delta\theta\sin\theta_0$ kept as constant. The parameters are the same as described in Fig. 2.3.

in Fig. 2.4 (c, d).

The fundamental reason of the transverse distortion and additional phase modulation (see discussions in Chap. IV) lies in the lack of time-reversal symmetry of the forward retrieval scheme. These problems can be avoided in a backward retrieval, wherein the time shift at each transverse point is exactly compensated during backward propagation. As a result, the fidelity remains high for all average angles θ_0 of interest.

However, due to the phase matching condition, it is not enough to merely switch the propagation direction of the control field to the opposite. In general, the symmetry of the system in backward retrieval requires a phase conjugation of the spin wave. Within the approximations discussed above, to achieve such a phase conjugation, we can just flip the

direction of the spin wave vector along direction $\mathbf{K} = \mathbf{k}_s - \mathbf{k}_c(t = 0)$ before the retrieval. This can be done by applying two non-colinearly propagating π pulses one followed by another [45, 105], both on resonance with level $|3\rangle$ and another energy level, say, $|4\rangle$. The transition frequency ω_{34} needs to be bigger than cK. The directions of the two π pulses are arranged in such a way that the wave vectors difference between them is along $-\mathbf{K}$. Another possibility is to generate spin wave vectors perpendicular to the signal wave vector [106]. In this case, k_c and k_s need to differ from each other significantly.

II.4.3 Experimental issues

The advantage of this PMC quantum memory scheme lies in its experimental convenience in many systems. For a single pulse to be stored or recalled in the free space, the minimum increment $|\Delta k_c/k_c|$ (or the rotation angle) of the control field wave vector k_c should be on the order of $10\lambda_c/L$. In other words, the ratio between the minimum angle of rotation and the beam diffraction angle (resolvable spot number) should be equal to ~ 10. This is confirmed by the numerical simulation, which shows that a single Gaussian pulse at 700 nm of duration $\Delta t = T/20$ with $T = 500$ ns can be stored and recalled with high efficiency and fidelity using transverse control field ($\theta_0 = \pi/2$) if $\Delta\theta/T \sim 10^3$ rad/s for $L = 1$ cm (in accordance with $2\Delta\theta \sim 10\lambda/L$). Such rate of beam deviation can be achieved by commercial equipment, and such wavelength can be implemented in nitrogen-vacancy centers in diamond (NVD) [107, 108].

In NVD system, the existence of lambda type optical transitions was demonstrated via EIT[109] and coherent population trapping [110]. The large inhomogeneous broaden-

ing can be reduced by optical pumping technique [111], and the interaction between spin excitation and the local environment can be untangled using dynamic decoupling [112--114]. The transfer of quantum states between the electron spins and nuclear spins is possible [115], which in combination with dissipative decoupling schemes allows long-lived quantum storage [116]. A more detailed discussion of the quantum memory implementation in NVD is given in Chap. III. Another promising system is cold atoms trapped in an optical lattice[117, 118]. The influence of regular atomic structure on the efficiency of quantum memory in such a system was analyzed in Ref. [119]. In principle, any spatially stationary atomic ensemble demonstrating off-resonant Raman interaction with relatively strong optical transitions (preferable possessing polarization selection rules to increase signal-to-noise ratio) is suitable for the implementation of the quantum memory based on control field angular scanning.

This scheme can be implemented also in a cavity [89]. Enclosing an atomic ensemble in a cavity makes it possible to achieve high efficiency of quantum storage with optically thin materials, which is typical for Raman transitions. This is especially important for the materials with relatively small dipole transition elements, such as rare-earth-doped crystals. A three-dimensional theory, which allows almost a perfect multimode storage for transverse excitation, was developed in Ref. [89]. The spatial multimode storage is crucially important for multiplexing in quantum repeaters, which can significantly increase the rate of quantum communication in possession of short-time quantum storage, and for holographic quantum computers. It was experimentally demonstrated using EIT [120--

123] and GEM [54, 55], but only in free space. As shown in Ref. [89], for a confocal cavity with Fresnel number 10, the total number of accessible transverse modes TEM_{mn} approaches 1000. Storage of such a multimode transverse field can be combined with that of the multimode longitudinal profile, i.e., with storage of a complicated pulse shape or a sequence of pulses. The minimum angle of rotation per pulse proves to be $\sim 10\lambda_c/L$, while accessible angular scanning range around transverse direction is about $\approx 20°$ for typical values of experimental parameters. Therefore, one can store about 100 of the spatially multimode pulses in a sequence. Thus we can predict a large storage capacity for the proposed memory scheme.

In this section we discussed a PMC quantum memory based on control field angular scanning. This method stores and retrieves weak pulses such as single-photon wave packets based on off-resonant Raman interaction. By changing the propagation direction of the strong classical control field, the temporal profile of the signal field is mapped into the spatial grating of Raman coherence. This specific realization of PMC quantum memory is easier to be experimentally realized than the PMC scheme based on refractive index manipulation. It has the advantage of GEM in that high efficiency can be achieved without backward retrieval. But unlike in GEM, this scheme can be implemented in resonant media which do not allow linear Stark or Zeeman effects.

II.5   Quantum storage via frequency chirp of the control field

The third method for PMC-based quantum memory is quantum storage via frequency chirp of the control field. Although this method is much more difficult to be realized due to the reason that will be explained in this section, we will provide theoretical discussion for the general interest and for the completion of the investigation on PMC quantum memory.

Our model is outlined in Fig. 2.5. We consider a single-photon signal field $E_s(z,t)$ and a strong classical control field $E_c(z,t)$ propagating collinearly along $\hat{z}$ direction with orthogonal polarizations. The two fields interact with each other through off-resonant Raman interaction [Fig. 2.1 (a)]. The control field has a frequency chirp, meaning that its frequency changes with time. Such a frequency chirp leads to a time dependent wave vector, which is used to achieve phase matching control in the process of quantum storage. It is worth noting that frequency chirped control field has been considered in an AFC scheme [124], where the chirp as an aide helps to increase the control filed bandwidth and thus reduce the requirement of the intensities. In present proposal, the chirp plays a principal role, leading to a time dependent excited spin wave vector, which records the temporal shape of the single-photon wave packet.

During storage, the Raman interaction between the signal and control fields creates spin coherence, and the temporal information of the signal field is recorded into the spin wave with difference wave vectors, as shown in Fig. 2.5 (a). During retrieval, the frequency chirp of the control field is reversed, resulting in an oppositely modulated control wave vector. Such a control field will read the spin wave into the signal field in a time-
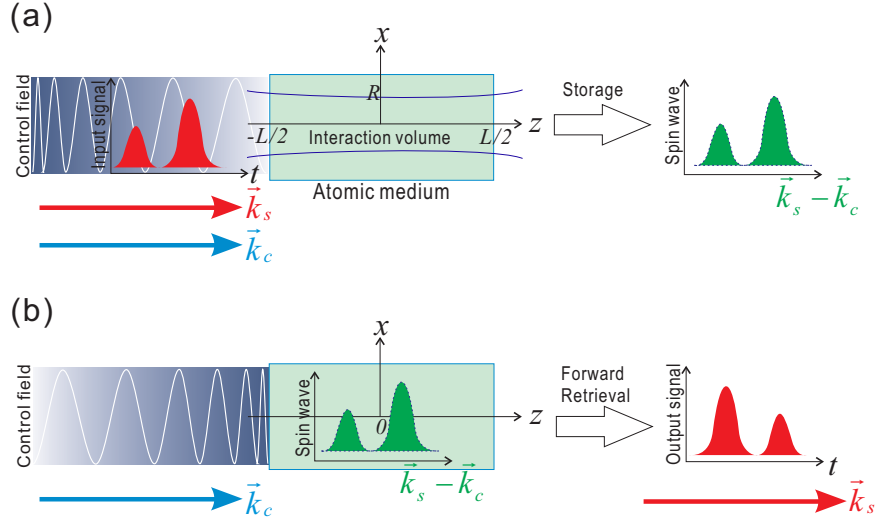
Figure 2.5: Model of quantum storage based on control field frequency chirp in a off-resonance Raman interaction. (a) During storage, the temporal profile of the signal field is mapped into the spin wave distributed over different spin wave vectors; (b) During forward retrieval, the spin wave profile is mapped back into the output signal field.

ordered manner, as illustrated in Fig. 2.5 (b).

The signal field is given by Eq. (II.1) with plain wave approximation, and the classical control field contains a frequency chirp:

$$E_c(z,t) = E_0 e^{i[k_{c0}z - \omega_{c0}t + \phi(z,t)]} + \text{c.c.}, \tag{II.25}$$

in which ω_{c0} is the angular frequency of the control field at $t = 0$, and $k_{c0} = \omega_{c0}/v_c$, where v_c is the phase velocity of the control field in the medium. We consider only the case of a linear chirp, so that the phase factor reads

$$\phi(z,t) = -\frac{1}{2}\alpha t^2 + \frac{\alpha}{v_{\text{cg}}}(z - z_0)t - \frac{1}{2}\alpha\frac{(z - z_0)^2}{v_{\text{cg}}^2}, \tag{II.26}$$

where α is the chirp parameter and v_{cg} is the group velocity of the control field. The first term on the right hand side of Eq. (II.26) is a time dependent phase from the frequency chirp. The second term is a time and space dependent phase coming from the

40

chirp-leaded wave vector modulation. $z = z_0$ is a phase stationary plane in which wave-vector-modulation part of the phase remains constant during storage or retrieval. In the long pulse regime, the higher spatial order term $-\frac{1}{2}\alpha(z-z_0)^2/v_{cg}^2$ may be neglected in Eq. (II.26).

Defining the slowly varying collective spin coherence operator as

$$s(z,t) = \sigma_{13}(z,t)e^{i\left[(\omega_s-\omega_{c0})t-\frac{1}{2}\alpha t^2-\frac{\alpha}{v_{cg}}z_0 t-(k_s-k_{c0})z\right]}, \qquad (II.27)$$

the quantum storage process can be described by the following equations:

$$\left(\frac{\partial}{\partial z} + \frac{1}{v_{sg}}\frac{\partial}{\partial t}\right)a(z,t) = -g^* N s(z,t)e^{i\frac{\alpha}{v_{cg}}zt}, \qquad (II.28)$$

$$\frac{\partial}{\partial t}s(z,t) = [-\gamma + i\delta(t)]s(z,t) + ga(z,t)e^{-i\frac{\alpha}{v_{cg}}zt}. \qquad (II.29)$$

Denoting $\delta_0 = \omega_s - \omega_{c0} - \omega_3 - |\Omega|^2/\Delta - (\alpha/v_{cg})z_0$ (where ω_3 is the Raman transition frequency), then $\delta(t) = \delta_0 - \alpha t$ is the time dependent two-photon detuning. The time dependent part originates from the changing of the control field frequency. Namely, the frequency chirp of the control field provides the phase matching control phase factor, but simultaneously introduces a shift of the resonant frequency.

Equations (II.28) and (II.29) are similar to the equations describing GEM scheme except for a presence of an inherent time dependent two-photon detuning. The term $i(\alpha/v_{cg})zt$ in Eqs. (II.28) and (II.29) is responsible for the creation and erasure of the spin grating (leading to quantum storage), while $i\delta(t)$, on the other hand, destroys the quantum storage by detuning the system away from two-photon resonance. In order to store a single photon wave packet, this time-dependent two-photon detuning has to be compensated. As-

suming it is compensated and defining new variable $S(z,t) = s(z,t)e^{i\frac{\alpha}{v_{cg}}zt}$, in the long-pulse regime Eqs. (II.28) and (II.29) become:

$$\frac{\partial}{\partial z}a(z,t) = -g^*NS(z,t),\tag{II.30}$$

$$\frac{\partial}{\partial t}S(z,t) = \left(-\gamma + i\frac{\alpha}{v_{cg}}z\right)S(z,t) + ga(z,t),\tag{II.31}$$

These equations are equivalent to those describing other PMC quantum memory schemes (namely, via refractive index modulation and/or angular scanning). It is convenient to introduce the "chirp depth" $\Delta_d = \alpha T$, which shows the amount of chirp during the storage or retrieval time T. Similar as before, high efficiency and field amplitude correlation can be achieved when

$$\frac{v_{cg}}{L}\frac{T}{\Delta t} \lesssim \frac{\Delta_d}{2\pi} \lesssim v_{cg}|g|^2NT.\tag{II.32}$$

Let us go back to consider how to compensate the time-dependent two-photon detuning in order to physically realize the evolution equations (II.30) and (II.31). To do that, one needs to modulate the atomic energy level $|3\rangle$ simultaneously with the chirp in a way to make two-photon detuning $\delta(t) = 0$, namely,

$$\omega_3(t) = \omega_s - \omega_{c0} - \frac{|\Omega|^2}{\Delta} - \frac{\alpha}{v_{cg}}z_0 - \alpha t.\tag{II.33}$$

At the retrieval stage the sign of the frequency chirp parameter should be changed (so that the equivalent "inhomogeneous broadening" would be reversed), while the modulation of the atomic level should be switched simultaneously to compensate the two-photon detuning introduced by this chirp and to ensure keeping of the two-photon resonance.

One way to achieve linearly shift of the ground state $|3\rangle$ is to use dc Stark or Zeeman

effect. The shift of the latter is proportional to $\mu_B/2\pi\hbar = 14$ GHz/T, where μ_B is the Bohr magneton. In the presence of polarization selection rules, the control field acts only on the transition of $|2\rangle$-$|3\rangle$ levels, which are essentially almost empty. So the medium is dispersionless for the control field. As a result, its group velocity v_{cg} is equal to phase velocity v_c, which is typically on the order of the speed of light in the vacuum. Then according to (II.32), for medium length $L = 2$ cm and signal field $T/\Delta t = 20$, the chirp depth $\Delta_d/2\pi$ should be on the order of 286 GHz. Numerical calculation shows that a chirp depth $\Delta_d/2\pi = 80$ GHz can store and recall such a signal pulse with high efficiency and fidelity in a medium with $|g|^2NT \sim 2000$ m^{-1}. A linear time dependent magnetic field up to ~ 1 T is able to compensate a chirp depth $\Delta_d/2\pi \sim 30$ GHz. Such a magnetic field can be modulated as fast as with 10 μs [125] time period. If the g-factors for the ground and excited state are the same, the levels $|1\rangle$ and $|2\rangle$ can be shifted roughly by the same amount, while the level $|3\rangle$ can be shifted substantially by different amount. As an example, in Fig. 2.6, a single photon wave packet of Gaussian temporal shape $\Delta t/T = 1/20$ is stored and retrieved with a chirp depth $\Delta_d/2\pi = 95$ GHz in a 2 cm medium with $|g|^2NT \sim 2650$ m^{-1} with high efficiency and fidelity. The lifetime of the spin wave is assumed to be much longer than the signal pulse duration.

Alternatively, another way to shift the ground state $|3\rangle$ is to take advantage of ac Stark effect, where a second coherent external control field (Stark field) with time-varying amplitude, propagating in the transverse direction with respect to the signal and the first control fields, is used for compensation of the time-dependent frequency shift. However,
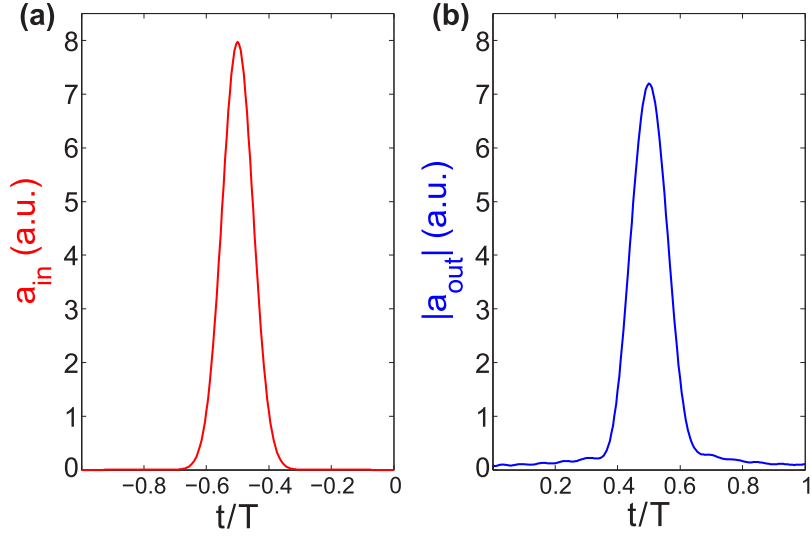
Figure 2.6: Incoming signal field $a_{in} = a(-L/2, \tau < 0)$ and forward retrieved field $a_{out} = a(L/2, \tau > 0)$ via Raman PMC quantum memory based on control field frequency chirp. The corresponding parameters are: $\lambda_s \approx \lambda_c = 700$ nm, $|g|^2 NT = 2650$ m^{-1}, $\Delta t/T = 1/20$, $L = 2$ cm, $\Delta_d = 6 \times 10^{11}$ rad/s. The efficiency η and fidelity $\mathscr{F}$ are 96%. The quantity $\mathscr{A}$, which describes the preservation of the pulse amplitude without taking into account possible phase modulation, is 98.6%.

it is not easy either, because the Stark laser's scattering at spin coherence would introduce a noise that decreases the fidelity. Its frequency should be carefully selected to provide, on one hand a large detuning to other levels to minimize a scattering rate, on the other hand small enough detuning sufficient for compensation of time-dependent two-photon detuning. The ac Stark gradient echo quantum memory scheme was suggested in [126], where a MHz shift can be obtained with 10 W Stark laser power (with 1 cm by 10 μm medium) in ^{87}Rb.

The next question is how to generate a long chirped control beam. Experimentally, sub-nanosecond chirp pulses at joule energy level can be produced using the ultra-fast optics technology [127, 128]. But first, the spectrum width (and thus chirp depth) of such a

pulse is too large for the compensation of the frequency shift induced by the chirp. Second, it becomes difficult to achieve a longer than nanosecond chirp pulse, which is required from the speed perspective, in order to provide a compensation of frequency shift via linear Stark or Zeeman effect as it was discussed above. In other words, if a slowly modulated control field allows to reduce chirp depth Δ_d, a long chirp pulse with narrow bandwidth is needed. By optical means such a chirp pulse would require an extraordinarily dispersive system which is very difficult to be achieved in conventional grating or prism pair. One possible solution to unravel the above difficulty is to stay in the narrow bandwidth regime and generate long chirp control field by electronic means. In this case, frequency chirp is added on top of a long control pulse by electronic modulation. Such technique is used, e.g., in high resolution lidar systems. The chirp depth Δ_d is determined by the RF-signal frequency tuning range, which can be as high as gigahertz. Using different techniques, 1-10 GHz chirp depth with pulse duration 0.1-0.5 μs [129--131] were demonstrated.

From the above discussion, it can be seen that the compensation of the two-photon-detuning drift due to spatial chirp is fairly difficult because of the mismatch of the parameter space between two techniques: On the one hand, the dc or ac Stark shift favors low bandwidth operation; On the other hand, the storage medium does not permit a ultra-low bandwidth because of its limited lifetime, and many techniques for frequency chirp operate on a picosecond time scale which is contradict with low bandwidth requirement. So such quantum memory scheme based on control field frequency chirp is not experimentally favorable comparing with the other two PMC schemes. But it is worth noting that another

type of quantum memory scheme based on control field spatial chirp, which is discussed in Chap. III, is free of such problem.

II.6 Conclusion

In this chapter, we propose a general method to realize quantum memory for a weak signal pulse (single photon wave packet) based on phase matching control (PMC). Depending on different wave vector manipulation methods, there are three different implementations, namely, via refractive index modulation, control field angular scanning, and control field frequency chirp. We analyze and compare these three PMC quantum memory schemes.

Specifically, we focus on PMC quantum memory based on control field angular scanning in a Raman configuration. The sweeping of the control field during storage is used to create a continuous set of spin waves with different spatial modes, which will record the temporal profile of the signal pulse. Later on, the same information can be read out by sweeping back. This scheme has very nice capability to deal with multiple spatial mode, and demonstrates very high efficiency and fidelity without relying on a backward retrieval in an all-optical manner. It can be experimentally implemented in cold atom, nitrogen-vacancy centers in diamond, or rare-earth-doped crystals (in a cavity-assisted set up to enhance the optical density).

We also discuss the PMC quantum memory based on frequency chirp of the control field. In such a case, to stay on two-photon resonance, the atomic level should be mod-

46

ulated in time through a dc or ac external field to compensate the two-photon detuning drift. In a dispersive medium the control field frequency chirp scheme involves also the refractive index modulation so that we actually have a combination of both approaches. This enhances the control field wave vector scanning rate and makes it easier for the sake of chirp-leaded two-photon detuning compensation.

Among the three PMC quantum memory schemes, the first and second ones are much easier to be implemented since there is no two-photon detuning drift. While the second one seems to be the easiest in the sense that no direct manipulation of the material is involved.

The phase matching control quantum memory demonstrates high efficiency and fidelity with the same performance as gradient echo memory. However the former (in cases of refractive index modulation and control field angular scanning schemes) does not require Stark or Zeeman effect, and no synchronization between signal and control fields is needed.

CHAPTER III

ALL OPTICAL QUANTUM STORAGE BASED ON SPATIAL

CHIRP OF THE CONTROL FIELD[*]

III.1   Introduction

Quantum memory schemes based on phase matching control (PMC) [85, 87--90] were discussed in Chap. II. PMC schemes get rid of the requirement of exact synchronization between signal and control fields, but still demand a manipulation with time of the refractive index or control field propagation direction.

In this chapter, we discuss a quantum storage method which also employs the Raman configuration as schemes discussed in Chap. II, but in principle requires neither the synchronization of the fields, nor the use of inhomogeneous broadening, nor the time variation of the control field amplitude or any other parameters of the system. The key element of this scheme is a spatial chirp on the control field, which means a varying frequency distributed across the laser beam. The result is very similar to the PMC quantum memory schemes, but it does not involve any temporal manipulation of the control field and, thus, is more robust to a time jitter.

It is interesting to compare the currently proposed quantum memory scheme with that based on control field frequency chirp, which was discussed in Sec. II.5. In the latter,

---

a time-dependent detuning drives the signal out of the two-photon Raman resonance. The compensation of this frequency shift creates a big experimental problem for implementation. In this chapter, we discuss the quantum memory based on the control field spatial chirp. We show that this scheme demonstrates a stationary two-photon detuning, thus is free of the above experimental difficulty. The effect of such a spatial chirp is analogous to the effect of frequency gradient in GEM. However, unlike GEM, the proposed scheme does not involve any direct operation on the medium itself. It does not require temporal modulation of the control field or the atomic levels, and can be realized without additional electric or magnetic fields. It means that materials demonstrating neither linear Stark nor Zeeman effects can be used and/or materials which are placed in specific external fields remain undisturbed.

III.2 The theoretical model and numerical simulation

We consider the off-resonant Raman interaction between a signal field E_s of full-width-half-maximum (FWHM) duration Δt and a three-level atomic ensemble under the control of a strong classical field E_c [Fig. 3.1 (a)]. The signal and control fields have angular carrier frequencies ω_s and ω_c, respectively. The corresponding one- (two-) photon frequency detuning is Δ (δ). The atoms are assumed to be stationary and uniformly distributed in space over a cylindrical excitation volume of length L and radius R (satisfying $\pi R^2/(L\lambda_s) \gg 1$). We assume the intensities of the signal and control fields to be constant across the dimensions transverse to their propagation directions, and their polarizations to
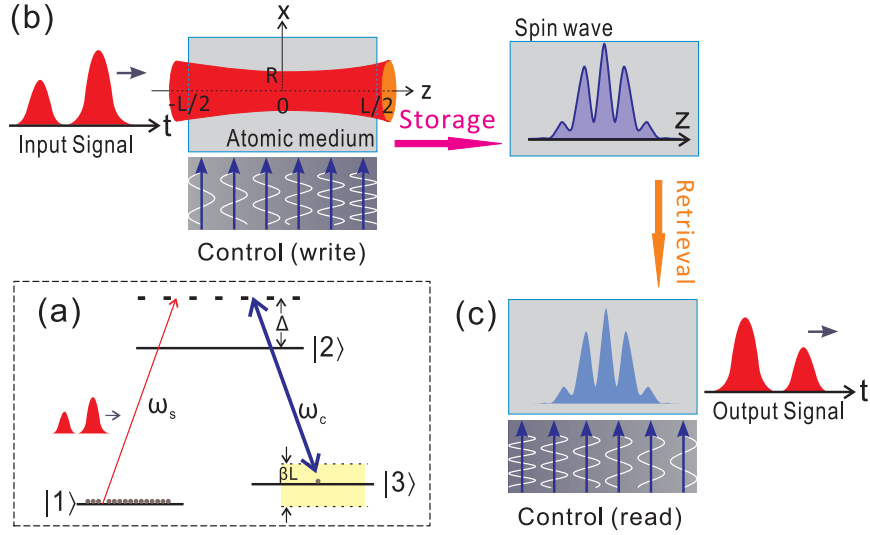
Figure 3.1: Illustration of quantum memory based on control field spatial chirp. (a) Energy diagram of the off-resonant Raman interaction in a three-level Λ system. The control field spectrum width is given by the spatial chirp, which is $|\beta|L$ for the transverse excitation setup. During storage (b), the temporal profile of the signal field is mapped into a pattern of the spin wave distribution due to the Raman interaction of the signal with the longitudinally chirped control field. During retrieval (c), the stored spin wave generates the output signal field and the spin wave spatial pattern is mapped back into the output signal's temporal profile.

be orthogonal so that they are coupled to the different atomic transitions due to polarization selection rules. The effect of the lack of such polarization selection rules is discussed in Sec. III.3. The control field frequency ω_c has a linear transverse spatial chirp, meaning that the frequency at different positions on the phase front varies as a function of space. The storage of the single-photon wave packet takes place during an interval of time $t \in [-T, 0]$, and the retrieval happens during $t \in [0, T]$.

In the transverse excitation regime [Fig. 3.1 (b, c)], the signal field propagates along $\hat{z}$ (the axis of the cylindrical medium) and the control field propagates perpendicularly to it. The signal experiences the inhomogeneity only along the longitudinal direction in the

Raman interaction with the control field that is spatially chirped along $\hat{z}$. The spatial chirp

of the control field creates an effective inhomogeneous broadening βL [Fig. 3.1 (a)] on

which the spectrum of the signal field is converted into the spatial spectrum of the spin wave

(Raman coherence) during the storage process and back during the retrieval process. The

storage time is defined by the Raman coherence decay time. But for the sake of simplicity,

a free decay of the spin wave between the end of the storage and the beginning of the

retrieval will be omitted.

The signal field of wave vector $k_s = \omega_s/c$ is given by Eq. (II.1), and the classical

control field with a large Fresnel number for the interaction volume is written as a plain

wave with a spatial chirp across the beam:

$$E_c(\mathbf{r},t) = E_0 e^{i[\mathbf{k}_c(\mathbf{r}_\perp)\cdot\mathbf{r}-\omega_c(\mathbf{r}_\perp)t-\varphi_{0c}(\mathbf{r}_\perp)]} + \text{c.c..} \tag{III.1}$$

We will consider a linear transverse spatial chirp $\omega_c(\mathbf{r}_\perp) = \omega_{c0} + \boldsymbol{\beta}\cdot\mathbf{r}_\perp$, where the radius-

vector $\mathbf{r}_\perp$ is perpendicular to the propagation direction of the control field, $\omega_{c0} = \omega_c(\mathbf{r}_\perp = 0)$, $\boldsymbol{\beta}$ is a frequency gradient. A transverse pattern of the wave vector of the control field

is described by a vector function $\mathbf{k}_c(\mathbf{r}_\perp) \perp \mathbf{r}_\perp$, $|\mathbf{k}_c(\mathbf{r}_\perp)| = \omega_c(\mathbf{r}_\perp)/c$, and a phase shift

$\varphi_{0c}(\mathbf{r}_\perp) = \mathbf{k}_c(\mathbf{r}_\perp)\cdot\mathbf{r}_0 - \omega_c(\mathbf{r}_\perp)t_0$ specifies the position $\mathbf{r}_0$ and time t_0 of the constant phase

plane. We assume the amplitude of the control field is constant in time and space, and the

switching of the field is instantaneous. For switching rate faster than $1/\Delta$, nonadiabatic

excitation of optical coherence may contribute to additional loss to the quantum memory

scheme. However, for a sufficiently large one-photon detuning compared with the Rabi

frequency, such influence is negligible [132].

The collective atomic operators are defined by Eq. (II.3), and the corresponding slowly varying part of the spin wave operator is

$$s(\mathbf{r},t) = \sigma_{13}(\mathbf{r},t)e^{-i(\mathbf{k}_s-\mathbf{k}_{c0})\cdot\mathbf{r}+i(\omega_s-\omega_{c0})t}. \tag{III.2}$$

Then the evolution equations are reduced to the same form of Eqs. (II.5) and (II.6), where δ is replaced with its averaged value $\delta_0 = \omega_s - \omega_{c0} - \omega_3$, and the phase factor ϕ is of the following form:

$$\phi(\mathbf{r},t) = [\mathbf{k}_c(\mathbf{r}_\perp) - \mathbf{k}_{c0}]\cdot\mathbf{r} - [\omega_c(\mathbf{r}_\perp) - \omega_{c0}]t - \varphi_{0c}(\mathbf{r}_\perp). \tag{III.3}$$

In obtaining Eqs. (II.5) and (II.6), we incorporated the Raman transition frequency shift $|\Omega|^2/\Delta$ in the average control field frequency ω_{c0}. For a control field of Gaussian spatial profile, this can not be done since the corresponding ac Stark shift is inhomogeneous in space. Its practical influence is discussed in Sec. III.3 as well as in Sec. V.2.

In transverse excitation regime of the proposed scheme, the frequency gradient of the control field lies along the longitudinal direction $\hat{z}$ and provides the spatial chirp $\omega_c(z) = \omega_{c0} + \beta z$, $z \in [-L/2, L/2]$. Choosing for convenience $x_0 = t_0 = 0$, the phase factor in Eq. (III.3) becomes the following:

$$\phi(\mathbf{r},t) = -\beta z(t - x/c), \tag{III.4}$$

where $x \in [-R,R]$ and $R < L$. We assume a short propagation time of the pulse through the medium compared to the inverse spectral broadening via spatial chirp, which, in its turn, is shorter than the pulse duration ($L/c < 2\pi/(\beta L) \lesssim \Delta t$). This allows us to neglect the retardation of the signal field, as well as the transverse dependent phase factor $\beta zx/c$.

Then the evolution equations describing the transverse excitation regime take the following form

$$\frac{\partial}{\partial z}a(\mathbf{r},t) = -g^*Ns(\mathbf{r},t)e^{-i\beta zt}\,, \qquad\qquad\text{(III.5)}$$

$$\frac{\partial}{\partial t}s(\mathbf{r},t) = -\gamma s(\mathbf{r},t) + ga(\mathbf{r},t)e^{i\beta zt}\,, \qquad\qquad\text{(III.6)}$$

where g is the Raman coupling constant, N is the constant atomic number density, γ is the decoherence rate of spin excitation, $z \in [-L/2, L/2]$. These equations can be reduced to the same form of GEM evolution equations. Therefore, we prove that the performance of the transverse excitation regime of the spatial-chirp quantum memory scheme is the same as that of GEM. Indeed, the essential part of GEM scheme is to create a non-uniformly distributed inhomogeneous broadening. Usually the translational symmetric is broken by external dc [44, 55] or ac [126] field which is used to introduce a level shift of the storage medium. In our scheme, the inhomogeneity is created by a spatial dependent dynamical phase of the control beam. So eventually we realize the GEM action with a completely different physical implementation.

Taking the analogy to the GEM scheme, the necessary condition for large efficiency (II.7) and fidelity (II.10) in the transverse excitation regime of the proposed scheme is (see discussions in Chap. II and references therein):

$$1 \lesssim \frac{\beta L \Delta t}{2\pi} < |g|^2 NL\Delta t\,. \qquad\qquad\text{(III.7)}$$

The forward retrieval is done by switching the frequency gradient to the opposite $\beta \to -\beta$ and keeping the same control beam propagation direction. Numerical simulations presented in Fig. 3.2 confirm that high efficiency and fidelity can be achieved following the

optimization condition Eq. (III.7). Although high efficiency is possible, there could be a strong phase modulation of the forward retrieval signal of the proposed scheme, especially at the large optical thickness. This is the reason that in Fig. 3.2 (f) the fidelity is only 75% although the retrieved pulse shape looks almost the same as the input [Fig. 3.2 (e)]. In Fig. 3.2 it can be seen that the fidelity in (f) is lower than that in (c) in despite of the same optical thickness. This is because a longer pulse duration experiences more phase modulation. The backward retrieval can be achieved by keeping the same frequency gradient $\beta \to \beta$ but with opposite control beam propagation direction. Because of the phase matching condition, a conjugate spin coherence should be prepared before backward retrieval by, for example, two successive non-collinearly-propagating π pulses as discussed in Sec. II.4. The backward retrieval signal field is free of phase modulation.

In a more general case, the propagating directions of the control and signal fields can make an arbitrary angle θ. We make the spatial chirp centered at control beam center, then $\omega_c(x,z) = \omega_{c0} + \beta z \sin \theta - \beta x \cos \theta$, with $x \in [-R, R]$, $z \in [-L/2, L/2]$. Without losing generality, we take $z_0 = x_0 = t_0 = 0$. The phase factor in Eq. (III.3) is the following function of the coordinates and time:

$$\phi(\mathbf{r}, t) = -\beta(z \sin \theta - x \cos \theta)\left(t - \frac{z \cos \theta + x \sin \theta}{c}\right). \tag{III.8}$$

Consider $k_c \approx k_s$, $\Delta t \gg L/c$, $\Delta k_{sx} \sim \Delta k_{cx} \sim \beta \Delta t$, $\beta R < \beta L \sim 2\pi/\Delta t$, the transverse evolution of the signal field can be neglected for large signal field Fresnel number $F \gg 1$. Under the same assumption made above, $L/c < 2\pi/(\beta L) < \Delta t$, the $(z \cos \theta + x \sin \theta)/c$ term in Eq. (III.8) can be neglected and we are able to approximate the phase shift in Eq. (III.3) by

54
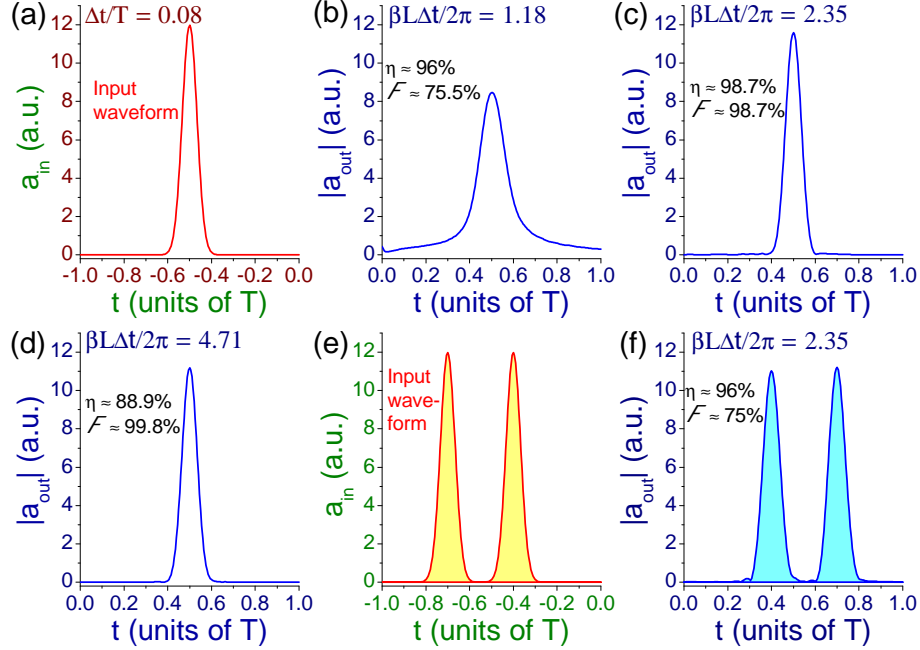
Figure 3.2: Forward retrieval of quantum memory based on control field spatial chirp. (a-d) Signal amplitude $|a_{out}(t)|$ (phase modulation is not shown in the figure but taken into account in the fidelity $\mathcal{F}$) as a function of time in the transverse excitation regime for different values of the spatial chirp βL across the control beam [(b) $2\pi\sqrt{2\ln 2}/\Delta t$, (c) $4\pi\sqrt{2\ln 2}/\Delta t$, (d) $8\pi\sqrt{2\ln 2}/\Delta t$] for the depicted in (a) Gaussian temporal shape input signal field $a_{in}(t)$ with a FWHM duration $\Delta t = (\sqrt{2\ln 2}/15)T$, where T is the duration of the writing process. (e, f) A double-peak Gaussian temporal shape input signal field (e) and its forward retrieval signal amplitude (f) for $\beta L = 4\pi\sqrt{2\ln 2}/\Delta t$. The graphs are plotted for the parameter $|g|^2 NL\Delta t = 13.78$.

$\phi(\mathbf{r},t) = -\beta(z\sin\theta - x\cos\theta)t$. Defining a variable $S(\mathbf{r},t) = s(\mathbf{r},t)e^{-i\beta(z\sin\theta - x\cos\theta)t}$, then we get the evolution equations describing the oblique excitation regime, which are the same as Eqs. (II.21) and (II.22). Therefore the performance of the oblique excitation regime can be fully analyzed in the same way as for quantum storage based on control field angular scanning in Sec. II.4. The forward and backward retrieval can be realized in the same manner as in the above transverse excitation. Other possibilities, such as retrieving at the control field angle equal to $-\theta$ or $\pi - \theta$ ($\theta \neq 0$), require external spin wave vector rotation before retrieval. Decreasing the angle θ to below the critical one, $\beta L\sin(\theta)\Delta t/(2\pi) < 1$, reduces the longitudinal absorption window, making it too small to accommodate the full Fourier components of the signal.

It is worth noting that the proposed all-optical GEM-like scheme provides some additional possibilities for manipulating the pulses, which are not available in the case of usual GEM implementation. For example, a transverse phase modulation of the read-out control field such as $\exp(i\beta zt')$ leads to the temporal shift of the output pulse on t' without its temporal squeezing or stretching. In other words, it is known that a temporal advance or delay in GEM scheme can be achieved by increasing or decreasing the retrieval gradient at the expense of compressing or stretching the temporal shape of the retrieved signal, while we can shift the pulse in time without changing the frequency gradient meanwhile keep the original duration of the input photon's wave packet. More advantages are demonstrated in the discrete version of our scheme, which is discussed in Chap. V.

III.3 The experimental implementation issues

Quantum memory based on control field spatial chirp requires en ensemble of atoms stationarily distributed in space. The Raman configuration calls for a rather strong optical transition. Based on these two requirements, nitrogen-vacancy (NV) centers in diamond (NVD) is a promising material for the realization of the suggested scheme. NVD has much stronger electric dipole Raman transitions compared with the commonly used rare-earth ions in quantum storage experiments. Different Λ-level structures in NV ensemble have been employed in the experimental demonstrations of EIT [109, 133], and also in the recent theoretical proposal for the traditional Raman quantum memory [134].

It is worth noting that quantum memories of a single-photon wave packet were not demonstrated yet in NVD. The scheme based on control field angular scanning and control field spatial chirp have important advantages compared with other methods for realization of NVD quantum memory [90]. Indeed, EIT technique requires rather high EIT contrast, while GEM and AFC based on optical transition require long life time of the excited state. Both are hardly achievable in NVD. EIT contrast in NVD is only $\sim 6\%$ [133], and AFC absorption peaks within inhomogeneous profile are strongly affected by the spectral diffusion inherent to NVD. An AFC comb structure in a Λ system will be limited by the small inhomogeneous broadening of the spin transition (e.g., ~ 200 kHz in Ref. [133]), and three-level GEM is difficult because the external electric or magnetic field strongly affects the excited spin state, which in turn affects the required Λ level structure (explained in the following). Besides, g factors of the excited [135] and ground [136] states in NV

57

are nearly equal to each other, which makes it difficult to introduce controllable inhomogeneous broadening via gradient magnetic field. So Raman scheme combined with PMC and/or control field spatial chirp approaches for quantum memory application is naturally suitable for NVD, especially for the realization of GEM-like memory performance.

Another candidate for our proposed quantum memory is silicon-vacancy (SiV) in diamond. It has similar oscillator strength as NV center [137] but larger Debye-Waller factor at 738 nm [138]. However, its spin coherence lifetime is not yet sufficiently long.

III.3.1 Nitrogen-vacancy centers in diamond

Nitrogen-vacancy centers in diamond (NVD) [139] consists of a carbon-vacancy in the diamond lattice with one of the neighboring carbon atoms substituted by a nitrogen atom [90]. This vacancy can be thought of as a carbon atom with zero nuclear charge. The effective energy level scheme of electronic transitions of NVD can be found in, for example, Refs. [140, 141].

NVD has some unique features such as strong coupling of light with an individual vacancy (2-4 orders of magnitude stronger transition than in rare-earth-doped crystals), room-temperature optical initialization of the electronic spin, long-lived electron spin coherence ($\sim$ 1 ms at the room temperature [108]), etc. The spin coherence time up to 0.6 s was demonstrated using decoupling techniques at temperatures below 100 K [142].

Quite a number of remarkable results dealing with interaction of light with the individual NV center in diamond [107] was demonstrated, including realization of the single photon emitter [143], individual electronic-^{13}C nuclear spins coherent interac-
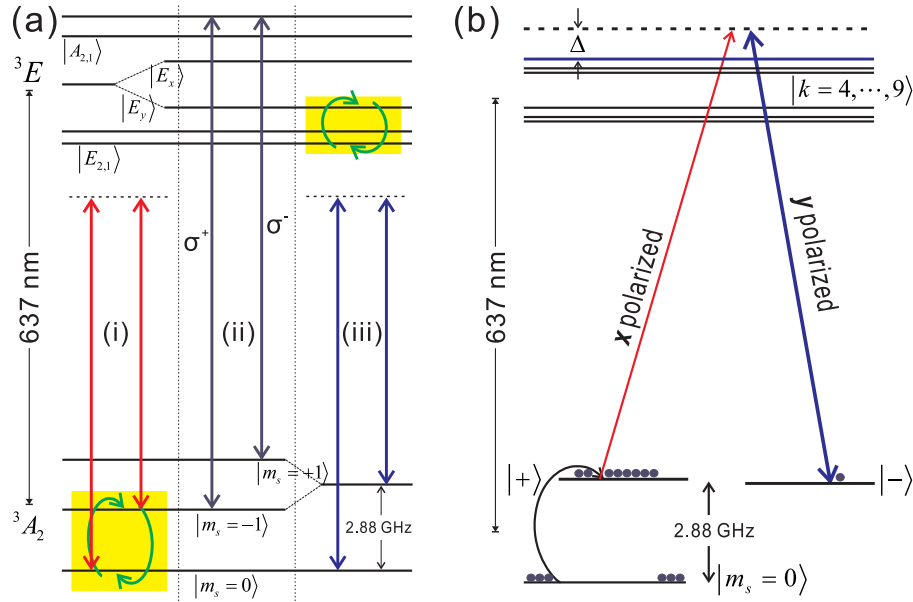
Figure 3.3: Energy level diagram of a nitrogen-vacancy center in diamond. (a) Three different Λ-level structures in NV. The yellow color with circulating arrow indicates a level mixing under external field or strain. (b) Λ-level structure suggested in Ref. [134].

tion [115, 144], electronic-electronic spins quantum register [145], spin-photon entangle-ment [146], etc., which proved that quantum information application can be realized in single NVD. Recently some important experimental works have been done in ensembles of NVD, including EIT [133], spin-superconducting resonator coupling [147], quantum correlation between phonon mediated Stokes/anti-Stokes pulses [148], etc. These results show the potential of bulk NVD for realization of quantum memory.

NVD is a spin $S = 1$ system with zero phonon line at 637 nm (containing $\sim 3\%$ of total fluorescence) between spin-triplet ground state $^3A_2$ and spin-triplet, orbit-doublet excited state ^3E [Fig. 3.3 (a)]. There is a 2.88 GHz zero-field splitting at ground state between $m_s = 0$ and $m_s = \pm 1$ due to spin-spin interaction [140]. The excited state ^3E undergoes spin-orbit and spin-spin interactions, and is highly affected by the diamond strain and external

59

electric and/or magnetic field [142, 149]. Raman-based quantum memory requires the realization of the Λ scheme. Since the ground states have a zero orbital angular momentum projection $m_L = 0$, each of them has a different spin projection m_s. So in order to have a Λ-level structure there has to be a spin-flip allowed transition. Spin flip is allowed by excited state spin-orbit interaction under very low strain and by strain-induced spin mixing under high strain. As a result different Λ-level structures can be realized in NVD between the spin triplet ground states manifold $^3A_2$ and excited ^3E under different transverse strain or electric field conditions.

A Λ system in the case of arbitrary strain was used in pioneering demonstration of EIT in NV-diamond [109] by using magnetic fields to tune to a ground state spin-level anti-crossing [level scheme (i) in Fig. 3.3 (a)]. The advantage of strain independence greatly releases the requirement of the sample preparation. However, since polarization selection rules are missing, a close spacing of the ground state spin levels could introduce additional noise due to allowed $|1\rangle$-$|2\rangle$ transition [Fig. 3.1 (a)] excited by the control field. In principle, a spin mixing of the excited state under magnetic field is also possible to achieve Λ-level structure. In such a case, the ground states spacing can be much larger.

A Λ system in the case of moderate transverse strain was used in the experiment of coherent population trapping [111] and in a recent demonstration of EIT in NV-diamond [133] [level scheme (iii) in Fig. 3.3 (a)]. In this scheme, the transverse strain lifts the orbital doublet of the excited state into E_x and E_y, each consists of three spin states m_s=0 and $m_s = \pm 1$. The upper branch E_x sublevels maintain uncrossed under strain thus result in optical spin-

conserving transitions, while the lower branch E_y experiences a spin mixing as a function of nonaxial strain [140] and results in optical spin-flip transitions. The Λ system based on such excited state E_y spin mixing can also be induced by external transverse electric field [149], which gives great flexibility for the realization of the level scheme. All orientations of the color centers can be involved by choosing the strain's direction [111].

A Λ-level structure also exists in the case of very low strain. In this situation, the axial spin-orbit interaction lifts the excited state into three twofold degenerate levels $E_{1,2}$, $E_{x,y}$ and $A_{1,2}$. The states $A_{1,2}$, which can be lifted by spin-spin interaction, has opposite orbital and spin quantum numbers. Consequently, optical transition is allowed between ground states $m_s = \pm 1$ and excited state A_1 or A_2 with polarization selection rules $\sigma^{\pm}$ [141] [level scheme (ii) in Fig. 3.3 (a)]. This Λ system has been used for spin-photon entanglement [146]. However, because it requires very low strain, sample preparation will be very difficult especially when high NV$^-$ density is needed for Raman-based quantum memory in free space. Quite recently, very similar Λ system with polarization selection rules under external electric field and low magnetic field due to mixing of the ground states $m_s = \pm 1$ was theoretically suggested for Raman scheme quantum storage [134] [Fig. 3.3 (b)]. The initialization of the population is achieved by a narrow microwave π pulse.

In addition to the above Λ systems, a principally different type of Raman transitions in room temperature diamond caused by excitation of optical phonons (in 40 THz range of phonon energy living for about 7 ps) was demonstrated in [148]. Potentially, any of the described Raman transitions can be used for the realization of PMC and/or control field

spatial chirp quantum memories.

III.3.2   Silicon-vacancy centers in diamond

Negatively charged silicon-vacancy (SiV) in diamond (Fig. 3.4 inset) caused a lot of attention in the field of quantum information due to some of its remarkable features. It has similar oscillator strength as NV center [137], but more than 70% of single SiV center fluorescence falls in zero phonon line at 738 nm [138], comparing with a small fraction of 3% in NV center [150]. This makes SiV a very promising candidate for room temperature bright single-photon source. Each of the ground ^2E_g and excited ^2E_u state has a twofold orbital and a twofold spin degeneracy [Fig. 3.4 (a)]. The orbital degeneracy is lifted by spin-orbit coupling and Jahn-Teller effect into double fine structure with $\Delta^2E_g = 50$ GHz and $\Delta^2E_u = 260$ GHz [137, 151]. This gives rise to 4 lines in the fluorescence spectrum with polarization selection rules [152], and in total makes Λ systems for Raman-based quantum memory schemes. Optical access to electronic spin shows a spin purity approaching unity in the excited state [153]. Small inhomogeneous broadening can be achieved to bring the linewidth of individual fine structure component of SiV ensemble to 9 GHz [154], and down to 1 GHz in recent experiment where much better crystal is produced [155, 156]. There is no spectral diffusion (only ± 4 MHz during 7 hours) which has been always a problem for NVD. There are also polarization selective EIT transitions that do not depend on getting the perfect crystal strain. However, its spin coherence lifetime, currently reported ~ 35 ns [155] at 4.5 K for Zeeman levels, has yet to be increased for longer storage time. The orbital spin population lifetime and coherence lifetime is of the
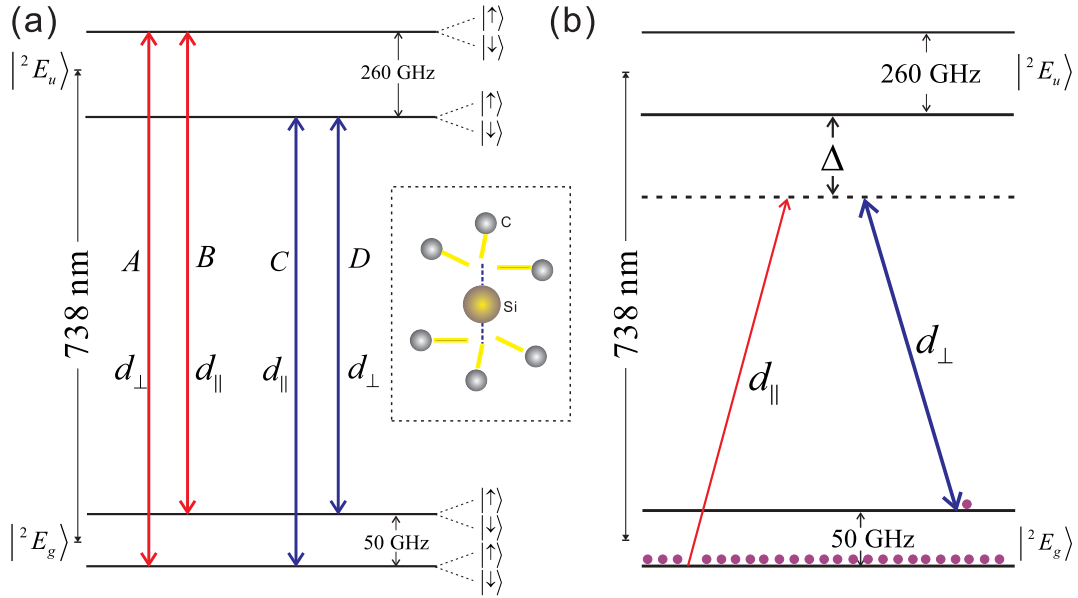
Figure 3.4: Energy level diagram of a silicon-vacancy center in diamond. (a) Different Λ-level structures in SiV with polarization selection rules. (b) Raman-based quantum memory energy scheme. The inset is the illustration of the molecular configuration of SiV in diamond.

same order, that is ~ 38 ns. There is no inhomogeneous broadening of the spin transition. Since the spin coherence time is limited by single-phonon processes at 47 GHz, cooling down the temperature or reducing the size of the sample into nanodiamond smaller than phonon wavelength ~ 250 nm will cease the phonon coupling decay and increase the spin coherence lifetime substantially. On the other hand, even with ~ 38 ns lifetime one can still do a proof-of-principle experiment demonstrating the storage of the signal field of duration ~ 10 ns via PMC and spatial chirp schemes. Such experiment requires almost no additional effort compared with that in NVD, and will be fully beneficial from the clean Λ system with polarization selection rules of SiV.

Since at 4 K 71% of the total zero-phonon-line fluorescence is contained in the tran-

sition of lower to lower orbital branch [which is denoted as transition C in Fig. 3.4 (a)], we can use transitions C and D as the Λ level structure [Fig. 3.4 (b)]. The effective dipole moment is about 5 times larger than that for NV. In Fig. 3.4 (a), transition C is $\hat{z}$-polarization allowed and transition D is $\hat{x}\hat{y}$-polarization allowed, where $\hat{z}$ is the SiV quantization axis along $\langle 111 \rangle$. In the recent experiment of coherent population transfer in SiV [155], the density of the color centers is estimated as $N \sim 2 \times 10^{17}$ cm^{-3}. The homogeneous broadening is on the order of 100 MHz, and the inhomogeneous broadening is on the order of 1 GHz. With such parameters there is no need to do hole burning to the sample. The spin coherence lifetime is limited by, and almost the same as, the orbital spin T_1, which is 38 ns. So we assume the signal field duration $\Delta t = 5$ ns, which requires $|g|^2 N \sim 1.2 \times 10^{11} s^{-1} m^{-1}$. The polarization selection rule and fairly large ground state splitting (50 GHz) and even much larger excited states splitting (250 GHz) essentially eliminate the possible spontaneous scattering noise within the spin coherence lifetime.

III.3.3   Adding spatial chirp to a control beam

Optical fields with a spatial chirp across the beam have been widely used in Fourier synthesis pulse shaping [157], multiphoton microscopy [158, 159], micromachining [160], etc. They commonly exist in the inhomogeneous dispersive medium, and can be produced by means of prism or grating diffraction [161], pulse spatial modulation [162], etc. Depending on the spectrum width of the chirp and control beam duration, the proposed scheme operates at different regimes.

Let us first consider the specific implementation of the spatial chirp via a spatial

dispersion of the Gaussian control beam [163]. Taking the transverse excitation regime as an example, and assuming the higher order chirp is absent [164], then the control beam with Gaussian spectrum and Gaussian transverse profile can be written in the frequency domain as

$$E_c(z,\omega) = \mathscr{E}_0 e^{-\left(\frac{\omega-\omega_{c0}}{\Delta\omega_c}\right)^2} e^{-\left(\frac{z-\zeta(\omega-\omega_{c0})}{\Delta w}\right)^2}, \tag{III.9}$$

in which $2\sqrt{\ln 2}\Delta\omega_c$ is the FWHM spectrum bandwidth, $2\sqrt{\ln 2}\Delta w$ is the FWHM spatial width of each spectrum component, ζ is the spatial dispersion, and the propagation (along $\hat{x}$) effect is neglected. The inverse Fourier transform of (III.9) gives the control beam in time domain:

$$E_c(z,t) = \frac{\Delta\omega_c\mathscr{E}_0}{\sqrt{2}\kappa} e^{-\frac{\Delta\omega_c^2 t^2}{4\kappa^2}} e^{-\frac{z^2}{\kappa^2\Delta w^2}} e^{-i\frac{\Delta\omega_c^2\zeta}{\kappa^2\Delta w^2}zt} e^{-i\omega_{c0}t}, \tag{III.10}$$

where the control beam is both transversely expanded and temporally stretched by a factor $\kappa = \sqrt{\Delta w^2 + \zeta^2\Delta\omega_c^2}/\Delta w$ comparing with a beam without spatial dispersion ($\zeta = 0$), and the frequency gradient is $\beta = \Delta\omega_c^2\zeta/(\kappa^2\Delta w^2)$. The term $e^{-i\beta zt}$ indicates that the control beam phase front rotates while the field is propagating.

For the quantum memory application, at least three conditions should be fulfilled: (i) spatial coverage: $2\sqrt{\ln 2}\kappa\Delta w > L$; (ii) temporal coverage: $4\sqrt{\ln 2}\kappa/\Delta\omega_c > \Delta t$; and (iii) spectral coverage: $\beta L = \Delta\omega_c^2\zeta L/(\kappa^2\Delta w^2) > 2\pi/\Delta t$, where L is the medium length, Δt is the signal field duration. Besides, as discussed in Sec. III.2, the z-dependence of the control field amplitude introduces a spatial variation of the induced frequency detuning. In our case, since the control beam has a Gaussian spatial profile, the corresponding Raman frequency shift (after incorporating a constant value into the definition of ω_c) is

$(|\Omega_0|^2/\Delta)\{1 - \exp[-2z^2/(\kappa^2 \Delta w^2)]\}$, where $\Omega_0 = \Omega(z = 0)$. The control intensity's spatial variation should be sufficiently smooth so that this Raman frequency shift would be negligible compared with the spatial chirp $|\beta z|$. Indeed, since $\kappa \Delta w \gg L \geqslant z$, taking into account condition (III.7) we get the ratio of the Raman shift and $|\beta z|$ approximately equal to $\frac{|\Omega_0|^2}{\beta \Delta} \frac{2|z|}{\kappa^2 \Delta w^2} \ll \frac{2|z|}{\kappa \Delta w} \frac{|\Omega_0^2|}{\Delta} \Big/ \frac{2\pi}{\Delta t} \ll 1$.

As one of the simplest schemes to generate control beam of the form Eq. (III.10) fulfilling the conditions (i) - (iii), let us consider a grating-lens pair with the grating and the medium placed at the back and front focal planes of the lens [165] [Fig. 3.5 (a)]. The switching of the spatial dispersion can be achieved by adding two additional lenses in a 6-F configuration. We take $\lambda_{c0} = 700$ nm and the focal length $f = 8$ m and assume the angular dispersion of the grating is $d\theta/d\lambda = 2.5 \times 10^{-3}$ nm^{-1}, the spatial dispersion $\zeta = -\frac{\lambda_{c0}^2}{2\pi c} f \frac{d\theta}{d\lambda}\big|_{\lambda_{c0}} = -5.2 \times 10^{-15}$ sm. For a 29 ps seed Gaussian pulse and $\Delta w = 10~\mu$m focal spot size of each individual frequency component, we get the frequency gradient $\beta = -1.9 \times 10^{14}$ m^{-1}rad/s, and the stretching factor $\kappa = 100$ which expands the transverse size of the control beam to 1 mm and stretches the duration to 2.9 ns. This corresponds to a sub-nanosecond-pulse quantum storage with signal field duration in between of 29 ps and 2.9 ns. The medium length $L < 1$ mm makes sure that the scheme operates at the long pulse regime. The difficulty of sub-nanosecond-pulse quantum storage is that a high optical depth is required. In the present example, the medium has to demonstrate $|g|^2 N > |\beta/2\pi| = 3 \times 10^{13}$ s^{-1}m^{-1}. Such coupling constant and atomic number density are not yet feasible in typical NV, but in principle are achievable in SiV.
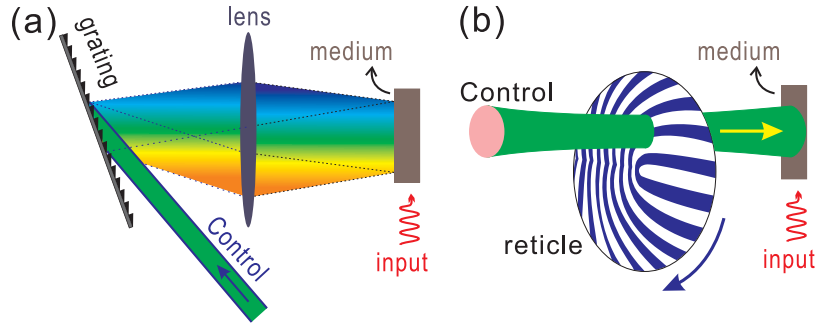
Figure 3.5: Adding spatial chirp to a control laser beam by using (a) grating-lens pair, and (b) a spinning reticle.

In the regime of sub-microsecond-pulse quantum storage, the spatial chirped beam has to be prepared by other means, for example, through frequency modulated reticles [166] [Fig. 3.5 (b)]. In this technique the bandwidth of the control beam will be determined by the pattern, size and the spinning speed of the reticle. For intensity modulation, one of the two side bands should be blocked for the current application. Assuming the pattern has a reciprocal wave vector $\Delta k = 1000 \, \mathrm{mm}^{-1}$, input beam size (or the radius of the reticle, whichever is smaller) 1 cm, and spinning speed 500 Hz [162], we have $\beta = 3.14 \times 10^9 \, \mathrm{m}^{-1}\mathrm{rad/s}$.

In principle, the gap between the above two regimes can be filled by generating chirped beam with $\sim$gigahertz spectrum width through, e.g., acousto-optic modulator (AOM). In such a case, a number of sub-beams are split from the original one, each with different central frequency due to AOM modulation, and aligned side-by-side to form a spatial-chirp control beam. A significant difference is that, if the number of the sub-beams is small, the frequency gradient becomes discrete, thereby forming an optical frequency comb. Contrary to AFC, such an optical comb is not limited by the inhomogeneous broadening of the atomic levels, and can be created and modified afterward without background

67

absorption. These features make the proposed scheme promising from the viewpoint of experimental realization, and will be discussed in Chap. V.

III.3.4 Specific example

Suppose we produce spatial chirp parameter $\beta = 3.14 \times 10^9$ m^{-1}rad/s using spinning reticles mentioned above. According to condition (III.7), a medium with $|g|^2N = 3 \times 10^9$ s^{-1}m^{-1} can store and retrieve ~ 200 ns signal pulse with high efficiency and fidelity. This can be fulfilled if NV diamond is used as storage medium. The inhomogeneous broadening of the optical transition in the whole ensemble of NV centers can be on the order of 10 GHz [111] at the NV density 8×10^{15} cm^{-3} [134]. The dipole moment corresponding to zero phonon line can be estimated as $\sim 2.3 \times 10^{-30}$ Cm based on oscillator strength ~ 0.1 and Debye-Waller factor 0.035. As an example, we take the Λ-level configuration recently suggested in [134] for realization of the traditional protocol of Raman quantum memory based on modulation of control field amplitude. The energy diagram is shown in Fig. 3.3 (b). Following Ref. [134], let us consider a sub-ensemble of NV with an effective inhomogeneous broadening 0.2 GHz with density $N = 2 \times 10^{13}$ cm^{-3}. Such sub-ensemble is to be produced by the hole burning and repumping technique. The spectral hole is characterized by sharp edges and small background absorption. Particularly, in considered scheme [134] a spectral hole of the width 2.87 GHz can be created by making $|+\rangle$ and $|-\rangle$ states empty (all NV centers are transferred into the $|0\rangle$ state). Then the $|+\rangle$ state is re-populated, which produces an inhomogeneously broadened optical transition with a narrow linewidth (limited from below by the homogeneous width of the optical transition)

inside the spectral hole. This can be done, for example, by optical pumping via two $\hat{y}$-polarized narrow-band lasers on-resonantly driving $|0\rangle$-$|k = 4\rangle$ and $|k = 4\rangle$-$|+\rangle$. Since the dipole moment of $|k = 4\rangle$-$|-\rangle$ transition is 1000 times weaker, such noise is negligible. The effective reduction of the inhomogeneous linewidth leads to proportional reduction of the effective density to the required value (so that the spectral density remains about the same). The produced narrow absorption line does not need to be Gaussian and may have the sharp edges, which allows us to use rather small one-photon detuning, 0.5 GHz. In its turn, as it is shown below, using such small detuning helps to suppress noise originating in the considered Λ-level scheme [134] from the off-resonant scattering of the control field via closely lying (separated by 1.5 GHz) excited state (due to the specific selection rules). The required $|g|^2 N$ is fulfilled with control field intensity ~ 140 W/cm^2. The intensity up to 280 W/cm^2 was used for demonstrating EIT in NV ensemble [109], and much higher intensities are used in single NV experiments. It should be noted that the noise can also be reduced by frequency filtering. In doing so, larger values of Δ are possible.

The rate of spontaneous Raman scattering of the control field into a specific spatial mode (corresponding to the signal field) can be estimated as $|g'|^2 NL$ [167], which is equivalent to $|g|^2 NL (\Delta/\Delta')^2 |d'_{21}/d_{21}|^2 |d'_{32}/d_{32}|^2$, where Δ, d_{21}, d_{32} are the control field one-photon detuning and dipole moments in the working Λ scheme, and g', Δ', d'_{21}, d'_{32} are the corresponding quantities in the noise channel. The total number of scattered photons during storage and retrieval processes each of duration T is consequently equal to $2|g|^2 NLT (\Delta/\Delta')^2 |d'_{21}/d_{21}|^2 |d'_{32}/d_{32}|^2$, which should be made smaller than 1 to neglect

spontaneous Raman scattering noise. In the considered case of the NV diamond Raman configuration [134], substituting the values of the corresponding parameters ($|g|^2 NL = 3 \times 10^7$ s^{-1}, $\Delta'/2\pi = \Delta/2\pi + 1.5$ GHz, taking for simplicity $d'_{32} = d_{32}$ and $d'_{21} = 0.75d_{21}$), we find the last condition fulfilled by $\Delta/2\pi < 0.6$ GHz, proving that signal-to-noise ratio remains greater than 1 for storage and retrieval of a single photon in a total time window > 700 ns.

III.4 Conclusion

In the photon echo based quantum memory schemes, the essential part is to produce a rephase of the dipole moments. The classical photon echo, for example, the two-pulse photon echo, uses the strong π pulses to produce the rephase, thus introducing a noise due to spontaneous emission and amplification originated from a population inversion, which makes it not suitable for the quantum field storage [168], unless techniques such as silent echo [169] is used. Instead, the controlled reversible inhomogeneous broadening (CRIB), and in particular the GEM schemes, create the rephase by manipulating an effective inhomogeneous broadening and introduces no population inversion. In order to achieve this, dc Stark or Zeeman effect should be used. In order to avoid complications due to required manipulations with the medium for the creation of the inhomogeneous spectral broadening structures, for example, by applying the external electric or magnetic fields with the spatial gradient, and for the material systems which do not demonstrate the dc-Stark or Zeeman effects, the alternative ways of creating effective controllable inhomogeneous broadening

should be adopted.

In the present scheme, we create an effective controllable inhomogeneous broadening of the Raman transition by a spatially inhomogeneous control field pattern with a frequency gradient across the control beam, that is the so-called spatial chirp. Since the control field wave pattern mimics the longitudinal inhomogeneous broadening, the atomic medium acts like a recorder which stores the spectrum components of the input signal as in GEM scheme. Meanwhile in terms of the phase matching control, a time dependent transverse wave vector βt created by the control field wave front rotation continuously records the signal field by the corresponding phase-matched spin wave components. Eventually the temporal shape of the signal field maps into the spatial distribution of the spin wave. In forward retrieval, reversing the frequency gradient of the control field has similar effect as reversing the dc-field gradient in the GEM scheme or reversing the phase matching sweeping in the PMC scheme.

By combining the basic ideas of the GEM scheme and the off-resonant Raman interaction based scheme in the proposed spatial-chirp scheme, we naturally come to the new memory scheme which contains the advantages of both, while, unlike the three-level GEM scheme, any direct manipulation of the resonant medium is avoided. As far as a practical implementation is concerned, any material demonstrating strong Raman transitions and long Raman coherence time can be employed. In particular, nitrogen-vacancy centers and silicon-vacancy centers in diamond seem to be very promising systems.

In summary, in this chapter we propose an all-optical quantum memory scheme

based on the off-resonant Raman interaction of the signal quantum field with a homogeneous atomic medium illuminated by a constant-in-time control field with a spatial chirp of frequency across its beam. Its mathematical model is similar to the GEM scheme. However, physically the proposed scheme is completely different and has very important experimental and implementation advantages compared to the controllable-reversible-inhomogeneous-broadening based and other schemes. These advantages originate from its all-optical nature. Unlike the Raman or phase-matching-control schemes, the proposed spatial-chirp one does not require, in principle, any synchronization or temporal manipulation of the control field and the atomic medium. Unlike the GEM scheme, it does not require the atomic medium possessing the Stark or Zeeman effect and the use of the external electric or magnetic fields.

CHAPTER IV

EXACT SOLUTION OF GRADIENT ECHO MEMORY[*]

IV.1   Introduction

In Chaps. II and III we proposed quantum storage schemes via phase matching control and control field spatial chirp. We proved that in free space they demonstrate the same performance as gradient echo memory. So essentially, from mathematical point of view, the analysis of all these schemes are reduced to the solution of the GEM evolution equations.

In GEM, an external dc electric or magnetic field with gradient along the longitudinal direction is applied to a medium with narrow transition linewidth (see Fig. 4.1). Due to Stark or Zeeman effect, the atomic transition frequency is shifted, acquiring a spatial dependence along photon propagation direction. This is equivalent to an artificial inhomogeneous broadening. As a result, different frequency components of the input photon are resonantly absorbed at different longitudinal locations of the medium, and the excited polarizations quickly get out of phase, suppressing reemission processes of the field. The on-demand retrieval is achieved by reversing the gradient of the external electric or magnetic field, which corresponds to an inverse of the inhomogeneous broadening. This will enforce a rewinding of the phase of the polarizations back to its original status, upon which

---

73

a photon echo emerges from the medium. GEM scheme can be implemented in both two-level and three-level [51] systems, and has been realized in many materials, including rare-earth-doped crystals [48--50], warm [51--55] and cold [56] atoms.

The evolution equation of GEM can be reduced from Maxwell-Bloch equation to Eqs. (I.1) and (I.2). Although the mechanism of GEM scheme is conceptually simple, its field-atom dynamics described by Eqs. (I.1) and (I.2) is highly nontrivial. The longitudinal distribution of the inhomogeneous broadening, i.e., the z-dependence of the resonant condition, is essential for GEM. For a uniformly distributed inhomogeneous broadening, after reversing the resonant condition, the forward retrieval efficiency is limited to 54% by reabsorption process [170]. But in GEM, since the resonant condition is assigned along the path of photon propagation, the reabsorption of the field during forward retrieval does not strongly confine the efficiency of the echo, allowing nearly 100% of the input energy to be recalled with high fidelity. In this process a phase matching plays a crucial role, as will be shown in this chapter. However, such inhomogeneity along propagation leads to a complicated field and atomic evolution. Theoretically, some analytical treatments of GEM have been done, including generalized investigation of time-reversible atom-light interaction [171], analytical calculation for narrow-band input signal [103, 104], analysis of GEM equation in spatial-Fourier space [44], and general GEM solution in terms of a response to the excited coherence [172].

In this chapter, we start from the derivation of the exact solution of GEM evolution equations (I.1) and (I.2) during storage and retrieval for an arbitrary linear gradient without

approximations [173]. The solution will be written in its final form, i.e., in terms of a response to the input signal. This solution describes not only GEM, but also quantum memory schemes based on phase matching control (PMC) [85, 87--90] and control field spatial chirp [91]. Moreover, the gradient absorption of a single photon is closely related to the single-photon superradiance [92--97]. So the solution and mathematical treatment presented here can also provide insights, for example, into the problem of the preparation and control of the timed Dicke state [98, 99].

IV.2 The exact solution of gradient echo: Storage

In a GEM experiment, a single-photon (or weak signal field) wave packet with slowly varying amplitude $a_{\text{in}}(t)$ and full-width-half-maximum (FWHM) field duration Δt propagating along the longitudinal direction $\hat{z}$ enters a resonant two-level (three-level) medium of length L. All the atoms in the medium initially stay in the ground state and mainly remain unexcited during the whole storage and retrieval processes. An external gradient electric or magnetic field is applied to the medium to create a photon detuning varying linearly as a function of position: $\Delta = \beta z$, where β is the frequency gradient along the photon propagation direction [see Fig. 4.1 (a)]. During retrieval, the gradient switches to a different value $\beta \to \beta'$, as shown in Fig. 4.1 (b). Very often $\beta' = -\beta$ is chosen to symmetrically reverse the photon detuning. Denoting the slowly varying amplitude of the single-photon annihilation operator as $a(z,t)$ and slowly varying amplitude of the collective atomic coherence operator as $S(z,t)$, the evolution equation for the field and atom within $z \in [-L/2, L/2]$ in
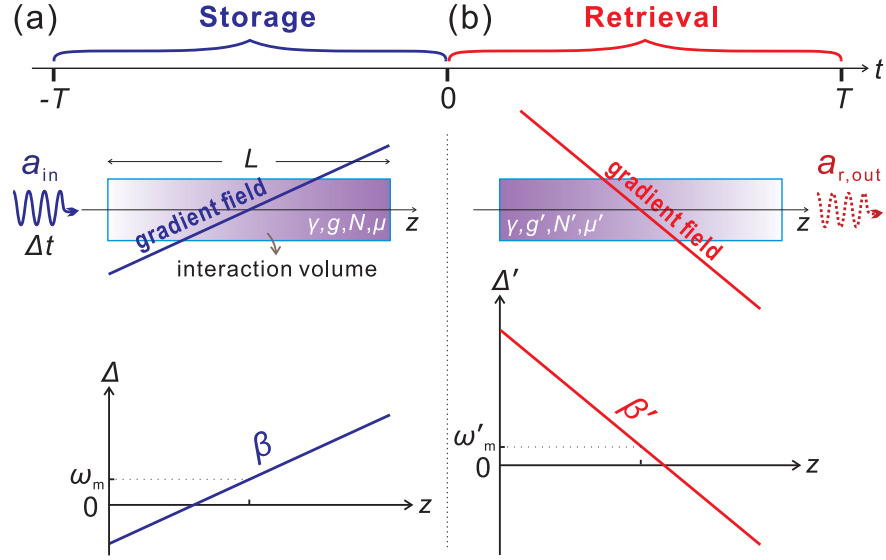
Figure 4.1: Illustration of gradient echo memory. (a) Storage process ($t \in [-T, 0]$). (b) Retrieval process ($t \in [0, T]$).

the long-pulse regime ($c\Delta t \gg L$, c is the speed of light in vacuum) is given by Eqs. (I.1) and (I.2).

In this section, the storage and retrieval processes are in time intervals $t \in [-T, 0]$ and $t \in [0, T]$ respectively (Fig. 4.1), where T is the duration of the storage or retrieval time window. The relevant parameters are defined as follows: γ is the single-atom decoherence rate of the optical transition in the two-level system, L is the medium length, β is the frequency gradient, g is the field-atom coupling constant, N is the atomic density, $2|g|^2 NL/\gamma$ is the optical thickness of the two-level medium, $\mu = |g|^2 N/\beta$, ω_m is an additional frequency shift on top of the frequency gradient. The parameters β', g', μ' and ω' carrying "$'$" indicate that they are quantities specifically for retrieval. The subscript "s" ("r") of a function denotes the storage (retrieval) process.

A general mathematical description of the problem we are solving in this chapter is

to find the exact analytical solution of the following differential equations:

$$\frac{\partial}{\partial z}a(z,t) = g^* N s(z,t)e^{i\phi(z,t)}, \tag{IV.1}$$

$$\frac{\partial}{\partial t}s(z,t) = -\gamma s(z,t) - ga(z,t)e^{-i\phi(z,t)}, \tag{IV.2}$$

where

$$\phi(z,t) = \int^t d\tau \Delta(z,\tau) + \phi_0(z), \tag{IV.3}$$

$$s(z,t) = S(z,t)e^{-i\phi(z,t)}, \tag{IV.4}$$

subjecting to different initial and boundary conditions and the following change of the

system's parameters for storage and retrieval, respectively.

$$\{\beta(t),g(t),N(t),\mu(t),\omega_m(t)\} = \begin{cases} \{\beta,g,N,\mu,\omega_m\}, & \text{if } t \leqslant 0 \\ \{\beta',g',N',\mu',\omega_m'\}, & \text{if } t > 0 \end{cases} \tag{IV.5}$$

Here $z \in [-L/2, L/2]$, and ϕ or Δ can be various functions of z and t. For example, a

stepwise-in-space ϕ (along with corresponding discrete interaction volume) reduces the

system to gradient frequency comb scheme, which will be discussed in Chaps. V and VI.

In this chapter we will restrict ourselves to a linear phase in space and time:

$$\phi(z,t) = \beta zt + \omega_m t, \tag{IV.6}$$

i.e., $\Delta = \beta z + \omega_m$. Here ω_m is a frequency shift in addition to the space dependent detuning

βz, which will shift the echo central frequency as discussed in Ref. [174] and experimen-

tally demonstrated in Refs. [53, 175].

In order to solve Eqs. (IV.1) and (IV.2), let us first change the spatial domain into

$z \in [0,L]$:

$$\frac{\partial}{\partial z}a(z,t) = g^*Ns(z,t)e^{i\beta zt}e^{-i(\beta L/2-\omega_m)t}, \tag{IV.7}$$

$$\frac{\partial}{\partial t}s(z,t) = -\gamma s(z,t) - ga(z,t)e^{-i\beta zt}e^{i(\beta L/2-\omega_m)t}, \tag{IV.8}$$

and then apply Laplace transformation method[1] over z. The solution of Eqs. (IV.7) and

(IV.8) in Laplace domain is given by Eqs. (B.15) and (B.16) in Appendix B.

The storage time window is $t \in [-T,0]$. Before storage, there is no collective atomic

coherence in the medium, so the initial condition is $s_s(z,-T) = 0$. The boundary condition

is given by the incoming signal field: $a_s(z = 0,t) = a_{\text{in}}(t)$. With the initial and boundary

conditions, the exact solution of Eqs. (IV.7) and (IV.8) during the storage process is ob-

tained in Appendix B by the inverse Laplace transformation of Eqs. (B.15) and (B.16) as

follows:

$$a_s(z,t \leqslant 0) = a_{\text{in}}(t) - \mu\beta z\int_{-T}^{t}d\tau a_{\text{in}}(\tau)e^{-i\left(\beta\frac{L}{2}-\omega_m\right)(t-\tau)}e^{-\gamma(t-\tau)} \times$$

$$_1F_1\left(i\mu+1;2;i\beta z(t-\tau)\right), \tag{IV.9}$$

$$s_s(z,t \leqslant 0) = -ge^{-i\beta zt}\int_{-T}^{t}d\tau a_{\text{in}}(\tau)e^{i\left(\beta\frac{L}{2}-\omega_m\right)\tau}e^{-\gamma(t-\tau)}\,_1F_1\left(i\mu+1;1;i\beta z(t-\tau)\right),$$

$$\tag{IV.10}$$

where $z \in [0,L]$.

In Eqs. (IV.9) and (IV.10), $_1F_1$ is the Kummer confluent hypergeometric function.

The second term of Eq. (IV.9) on the right hand side tells how a weak input field gets

absorbed by a medium with longitudinally distributed, linear, gradient transition frequency.

---

[1]Equations (I.1) and (I.2) are easily solved in frequency domain using Fourier transformation method over t. However, this method proves to be easy only for the storage process, and becomes difficult for the retrieval process. By Laplace transformation method over z, we obtain a general solution for both storage and retrieval processes.

In Fourier domain, such absorption of the input spectrum is equal to

$$a_{\text{in}}(\omega)\left[\left(\frac{\omega+\omega_m-\beta L/2+i\gamma}{\omega+\omega_m+\beta(z-L/2)+i\gamma}\right)^{i\mu}-1\right],\qquad\text{(IV.11)}$$

which can also be obtained by solving Eqs. (I.1) and (I.2) using Fourier transformation on t.

In Fig. 4.2 we plot the gradient absorption process of an input photon (with Gaussian waveform) of duration Δt in a medium of length L when $\omega_m = 0$. It shows that the analytical solution (IV.9) - (IV.10) and numerical simulation agree with each other. From Fig. 4.2 (a-d, g-h), for fixed $|g|^2 N$ the gradient absorption experiences more amplitude and phase modulation in the case of small storage bandwidth βL due to the cutoff of the absorbed frequency components [Fig. 4.2 (a, b)], and for fixed μ a large storage bandwidth βL compresses the collective coherence distribution into a narrow region corresponding to the spectrum of the input field [Fig. 4.2 (h)]. So β determines the spatial width of the polarization distribution in the medium. Since $2|g|^2 NL/\gamma$ is the optical thickness of a two-level system, for enough storage bandwidth a larger $|g|^2 N$ indicates a faster absorption of the input field, as shown in Fig. 4.2 (c, e). Comparing Fig. 4.2 (d, f, h), we see that for sufficient absorption bandwidth and optical density, μ determines the central position of the polarization distribution in the medium. Indeed, if we divide the medium into a number of spectrally resolved units according to $\beta L/(2\gamma)$, μ is proportional to the optical thickness of each of such units. In an optically dense medium, the absorption width is broadened by optical thickness compared with the single-atom absorption linewidth, so the input field gets absorbed near the entrance (rather than in the center) of the medium even though the
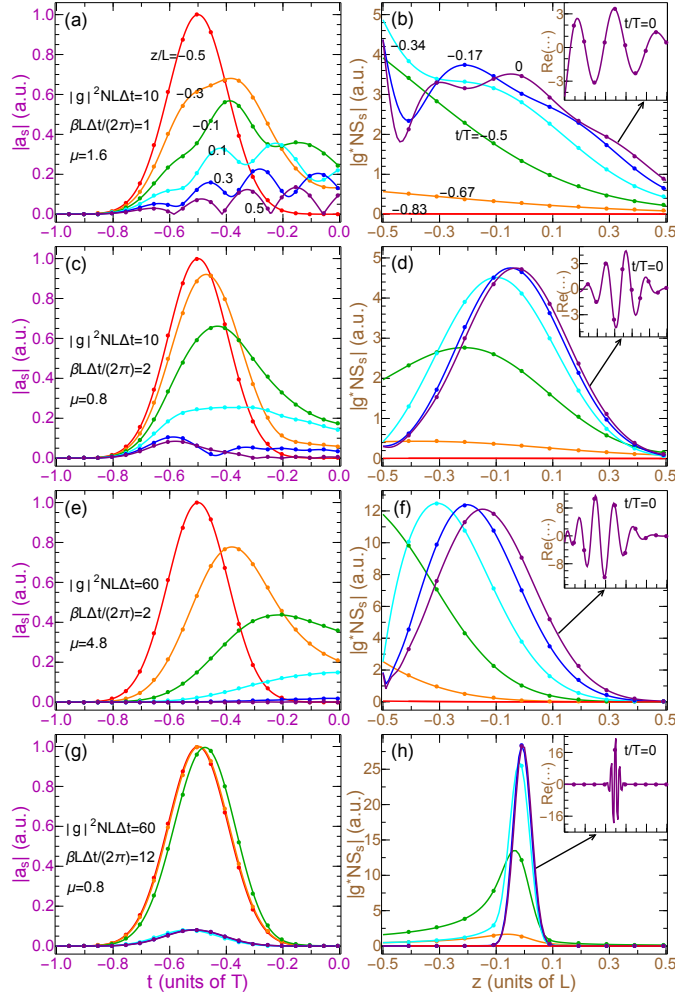
Figure 4.2: Analytical solution (dotted) based on Eqs. (IV.9)-(IV.10) and numerical simulation (solid) of Eqs. (I.1)-(I.2) for GEM storage process. The input single photon has a Gaussian waveform (red curves in the left panels) of duration $\Delta t/T = 0.25$ peaked at $t_{\text{in}}/T = -0.5$. Spatial variable z is converted to the interval $[-L/2, L/2]$. (a, c, e, g) Absolute value of the field $|a_s(z,t)|$ as a function of time at different locations of the medium. The colors of red, orange, dark green, cyan, blue and purple represent $z/L = -0.5, -0.3, -0.1, 0.1, 0.3, 0.5$ respectively. (b, d, f, h) Absolute value of the collective coherence $|g^*Ns_s(z,t)e^{i\beta zt}|$ as a function of space at different times. The colors of red, orange, dark green, cyan, blue and purple represent $t/T = -5/6, -2/3, -1/2, -1/3, -1/6, 0$ respectively. The insets show the corresponding real values at the end of the storage, i.e., t/T = 0. The figures are obtained under $\gamma = 0$ and $\omega_m = 0$. The value of μ is 1.6 in (a, b), 0.8 in (c, d), (g, h), and 4.8 in (e, f).

80

resonant absorption frequency in this region does not exactly match the input spectrum [Fig. 4.2 (f)]. But when μ gets smaller, this central position of the polarization distribution is pushed back to the center of the medium because the optical density of each spectrally resolved unit is "diluted" by large storage bandwidth [Fig. 4.2 (h)].

IV.3   The exact solution of gradient echo: Retrieval

The retrieval time window is $t \in [0, T]$. Let us assume that right after storage, at $t = 0$, the parameters of the system are switched in the following way: the frequency gradient $\beta \to \beta'$, coupling constant $g \to g'$, atomic density $N \to N'$, $\mu \to \mu' = |g'|^2 N'/\beta'$, and the additional frequency shift $\omega_m \to \omega'_m$. The initial condition is given by the collective coherence distribution determined by the result of the storage process. In usual GEM, this is $s_r(z, 0) = s_s(z, 0)$ where the subscript "r" denotes the retrieval process. Since there is no input field during retrieval, the boundary condition is $a_r(z = 0, t) = 0$.

In Appendix B we derive the general retrieval solution (B.35) and (B.36) for arbitrary parameters. In a typical GEM experiment, only the frequency gradient is switched to the opposite during retrieval, meaning that $g' = g$, $N' = N$, $\beta' = -\beta$, $\mu' = -\mu$. In such a case, the solution reduces to:

$$a_{\mathrm{r,out}}(t \geqslant 0) = \int_{-T}^{0} d\tau\, a_{\mathrm{in}}(\tau) K(t, \tau), \tag{IV.12}$$

$$K(t, \tau) = -\mu \beta L e^{i\beta \frac{L}{2}(t+\tau)} e^{i(\omega'_m t - \omega_m \tau)} e^{-\gamma(t-\tau)} \Phi_2\left(i\mu + 1, -2i\mu; 2; -i\beta L(t+\tau), -i\beta L t\right),$$

$$\tag{IV.13}$$

where $t \in [0, T]$. Here the essential part of the integral kernel K is Φ_2, which is the Humbert
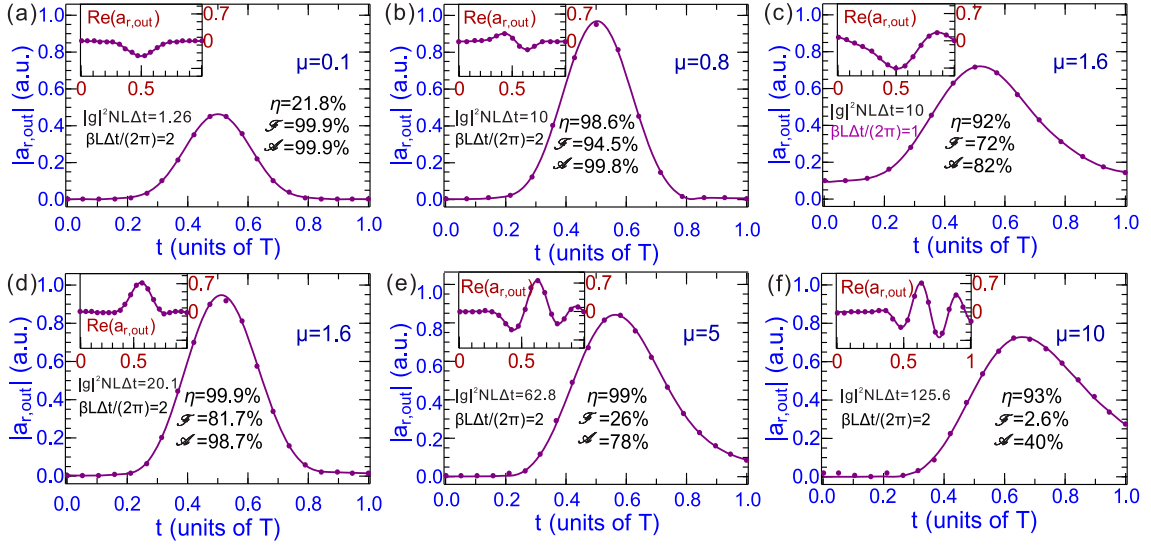
Figure 4.3: Analytical solution (dotted) based on Eq. (IV.12) and numerical simulation (solid) for the output gradient echo $a_{\mathrm{r,out}}(t)$ for different parameters shown in the figure. The incoming photon has a Gaussian temporal shape peaked at $t_{\mathrm{in}}/T = -0.5$ with $\Delta t/T = 0.25$.

double hypergeometric series. Some of this special function's properties are discussed in Appendix B. Some examples of the output field are plotted in Fig. 4.3.

As shown in Fig. 4.4 (a1), the absolute values of the integral kernel $|K|$ behave like dirac delta functions that peak at $\tau = -t$ to select the corresponding moments from the input photon wave packet $a_{\mathrm{in}}(\tau)$ in the integral (IV.12), which recovers the signal field in a
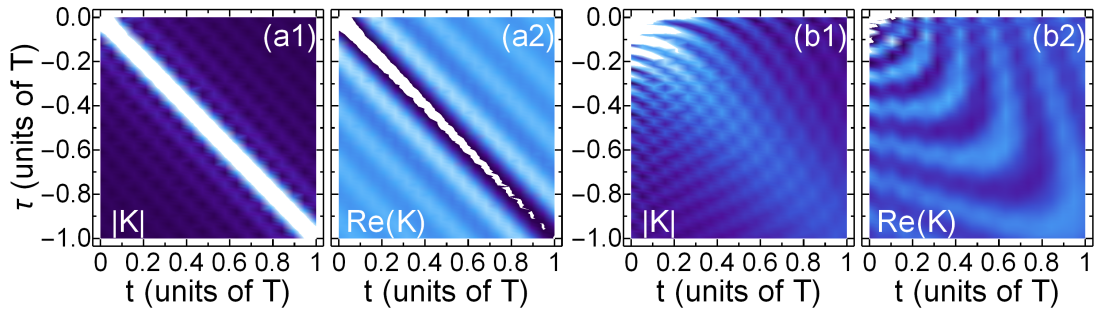
Figure 4.4: The absolute value (a1 and b1) and real part (a2 and b2) of the integral kernel K at the output of the medium. (a1, a2) are plotted for the parameters corresponding to Fig. 4.3 (a), and (b1, b2) are plotted for the parameters corresponding to Fig. 4.3 (f).

82

time-reversed order. This is governed by the argument $i\beta z(t+\tau)$ in Φ_2, which is the total phase carried by the polarization as a function of time t during retrieval. From the time when the gradient is reversed ($t = 0$), this phase starts to regress back towards its original value zero. The complete rephasing happens at $t = -\tau$, which determines the moment of a constructive interference and manifests itself as the moment at which $|K|$ is maximized. However, the rephasing itself is not enough for understanding GEM, and the longitudinal dependence of the resonant condition plays a crucial role in the field evolution. Without this z-dependence, for a system with longitudinal-uniformly distributed inhomogeneous broadening, the forward echo due to the reverse of this broadening contains at most 54% of the input energy because of the reabsorption on its path during propagation [170]. But in GEM, since $i\beta(t+\tau)z$ is valid for all space in the medium, we can treat $k_s = \beta\tau$ and $k_r = \beta't = -\beta t$ as the wave vectors characterizing the spatial mode of the polarization in the medium during storage and retrieval, respectively. This spatial mode of the polarization is caused simply by the free evolution of the phase due to position-dependent transition frequency. The gradient echo is mapped out from the collective excitation in the medium in a way that the retrieval procedure finds its correct spatial mode of the polarization in time according to the phase matching condition $k_r = k_s$. In this manner the echo can avoid the strong reabsorption during its evolution.

On the other hand, when the optical thickness becomes too high, as shown in Fig. 4.4 (b1), the integral kernel $|K|$ loses its dirac-delta property. This is because in an optically thick medium, the linewidth of each transition frequency is broadened by an amount of

optical thickness, which eventually smears out the phase matching condition. As result, the peak of the echo is delayed and the temporal shape becomes deformed. This waveform deformation is quantified by the amplitude preservation $\mathscr{A}$ defined by Eq. (II.11).

Comparing the Fig. 4.3 (c) and (d), for fixed μ, the smaller bandwidth βL corresponds to a wider peak width of the kernel $|K|$, which decrease the retrieval field amplitude preservation $\mathscr{A}$. This is expected from Eqs. (IV.12) and (IV.13), since βL (or βz in a general case inside medium) enters Φ_2 as a scaling factor in from of time variable.

Comparing Fig. 4.3 (a-b, d-f), for fixed bandwidth βL that covers the input spectrum, for example here $\beta L = 4\pi/\Delta t$, if $\mu \ll 1$, the optical thickness is too thin to retain the input energy as determined by the factor μ in front of Φ_2 in Eq. (IV.13). This is the reason in Fig. 4.3 (a) the memory efficiency is only 22%. On the other hand, for large $\mu \gg 1$, the peak of the integral kernel $|K|$ becomes wide for the reason explained before. As can be seem from Fig. 4.3 (f), for large μ, the gradient echo of an input Gaussian wave packet peaked at $t_{\text{in}} = -0.5T$ becomes right-shifted in time and asymmetric in shape, which reduces $\mathscr{A}$ down to 40%. Moreover, from Fig. 4.4 (a2, b2), it is seen that a large optical thickness also introduces a phase modulation. So the strong light-matter interaction not only drags and distorts the echo waveform, but also intensely modulate its phase. This phase modulation on the echo, shown in the insets of the left panels of Fig. 4.3, will rapidly decrease the memory fidelity $\mathscr{F}$. In order to keep high fidelity, μ should be kept small enough such that the phase variation of K on the scale of input photon duration Δt is small, such as in Fig. 4.3 (a) and (b).

From the above analysis, in order to optimize the gradient echo, i.e., to maximize both efficiency and fidelity, the bandwidth βL should cover the input bandwidth, and the parameter μ should be on the order of 1:

$$\beta L \gtrsim 2\pi/\Delta t, \tag{IV.14}$$

$$\mu \sim 1. \tag{IV.15}$$

Too small μ results in small efficiency, and too large μ results in small fidelity (as well as efficiency and amplitude preservation $\mathscr{A}$). An example of high efficiency and fidelity is shown in Fig. 4.3 (b), with $\eta = 99\%$ and $\mathscr{F} = 95\%$.

Although we mainly focus on the output field at the end of the retrieval process, we mention here that in Appendix B the retrieval coherence in the medium as a function of time and space is also derived:

$$s_r(z,t \geqslant 0) = -g \int_{-T}^{0} d\tau a_{\mathrm{in}}(\tau) e^{i\left(\beta \frac{L}{2} - \omega_m\right)\tau} e^{-\gamma(t-\tau)} \Phi_2\left(i\mu + 1, i\mu; 1; -i\beta z\tau, i\beta zt\right),$$

$$\tag{IV.16}$$

where $z \in [0,L], t \in [0,T]$.

IV.4   Conclusion

Gradient echo memory evolution equations (I.1) and (I.2) are important because they do not only describe the GEM scheme but also the PMC scheme and quantum storage based on control field spatial chirp. In this chapter we derive the exact analytical solution for GEM scheme under arbitrary optical thicknesses and frequency gradient for both storage and retrieval process. This is important for the understanding the field-atom dynamics of

GEM and GEM-like schemes.

The analytical solution shows the reason why GEM can achieve high efficiency and fidelity in forward retrieval, and identify the optimal regime for good quantum memory. These optimal conditions (IV.14) and (IV.15) agrees with the previous conditions (II.18) for control field angular scanning, (II.32) for control field frequency chirp, and (III.7) for control field spatial chirp. However here the analysis is based on the exact analytical solution rather than some rough arguments.

CHAPTER V

QUANTUM STORAGE BASED ON DISCRETE SPATIAL CHIRP: GRADIENT FREQUENCY COMB AND STEPWISE GRADIENT ECHO MEMORIES[*]

V.1   Introduction

As explained in Chap. I, the major techniques for the storage and retrieval of a time-bin single-photon wave packet [26] in atomic ensembles, such as EIT, Raman, GEM and AFC, divide into two groups, and both of them have some fundamental and practical limitations. Since the concept of quantum information is rather broad and its applications are versatile, a quantum memory scheme should be implementable in as many quantum interfaces as possible to be integrated into different information processing devices, and had better to be able to store incoming photon without knowing its information. So the specific requirements of each of the above mentioned quantum memory methods may limit its applications in different cases.

In this chapter, we propose a method combining these two types of techniques, which overcomes the above hassles and demonstrates many other interesting advantages. We suggest an all-optical scheme for the storage, retrieval and sequencing of a single-photon wave packet through its off-resonant Raman interaction with a series of coherent control

---

[*]The preprint of the related work "Quantum storage based on controllable frequency comb" by Xiwen Zhang, Alexey Kalachev, Philip Hemmer, and Olga Kocharovskaya is available on arXiv:1602.02322 (2016), and will be submitted to journal publication soon.

beams [176]. These control beams, each with distinct carrier frequency, are distributed along the way of single-photon propagation, thus effectively forming a gradient absorption structure which can be controlled in various ways to achieve different single-photon processing functionalities. Such a controllable frequency comb is a hybrid of Raman, GEM and AFC methods, therefore demonstrates many of their advantages all together in one.

V.2   Gradient frequency comb

Consider a single photon wave packet $\mathbf{E}_s(\mathbf{r},t)$ of carrier frequency ω_s and duration Δt passing through a three-level atomic ensemble along the longitudinal direction $\hat{z}$ with one-photon detuning $\Delta = \omega_s - \omega_{21}$, where ω_{ij} is the transition frequency between levels $|i\rangle$ and $|j\rangle$ [Fig. 5.1 (a)]. The control field propagates perpendicularly to the signal field's propagation direction, and has a spatial chirp across the beams. The interaction volume consists of discrete sections distributed along $\hat{z}$, due to either disconnected pieces of ensembles or spatially separated individual controlling beams [Fig. 5.1 (b)]. Because of the spatial chirp, each section sees different frequency of the control field, resulting in an overall comb structure in the photon's absorption spectrum. But unlike AFC, the comb teeth are distributed linearly on the path of photon propagation, therefore forming a gradient frequency comb (GFC). This gradient frequency comb, determined by the two-photon resonance condition $\delta(\mathbf{r},t) = \omega_s - \omega_c(\mathbf{r},t) - \omega_{31} = 0$ [Fig. 5.1 (a)], will be used to store the input single-photon wave packet.
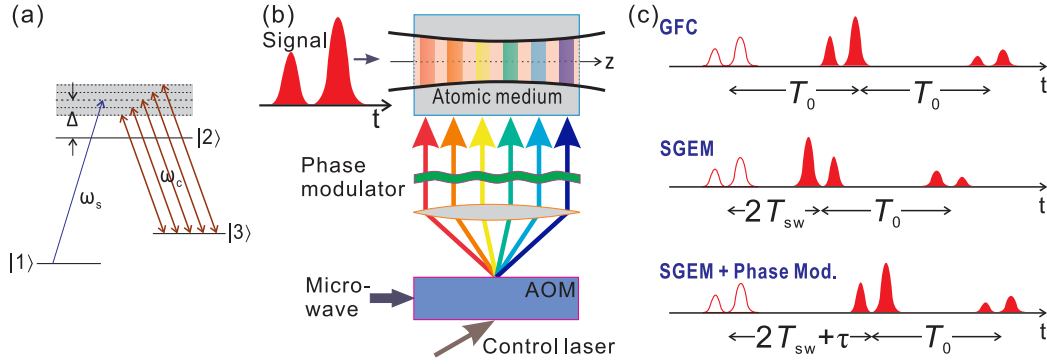
Figure 5.1: Scheme of quantum memory based on discrete spatial chirp. (a) In a Λ-level structure, the control field consists of a number of spatially separated beams each with different frequencies. (b) Illustration of a implementation of the proposed quantum memory scheme. (c) Different regimes of the scheme, including gradient frequency comb (GFC), stepwise gradient echo memory (SGEM) and that with additional phase modulation.

V.2.1 Theoretical model of gradient frequency comb quantum memory

Let us write the signal field $\mathbf{E}_s(z,t)$ and control field $\mathbf{E}_c(\mathbf{r},t)$ as [177]:

$$\mathbf{E}_s(z,t) = \hat{\epsilon}_s \frac{i}{n_{\text{bg}}} \mathscr{E}_s a(z,t) e^{-i(\omega_s t - k_s z)} + H.c., \tag{V.1}$$

$$\mathbf{E}_c(\mathbf{r},t) = \hat{\epsilon}_c E_0(z) e^{i[k_c(z)x - \omega_c(z)t - \varphi_{0c}(z)]} + c.c., \tag{V.2}$$

in which $\hat{\epsilon}_{s,c}$ are the polarization vectors of the signal and control fields, $a(z,t)$ is the slowly varying amplitude of the signal field, $\mathscr{E}_s = \sqrt{\hbar\omega_s/(2\varepsilon_0 V)}$, φ_{0c} is a stationary phase on the control beam, $k_s = n\omega_s/c$, $k_c = n_{\text{bg}}\omega_c/c$, $n = n_{\text{bg}}n_{\text{int}}$ is the refractive index taking into account the atom-environment interaction (background) n_{bg} and the Raman interaction n_{int}, and c is the speed of light in vacuum. We assume each control beam has a duration much longer than Δt, so that the time dependence of E_0 can be neglected. The control field spatial chirp is characterized by its position-dependent frequency: $\omega_c(z) - \omega_{c0} = m(z)\delta\omega_c$, where $\omega_{c0} = \omega_c(z=0)$, m is the sequence of the control beams, and $\delta\omega_c$ is their adjacent

frequency spacing.

Let us define the slowly varying part of the spin wave operator as

$$S(\mathbf{r},t) \propto g^* N \sigma_{13} e^{i(\omega_s - \omega_c)t} e^{i[\mathbf{k}_c(z) - \mathbf{k}_s] \cdot \mathbf{r}} e^{-i\varphi_{0c}}, \tag{V.3}$$

where $\sigma_{nn'}(\mathbf{r},t) = \frac{1}{N} \sum_j |n\rangle_{j,\mathbf{0}} \langle n'| \delta(\mathbf{r} - \mathbf{r}^j)$ is the collective atomic operator for the nth state

of atom j with velocity $\mathbf{0}$, N is the atomic density, $g = \sqrt{\omega_s/(2\hbar\varepsilon_0 cn_{bg}n_{int})}[d_{21}\Omega_c(z)/\Delta]$,

$\Omega_c(\mathbf{r},t)$ is the control field Rabi frequency. As shown by Eqs. (C.43a) and (C.43b) of

Appendix C, in long-pulse and far off-resonant regime, the evolution equations read

$$\frac{\partial}{\partial z}a(z,t) = -S(z,t)\exp\left(-\frac{t^2}{2t_d^2}\right), \tag{V.4}$$

$$\frac{\partial}{\partial t}S(z,t) = -[\gamma - i\delta(z)]S(z,t) + |g(z)|^2 Na(z,t), \tag{V.5}$$

where γ is the decoherence rate of the spin coherence. Let us choose the control field central

frequency as $\omega_{c0} = \omega_s - \omega_{31} - |\Omega_c(z=0)|^2/\Delta$, then the two-photon detuning becomes

$$\delta(z,t) = -\sum_{m=-M_0}^{M_0} m\delta\omega_c(\Theta_-^m - \Theta_+^m) - \delta_{AC}, \tag{V.6}$$

where $\delta_{AC}(z,t) = [|\Omega_c(z,t)|^2 - |\Omega_c(z=0,t)|^2]/\Delta$ is the uncompensated ac-Stark shift due

to the spatial inhomogeneity of the individual control beams, and $\Theta_\mp^m = \Theta(z - mL_0 \pm d/2)$

are the Heaviside step functions. The Gaussian factor in Eq. (V.4) describes the spin wave

Doppler dephasing along the longitudinal frequency gradient due to the atomic motion with

Maxwellian velocity distribution [178]. In general, a transverse atomic motion also leads

to similar dephasing of the spin wave, which will be neglected for the sake of simplicity.

So, as discussed in Appendix C, the dephasing time is $t_d = 1/(\sqrt{k_BT/m_a}k_s)$, where k_B is

the Boltzmann constant, T is the gas temperature and m_a is the atomic mass.

Due to the periodicity of the two-photon resonance condition, the spin waves get recurrently inphase after each $T_0 = 2\pi/\delta\omega_c$. If the Doppler dephasing and control beam spatial inhomogeneity are neglected, approximate analytical solution of Eqs. (V.4) and (V.5) can be obtained in the high comb finesse $\mathcal{F} = \delta\omega_c/(2\gamma)$ regime. This solution up to $t = T_0$ is expressed as follows [173] (see Appendix D)

$$a_{\text{out}}(t) \approx e^{-\frac{\pi}{4}\zeta_{\text{eff}}^0} a_{\text{in}}(t) - \frac{\pi\zeta_{\text{eff}}^0}{2} e^{-\frac{\pi\zeta_{\text{eff}}^0}{4}} e^{-\frac{\pi}{\mathcal{F}}} a_{\text{in}}(t - T_0), \qquad (\text{V.7})$$

where $\zeta_{\text{eff}}^0 = 4|g|^2 Nd/\delta\omega_c$ is the individual effective optical thickness. Since for spin transitions the docoherence rate γ usually is very small, we will assume that $\mathcal{F} \gg 1$ is always satisfied. The first term of Eq. (V.7) is the leakage field that did not interact with the medium, and the second term is the first GFC echo. In this dissertation we mainly focus on the first echo. We use efficiency η [Eq. (II.7)] to describe the ratio of retrieved energy out of the input signal, and fidelity $\mathscr{F}$ [Eq. (II.10)] to characterize the waveform preservation. So Eq. (V.7) tells that the maximum efficiency for the forward GFC echo is 54%, and the corresponding optimization conditions are:

$$\mathcal{F} \gg 1, \qquad (\text{V.8})$$

$$\zeta_{\text{eff}}^0 = 4/\pi, \qquad (\text{V.9})$$

$$\Delta t < T_0 < M\Delta t. \qquad (\text{V.10})$$

V.2.2 Experimental example of gradient frequency comb quantum memory

From Eq. (V.7), we see that in the high finesse regime, our method demonstrates the same action as AFC scheme. But unlike AFC, our scheme can be implemented in
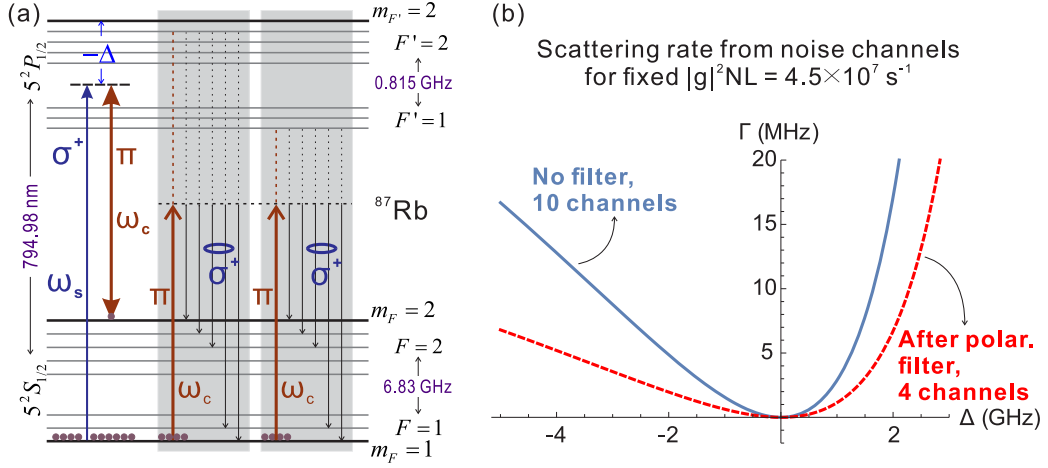
Figure 5.2: (a) Λ-level scheme consisting of $|F=1, m_F=1\rangle$-$|F'=2, m_{F'}=2\rangle$-$|F=2, m_F=2\rangle$ of rubidium 87 D1 line. The signal photon excites σ^+ transition and the control field works on the π transition. The shaded area shows the major noise channels. (b) The noise scattering rate as a function of one-photon detuning for fixed $|g|^2 NL = 4.5 \times 10^7$ s^{-1}. The scattering rate is estimated using the treatment introduced in Sec. III.3.4, which is valid only under off-resonant Raman condition. So the values near resonances should not be read form this figure. In addition, $\Delta \rightarrow \infty$ indicates infinite control power which is not realistic either.

materials without inhomogeneous broadening, such as cold atom. Let us consider the Λ-level scheme of cold ^{87}Rb shown in Fig. 5.2 (a). Typically the temperature of such system is 100 μK and the atomic density can reach 10^{11} cm^{-3} [56]. Under this temperature, the dephasing time due to Doppler broadening is $t_d = 1$ μs, and the atom loss time due to the atomic migration out of interaction volume is 77.7 μs. These limit the storage time to a microseconds level. This storage time, in turn, determines a minimum bound of the storage bandwidth. Let us consider a storage time $T_0 = 400$ ns, which is smaller than the dephasing time. The signal duration must be further smaller than the echo rephasing time (or the storage time) T_0, say, $\Delta t = 50$ ns. This FWHM duration of the signal field eventually determines a combination of one-photon detuning, control power, and atomic

density through required storage bandwidth of the medium, which is optimized via Eqs. (V.8) - (V.10).

The one-photon detuning is further limited by spontaneous Raman noise. As shown in Fig. 5.2 (a), the control field can act on the first ground state, promoting the population to the second ground state through spontaneous scattering with a noise photon. Such process can be eliminated or alleviated by using polarization and frequency filters. Without these filters, one has to carefully choose the one-photon detuning in order to increase signal-to-noise ratio (SNR). In our case, there are 10 major such noise channels. The scattering rate as a function of frequency detuning is plotted in Fig. 5.2 (b) by the solid line. By considering the polarization of the scattered photon, a simple polarization filter can exclude six channels of the ten, and the resulted scattering rate versus one-photon detuning is shown by the dashed line of Fig. 5.2 (b). In order to keep the SNR larger than 1, the inverse of the scattering rate should be larger than the storage time. So a one-photon detuning should be chosen on the one hand to keep reasonably small noise, on the other hand to satisfy off-resonant Raman condition. Let us consider a one-photon detuning $\Delta = -0.7$ GHz, which will allow an operation window < 1.21 μs to keep SNR greater than one if no filtering is performed, in accordance with the spin wave dephasing time ~ 1 μs. A simple polarization filter will enlarge this time window from < 1.21 μs to 3 μs.

According to Eqs. (V.9) and (V.10), for a $\Delta t = 50$ ns signal photon, the required $|g|^2 N$ is 9×10^9 s^{-1}m^{-1}. This can be achieved with a control power of 0.18 W under a one-photon detuning $\Delta = -0.7$ GHz. The control beams can be generated, for example,
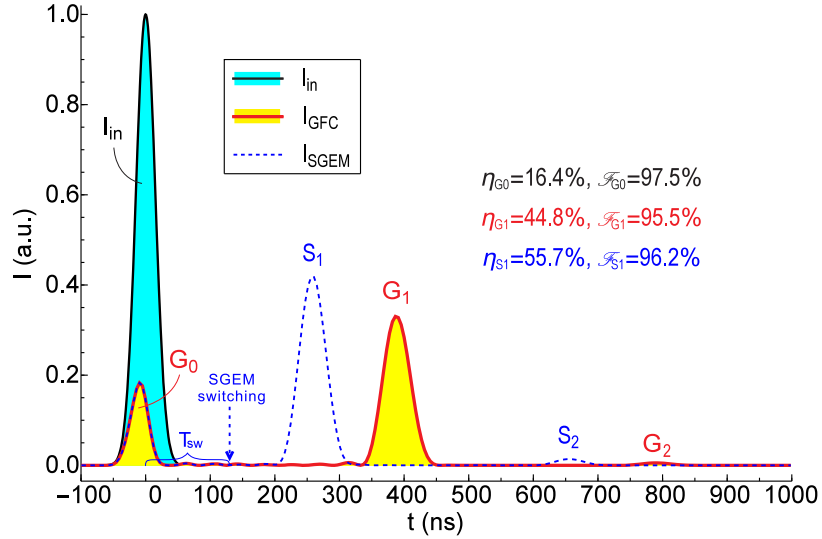
Figure 5.3: GFC and SGEM echoes in a cold ^{87}Rb ensemble. The medium is divided into $M = 9$ sections each of length $d = 0.56$ mm. The σ^+-polarized signal photon ($\Delta t = 50$ ns, width 50 μm) is frequency detuned by -0.7 GHz from the excited state. The nine π-polarized control beams of total power 0.18 W are assigned to a frequency spacing such that $T_0 = 400$ ns, giving $\zeta_{\text{eff}}^0 = 1.28$. In SGEM regime, $T_{\text{sw}} = 130$ ns, where T_{sw} is the time interval between the arrival of the signal photon and the switch of the control beam frequencies.

by passing phase-locked short laser pulse train through an Acousto-optic modulator and arbitrary wave generator, which permits a bandwidth ~ 100 MHz [see Fig. 5.1 (b)].

The result is shown in Fig. 5.3. Notice that here we assume $\delta_{AC} = 0$. Otherwise the efficiency will be strongly decreased since $\delta_{AC}/(2\pi) = 46.2$ MHz, larger than the 20 MHz input bandwidth. Thus we should prepare a flat-topped control beam profile to keep the efficiency. In the following we assume this is always the case.

V.3 Stepwise gradient echo memory and photon processing

The GFC regime of the proposed quantum storage scheme has upper bound efficiency 54%, and the memory is on pseudo-demand since the storage time is adjustable

94

but pre-determined before the retrieval. On-demand retrieval is an essential requirement of quantum memory. Otherwise the application of multichannel synchronization becomes difficult, and very often there is no need to resort to light-mater interaction since a simple low-loss fiber delay line can achieve a time delay of a photon. In AFC scheme, this is done through transferring the atomic excitation down to another ground state by a π pulse [47, 60], or changing the comb teeth spacing by external field [72]. In our case we can simply shut down the control beams, or in practice take advantage of the finite duration of the control field, to achieve arbitrary storage time allowed by the spin-wave lifetime. Meanwhile, the π-pulse technique can also be used in our scheme for the purpose of backward retrieval [88], which in principle promises perfect efficiency and fidelity.

Another way to achieve on-demand retrieval is through the second regime of the proposed scheme, where we switch the two-photon frequency detuning to the opposite before the emergence of the first echo. In such a case, the spin wave starts to dephase immediately after the storage process. Before the phases of the spin wave evolve into the constructive interference status, the switch of the control field frequency enforce them to regress back. When the spin waves rewind to their starting state, an echo is emitted. The total storage time consists of the dephasing and rewinding time [see Fig. 5.1 (c)]. So depending on the moment of the frequency switching, one can control the echo emergence time. Since our comb has a discrete frequency gradient along $\hat{z}$, which means by reversing the control beam sequence we realize a GEM scheme in a discrete manner. We call this regime stepwise gradient echo memory (SGEM).

The advantage of SGEM regime does not only lies in its on-demand retrieval, but also lies in its higher theoretical upper bound of efficiency. As we discussed in Chap. IV, the GEM demonstrates almost 100% efficiency in a forward retrieval. For similar reason, we expect that the efficiency of SGEM can also become as close to 100% as possible when the scheme approaches its continuous limit. In Fig. 5.3 (dashed blue line) we show a simple example of SGEM echo with efficiency 55.7%, larger than the upper bound of GFC regime 54%. Higher efficiency can be achieved with larger amount of discrete sections. The SGEM regime also allows a read out of reversed sequence of the input photon without multiple stages of phase modulation (as discussed below). More discussions on SGEM are given in Chap. VI.

In AFC, since the absorption structure can not be much manipulated once created, the signal processing has to be achieved via multiple combs made in advance, and a frequency modulation has to be applied to the single photon to determine which storage channel to go [80]. This technique is also readily applicable in our scheme, but in general the multi-comb configuration consumes the storage bandwidth, and a direct manipulation to the fragile single photon may not be feasible in some real applications.

The fact that our frequency comb is implemented through two-photon detuning by external control beams gives us two additional degrees of freedom for the manipulation of the single-photon wave packet. The first is the ability of switching the frequencies of control beams, which leads to SGEM regime of the scheme as discussed above. Second, the control beam can each be imposed on a different phase at any moment of time, which is
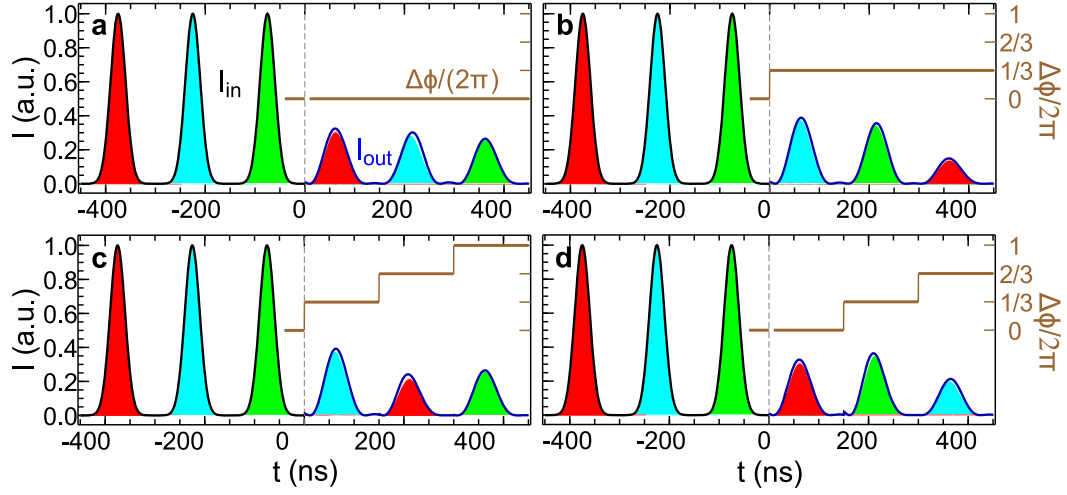
Figure 5.4: Single-photon processing. The black solid lines ($t < 0$ ns) are input three-peak single-photon intensities, and the blue solid lines ($t > 0$) are retrieved signals of different sequences. The brown solid lines show adjacent phased difference $\Delta\phi$ introduced by additional modulation as a function of time. (a, b): Retrieved signal with circular permutation. (c, d): Retrieved signal with non-circular permutation. Common parameters: $\Delta t = 50$ ns, $T_0 = 450$ ns, $M = 9$, $\zeta^0_{\text{eff}} = 4/\pi$. Parameters for material are the same as in Fig. 5.3.

shown in Fig. 5.1 (b, c). From Eq. (V.3) we see that the phase of the control beams modifies the collective operator S. Without additional phase modulation, the echo emission time T_0 is determined by the discreteness of $\omega_s - \omega_c$, namely, when $\delta\omega_c T_0 = 2\pi$. If we add phases to the control field such that between two adjacent beams $\Delta\phi = \delta\omega_c\tau$, meaning that the phases of the spin waves are advanced by a time τ, the echo will instead emerge at $T_0 - \tau$, where $0 \le \tau \le T_0$. This can be used to achieve single photon processing, as shown in Fig. 5.4.

V.4 Conclusion

In this chapter, we suggest an all-optical scheme for the storage, retrieval and sequencing of a single-photon wave packet through its off-resonant Raman interaction with

a sequence of coherent control beams. Compared with EIT and Raman scheme, it does not require a prior knowledge of the signal photon's waveform, neither the synchronization of the signal and control fields. Compared with AFC, it demonstrates lots of advantages in its implementation and its controllability over the single photon wave packet, including on-demand retrieval and photon processing. Compared with GEM, it does not relay on the existence of Zeeman and/or Stark effect. Such a controllable frequency comb is a hybrid of Raman, gradient echo memory and atomic frequency comb methods, therefore demonstrates many of their advantages all together in one.

CHAPTER VI

NUCLEAR QUANTUM MEMORY AND CONTROL OF A SINGLE

γ-RAY PHOTON[*]

VI.1   Introduction

Quantum information has been developed for thirty years from many aspects of dif-
ferent branches of physics. Specifically, from optical point of view, so far the related
research mainly focuses on infrared, visible and nearby frequency regime because of the
richness of the tool box and variousness of the interaction media. However, there are
both practical and fundamental limitations on optical single-photon qubit, such as the lack
of reliable, economical single-photon sources, low efficiency and high dark-count rate of
single-photon detectors [179], diffraction limit of the size (down to ~ 1 μm) of quantum
photonic circuits, etc.

In γ-ray range (10 -100 keV), on the other hand, these problems are resolved. The
single photon detector has nearly 100% detection efficiency with almost no false detection,
and radioactive decay in a cascade scheme can be used as the natural heralded single γ-ray
source. Realization of quantum memory, as will be discussed in this paper, would provide
single γ photons on demand. The small wavelength of the γ photon allows nano-scale
or even smaller photonic circuit. Moreover, the Mösbauer solid provides almost perfect

---

nuclear-resonant medium for quantum information application in γ-ray range: even at room temperature, it may have several orders of magnitude higher density with several orders of magnitude smaller linewidth compared with resonant media in optical range at cryogenic temperature based on electronic transitions. Thus higher optical density and longer coherence time can be simultaneously achieved, providing strong light-matter interaction for information processing while leaving sufficient lifetime of qubit for gate operation, nearby entanglement preparation, etc. The downside of γ-ray quantum information is also obvious: it is rather difficult to control γ photons because of the absence of bright coherent sources and high finesse cavities. In fact, most of the tools for controlling optical photons become difficult, inefficient or even missing in γ-ray regime.

However, the situation has been substantially improved by recent works, including coherent sources up to 849 eV via stimulated emission of core-excited state [180], 1.6 keV via high-harmonic generation [181], 9 keV via self-seeding x-ray free-electron laser [182], etc. As for γ-ray cavities, over 99% back Bragg reflectivity of hard x rays is demonstrated in perfect diamond [183], and four-mirror resonator is built out of mosaic graphite crystals at 5 keV [184]. In addition, coherent effects, such as level-mixing-induced transparency [185], electromagnetically induced transparency (EIT) [186], γ echo [187, 188] and its complement position-induced phase modulation [189, 190], nuclear lighthouse effect [191], spontaneously generated coherence [192], x-ray parametric down conversion [193] and second harmonic generation [194], nuclear coherent population transfer [195], single photon entanglement [196], etc, can be adopted to control γ-ray photon.

Recently, coherent control of the waveforms of recoilless single γ-ray photon is demonstrated by tuning the Mösbauer absorber into different vibrational sidebands [197]. Shaping of single photon can be as well achieved by abrupt change of the excited nuclear state [198]. The ability to shape single γ-ray photon allows the information to be encoded in time-bin qubit [26] or more complicated temporal wave packet [43] out of qusi-monochromatic γ-ray radiation, thus lays the foundation of γ-ray quantum information. In particular, in the first part of this chapter we discuss one of the main building blocks of quantum information processing, namely, quantum memory and time processing of a photon's waveform using Doppler frequency comb.

Apart from the manipulation of the temporal mode of a single γ photon, it is as well important to demonstrate the controllability of its spatial mode, such as γ-ray switch. The development of a fast switch of γ photons could be important for extending the time resolution of γ-ray sources and for increasing the operating speed of γ-ray quantum information processing. Nanosecond γ-ray switching has been realized by magnetically manipulating nuclear excitation based on quantum beat in the nuclear Bragg scattering [199]. Picosecond x-ray Bragg switch utilizing laser generated phonons was proposed [200] and later demonstrated experimentally [201, 202]. In the second part of this chapter we investigate an all-optical way to control the propagation direction (Bragg mode) of a γ-ray beam using a vibrating Mössbauer crystal.

VI.2 Storage and processing of a γ photon's temporal mode

Quantum memory is considered to be *condicio sine qua non* of the definition of quantum computing device [16], and lies in the heart of the realization of long-distance quantum communication [12]. However, a direct transfer of the quantum memory technology from optical frequency range to γ-ray range is rather challenging, sometimes impossible. For example, quantum memory based on EIT [32] and off-resonant Raman interaction [39] require Λ-level system and shaped strong control field, thus are too far from being implemented in γ-ray frequency range in Mösbauer solids. Among two-level photon-echo-based quantum memory schemes, atomic frequency comb (AFC) [47, 59, 60] is achieved by delicate preparation of an absorption comb in the wide inhomogeneous broadening profile of the excited state, while in Mösbauer solids such inhomogeneous broadening, as well as strong lasers for hole-burning are not available. Another echo scheme is gradient echo memory (GEM) [44, 50] where an switchable artificial position-dependent inhomogeneous broadening is created by external gradient field. For nuclear transition, nuclear magneton is three orders of magnitude smaller than Bohr magneton. Taking one of the most widely studied Mösbauer isotope, ^{57}Fe for example, in order to store a photon, a much broader artificial inhomogeneous broadening compared to the life-time broadening (1.1 MHz) should be prepared. This requires tens of tesla external magnetic field which should be switched within ~ 10 ns, thus would be challenging for current technology. In principle, nuclear Zeeman levels could be used as natural frequency comb, and such comb can be switched within several nanoseconds in antiferromagnetic material such as iron borate $FeBO_3$ by

tens of tesla internal hyperfine magnetic field [203, 204]. But due to selection rules no more than three comb teeth can be used per ground state, and there is not much tunability of the comb either. Such scheme can be used to store nuclear excitation energy [205, 206] but not a time-bin state of a single photon yet. To the best of our knowledge, up to date there is no feasible quantum memory scheme to faithfully store a single γ-ray photon yet.

In this section, we propose to store and process a single γ-ray waveform using Doppler frequency comb, which will be explained in the following.

VI.2.1 Theoretical description of Doppler frequency comb: gradient frequency comb (GFC) and stepwise gradient echo memory (SGEM)

We consider the storage of a single γ-ray wave packet of carrier frequency ω_0 and wave vector $k_0 = \omega_0/c$ in a two-level resonant medium ($\omega_{ab} = \omega_0$) [207]. The resonant medium is composed of $M = 2M_0 + 1$ identical Mösbauer targets, stainless steel for example, each of which has thickness d and moves with different velocities v_m with equal velocity spacing Δv: $v_m = m\Delta v, m = 0, \pm 1, \pm 2, \cdots \pm M_0$ [Fig. 6.1 (a)]. Such velocity spectrum forms a frequency comb due to Doppler effect, which we name as Doppler frequency comb. Since the comb teeth are distributed along the γ photon propagation direction, it is also a gradient frequency comb (GFC) which was discussed in Chap. V. In this comb, the one-photon detuning of the γ-ray field with respect to the nuclear transition frequency is $\Delta_m = m\beta\omega_0$ where[1] $\beta = \Delta v/c$. Echoes are produced because of the beating of different frequency components of the excited polarization in the medium, which are represented by

---

[1] In this chapter, β is used to denote a dimensionless velocity, which is different from a changing rate of wave vector in Chap. II or a frequency gradient in Chaps. III and IV.
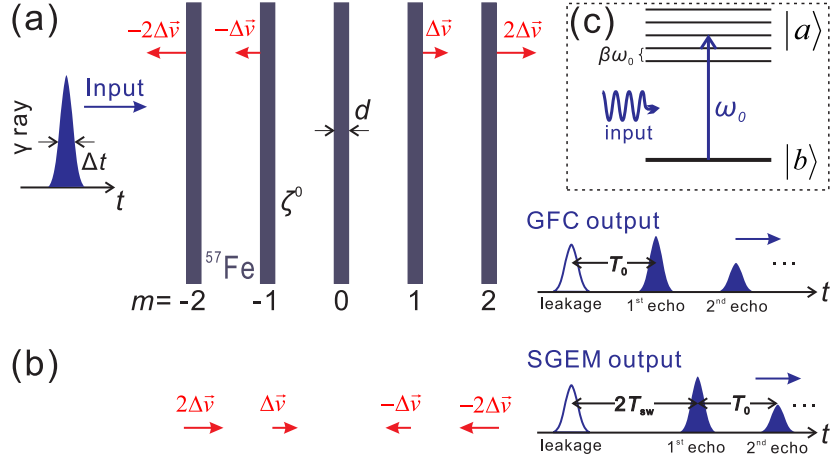
Figure 6.1: Illustration of the proposed γ-ray quantum memory scheme. (a) In GFC regime, the input single γ-photon wave packet is absorbed by the Doppler frequency comb formed by a number of Mösbauer targets moving with velocities $m\Delta v$, $m = 0, \pm 1, \pm 2, \cdots \pm M_0$. The periodic beating of the comb teeth generates echo signals. (b) In SGEM regime, after absorbing the input photon, the Mösbauer targets switch their moving directions to the opposite, and the echo is generated after twice of the switching time T_{sw}. (c) The effective energy level scheme of the quantum memory method.

these spectrum teeth of GFC.

The evolution equation of the light-matter interaction in a one dimensional model is derived from Maxwell equation in the laboratory frame F

$$\left(\frac{\partial^2}{\partial z^2} - \frac{1}{c^2}\frac{\partial^2}{\partial t^2}\right) E(z,t) = \mu_0 \wp_{ba} \frac{\partial^2}{\partial t^2} \sum_j \left[\rho_{ab}^{'j}(t) + c.c.\right] \delta(z - z_j(t))\frac{1}{A}, \qquad (VI.1)$$

and Schrödinger equation of the nuclei in mth target in its moving frame F_m'

$$\frac{\partial}{\partial t'}\rho_{ab}^{'j}(t') = -i\omega_{ab}\rho_{ab}^{'j}(t') + i\frac{\wp_{ab}}{\hbar}E(z_j,t), \qquad (VI.2)$$

where $E(z,t)$ is the corresponding electric field of the γ-ray quanta in the laboratory frame F, $\rho_{ab}^{'j}(t')$ is the off-diagonal element of the density matrix of jth nucleus in its moving frame F_m' with laboratory position $z_j(t)$, $\wp_{ab}$ is the dipole matrix element of the two-level nuclear system, A is the transverse cross section of the input γ-ray field. Assum-

ing each Mössbauer target has thickness d and initial central position l_m, then the relations between the laboratory frame (F) variables and the moving frame (F'_m) variables are $z = z' + l_m + v_m t'$, $t = t'$, with $z' \in [-d/2, d/2]$. Notice that in ^{57}Fe it is the magnetic component that actually interacts with the nuclei, while the above equations are written for electric component of electromagnetic field. However, they are still valid for magnetic transition after rescaling the interaction constants. The number density distribution is $N(\Theta^m_- - \Theta^m_+)$ where N is the nuclear number density and $\Theta^m_\pm = \Theta(z - l_m \mp d/2)$ is the Heaviside step function.

Let us define the collective operator ρ'^m_{ab} of the mth Mössbauer target in its moving frame F'_m as:

$$\rho'^m_{ab}(z', t') = \frac{1}{NAdz'} \sum_{j'=1}^{NAdz'} \rho'^j_{ab}(t'), \tag{VI.3}$$

where $NAdz'$ is the number of nuclei in a small slice dz' of the mth target at position z'. We can write the γ-ray field and the nuclear coherence in the laboratory frame F into the form of

$$E(z,t) = \mathcal{E}(z,t)e^{-i(\omega_0 t - k_0 z)} + c.c., \tag{VI.4}$$

$$\rho'^m_{ab}(z - l_m - v_m t, t) = -i\frac{\wp_{ab}}{\hbar|g|^2 N}\mathcal{P}'^m(z - l_m - v_m t, t)e^{-i(\omega_0 t - k_0 z)}, \tag{VI.5}$$

where ω_0 is the central frequency of the incoming γ photon, $k_0 = \omega_0/c$, $g = \wp_{ab}\sqrt{\omega_0/(2\hbar\varepsilon_0 c)}$ is the coupling constant of the γ-ray-nucleus interaction, $\mathcal{E}(z,t)$ is the slowly varying amplitude of the γ-ray field in the laboratory frame and $\mathcal{P}'^m(z', t')$ is proportional to the slowly varying amplitude of the medium polarization of mth target in its moving frame.

To proceed, we adopt slowly varying amplitude approximation and rotating wave approximation, and apply the transformation $\frac{\partial}{\partial z'} = \frac{\partial}{\partial z}$, $\frac{\partial}{\partial t'} = \frac{\partial}{\partial t} + v_m \frac{\partial}{\partial z}$. Moreover, in order to simplify the evolution equations, two additional approximations will be used: In the slow-motion regime, $v_m \Delta t \ll d$, we neglect $v_m t$ with respect to $z - l_m$ and $v_m \partial / \partial z$ with respect to $\partial / \partial t$; while in the long-pulse regime, $L \ll c\Delta t$, we neglect the term $\partial / \partial (ct)$ with respect to $\partial / \partial z$. Here L is the length of the whole medium. In this chapter we have the target velocity $v_m \sim$ 1-10 mm/s, input field duration $\Delta t \sim$ 1-10 ns, and ^{57}Fe thickness $d \sim 10\ \mu$m, so these conditions are fulfilled. Thus in the regime

$$v_m \Delta t \ll d < L \ll c\Delta t, \tag{VI.6}$$

adding the nuclear decoherence rate Γ by hand, one derives the evolution equation as follows:

$$\frac{\partial}{\partial z}\mathcal{E}(z,t) = \sum_{m=-M_0}^{M_0} \mathcal{P}^m(z,t)\left[\Theta\left(z - l_m + \frac{d}{2}\right) - \Theta\left(z - l_m - \frac{d}{2}\right)\right], \tag{VI.7}$$

$$\frac{\partial}{\partial t}\mathcal{P}^m(z,t) = (-\Gamma - i\Delta_m)\mathcal{P}^m(z,t) - |g|^2 N\mathcal{E}(z,t), \tag{VI.8}$$

where $\Delta_m = \beta_m \omega_0 - \delta$ is the input photon detuning in mth Mössbauer target, $\delta = \omega_0 - \omega_{ab}$, $\omega_m = \beta_m \omega_0$, $\beta_m = v_m/c$. The initial condition is the absence of the nuclear coherence $\mathcal{P}^m(z,0) = 0$ and the boundary condition is the input signal field $\mathcal{E}(0,t) = \mathcal{E}_{\text{in}}(t)$. We consider equally spacing Doppler frequency comb and assume resonant interaction ($\delta = 0$), so the photon detuning $\Delta_m = m\beta \omega_0$ where $\beta = \Delta v/c$.

The output field will be determined by some important characteristic parameters of the medium and the comb: the rephasing time $T_0 = 2\pi/(\beta \omega_0)$, the individual optical thick-

ness of each Mössbauer target $\zeta^0 = 2|g|^2 Nd/\Gamma = |\wp_{ab}|^2 \omega_0 Nd/(c\hbar\varepsilon_0\Gamma)$, the total optical

thickness for the whole medium $\zeta = M\zeta^0$, and the individual effective optical thickness

$\zeta^0_{\mathrm{eff}} = \zeta^0/\mathcal{F}$ where $\mathcal{F} = \beta\omega_0/(2\Gamma)$ is the finesse of the comb.

The efficiency η_i and fidelity $\mathscr{F}_i$ of ith echo signal are defined as follows: Efficiency

$$\eta_i = \frac{N^i_{\mathrm{out}}}{N_{\mathrm{in}}}, \tag{VI.9}$$

where $N_{\mathrm{in}} = \int_{t_{\mathrm{in}}-\tau}^{t_{\mathrm{in}}+\tau} dt \mathcal{E}^\dagger_{\mathrm{in}}(t)\mathcal{E}_{\mathrm{in}}(t)$ and $N^i_{\mathrm{out}} = \int_{t^i_{\mathrm{ec}}-\tau}^{t^i_{\mathrm{ec}}+\tau} dt \mathcal{E}^\dagger_{\mathrm{out}}(t)\mathcal{E}_{\mathrm{out}}(t)$, and fidelity

$$\mathscr{F}_i = \frac{1}{N_{\mathrm{in}}N^i_{\mathrm{out}}} \left| \int_{t_{\mathrm{in}}-\tau}^{t_{\mathrm{in}}+\tau} dt \mathcal{E}^\dagger_{\mathrm{in}}(t)\mathcal{E}_{\mathrm{out}}\left(\pm(t-t_{\mathrm{in}})+t^i_{\mathrm{ec}}\right) \right|^2, \tag{VI.10}$$

in which t_{in} and t^i_{ec} are the single photon's arrival time and ith echo's emergence time (for

numerical simulation t^i_{ec} is determined by the local maximum of the echo signal). In GFC

regime $\tau = T_0/2$ and "+" sign is chosen in Eq. (VI.10), while in SGEM[2] regime $\tau = $

$\min\{T_{\mathrm{sw}}, T_0/2\}$ and "−" sign is used. In all cases we assume the integrate interval $\tau > \Delta t/2$

is very well satisfied.

From Eqs. (VI.7) and (VI.8), it can be seen that the periodic spectrum of the polar-

ization will tailor the evolution of the γ-ray field via a spatial interference of the re-emitted

wave, leading to a series of GFC echoes. The analytical solution of the first GFC echo is

derived in Appendix D, which reads the following:

$$\mathcal{E}_{\mathrm{out}}(t) = e^{-\frac{\pi}{4}\zeta^0_{\mathrm{eff}}}\mathcal{E}_{\mathrm{in}}(t) - \frac{\pi\zeta^0_{\mathrm{eff}}}{2}e^{-\frac{\pi\zeta^0_{\mathrm{eff}}}{4}}e^{-\frac{\pi}{\mathcal{F}}}\mathcal{E}_{\mathrm{in}}(t-T_0). \tag{VI.11}$$

The first term of Eq. (VI.11) is the leakage field without interaction with medium. The sec-

ond term represents the first GFC echo. Its efficiency can be extracted from the analytical

---
[2]SGEM stands for stepwise gradient echo memory, which is explained in the following of this section.

solution as:

$$\eta_{G1} = \left(\frac{\pi \zeta_{\text{eff}}^0}{2} e^{-\frac{\pi \zeta_{\text{eff}}^0}{4}} e^{-\frac{\pi}{\mathcal{F}}} \right)^2. \tag{VI.12}$$

This efficiency demonstrate maximum value 54%. The corresponding optimization condition derived from Eq. (VI.12) reads:

$$\zeta^0 \approx \frac{4}{\pi} \mathcal{F} \gg 1, \tag{VI.13}$$

$$\frac{\pi}{M \Delta t \Gamma} < \mathcal{F} < \frac{\pi}{\Delta t \Gamma}. \tag{VI.14}$$

From the left-hand-side of Eq. (VI.13) we see, for given input signal bandwidth, it is the individual effective optical thickness $\zeta_{\text{eff}}^0 = \zeta^0 / \mathcal{F}$, instead of total optical thickness $\zeta = M \zeta^0$, that plays an important role in GFC method[3]. It represents the portion of the individual optical thickness covered by the frequency comb, and has an optimized value approximately equal to $4/\pi$. The right-hand-side of Eq. (VI.13) requires a large finesse, which means that the efficient storage and retrieval of the signal demand a clean, sharp frequency comb. But this indicates a weak covering of the signal spectrum by the discrete absorption structure, making it difficult to retain the input energy and leading to a very low efficiency. Thus, correspondingly, a certain amount of the individual optical thickness ζ^0 has to be attained in order to make each comb tooth effectively wide enough to fill out the comb bandwidth, which all together translates into an optimized value of ζ_{eff}^0.

On the other hand, indeed the total optical thickness ζ eventually matters because it determines the storage bandwidth: If a shorter input photon is to be stored, in order to

---

[3]For SGEM regime, which is explained in the following of the text, in the context of its analogy to GEM method, $\zeta_{\text{eff}}^0 = 4|g|^2 N/\alpha$, where $\alpha = M \beta \omega_0 / (Md)$ is the frequency gradient. In GEM scheme this combination is the key parameter determining the action of the quantum memory [88, 91].

ensure spectrum coverage and echo's temporal resolvability, $\mathcal{F}$ has to be increased accordingly to satisfy Eq. (VI.14). Then Eq. (VI.13) requires a larger individual and/or total optical thickness. From this point of view, using an optical denser medium can help to improve the efficiency because it accommodates a shorter input signal, which allows less storage time without loosing temporal resolvability. This means the storage suffers less incoherent decay, consequently manifesting higher efficiency.

Based on Eq. (VI.11), we plot in Fig. 6.2 the efficiency of the first GFC echo as a function of different parameters. From these plots it can be seen that the analytical solution and numerical simulation agree with each other very well.

Suppose now after absorption of the input γ-ray signal all Mössbauer targets switch their velocities at a switching time $t_{\mathrm{sw}} = t_{\mathrm{in}} + T_{\mathrm{sw}}$ (t_{in} is the signal arrival time) to the opposite directions, as shown in Fig. 6.1 (b). Since the moving targets form a gradient absorption spectrum, the switching of the targets' moving directions corresponds to an inversion of an effective "artificial inhomogeneous broadening". Therefore, this scheme is resembling the GEM scheme, but in a discrete way. So similar to Chap. V, we call it stepwise gradient echo memory (SGEM). If $T_{\mathrm{sw}} > T_0$, GFC echo will appear before SGEM echo. Otherwise SGEM signal appear first at time $t = t_{\mathrm{in}} + 2T_{\mathrm{sw}}$. In such way, the retrieval time of the signal can be completely controlled (up to $2T_0$), which leads to an on-demand single γ-ray photon source. In addition, as compared to GFC regime, a series of input γ-ray signals can be retrieved in a reversed order of the input signals. Numerical simulation of the efficiency and fidelity in SGEM regime is shown in Fig. 6.3.
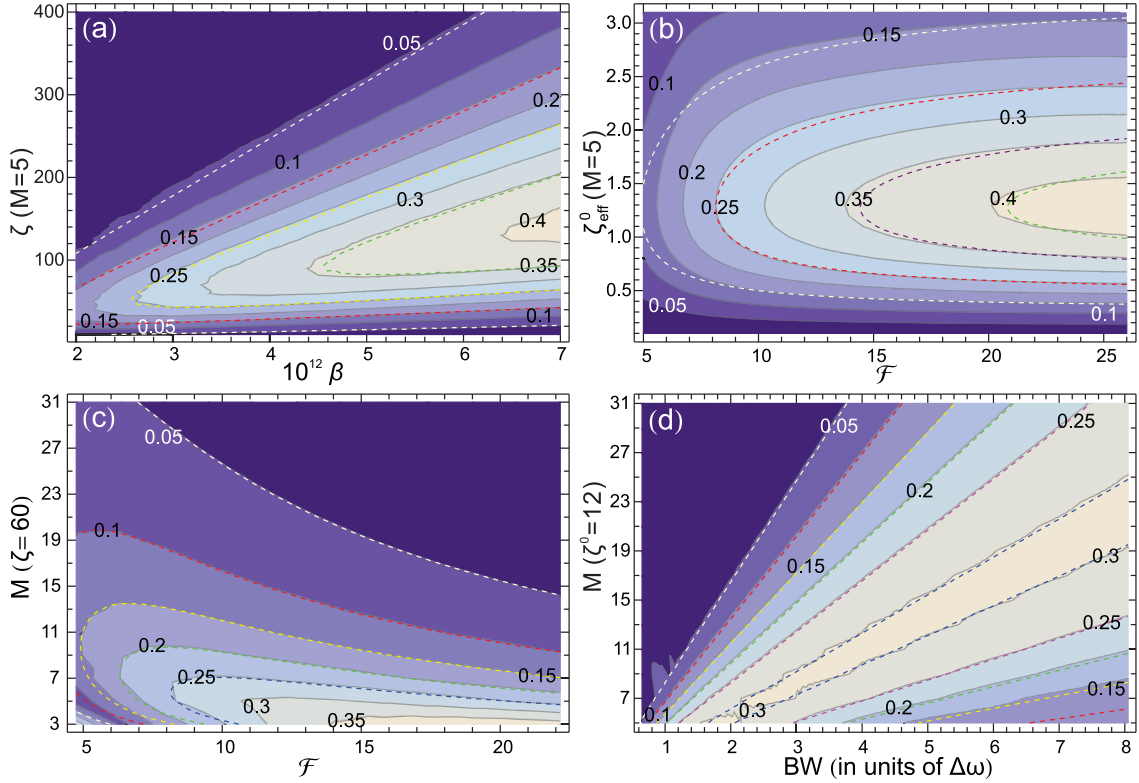
Figure 6.2: Numerical simulation (background contour plot) and analytical calculation [based on Eq. (VI.11)] (dashed line) of the efficiency of GFC first revival signal as function of different parameters. (a) Retrieval efficiency vs. total optical density ζ and velocity spacing β (multiplied by 10^{12}) for fixed number of targets $M = 5$. (b) Retrieval efficiency vs. individual effective optical thickness ζ_{eff}^0 and comb finesse $\mathcal{F}$ for fixed $M = 5$. (c) Retrieval efficiency vs. M and comb finesse $\mathcal{F}$ for fixed total optical thickness $\zeta = 60$. (d) Retrieval efficiency vs. M and comb bandwidth BW (in units of the input signal's FWHM bandwidth $\Delta\omega$) for fixed individual optical thickness $\zeta^0 = 12$. Common parameters: the FWHM duration of the input signal is $\Delta t = 23.3$ ns, and the decoherence rate is $\Gamma/(2\pi) = 0.55$ MHz.
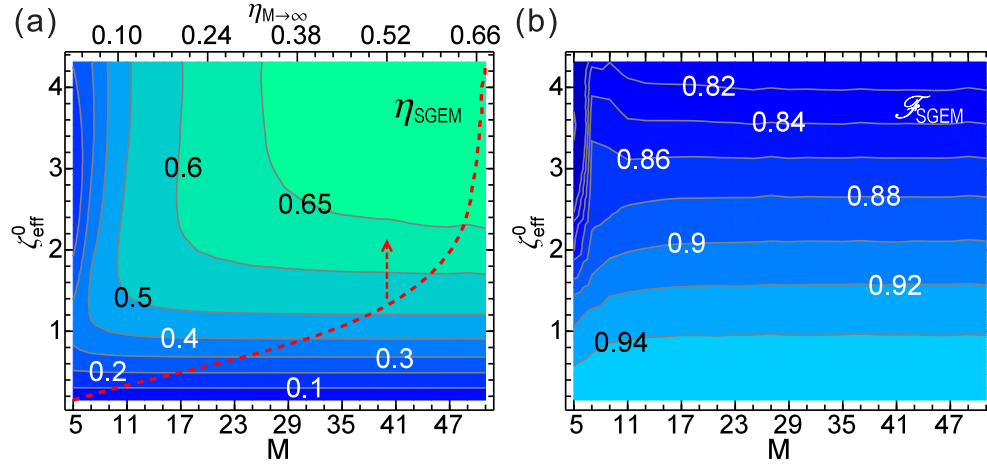
Figure 6.3: Numerical simulation of the efficiency and fidelity of the SGEM echo as a function of ζ_{eff}^0 and number of targets M. The red, dashed line in (a) shows the efficiency as a function of ζ_{eff}^0 in the continuous limit $M \to \infty$. In all cases $\Delta t = 7$ ns, $T_{\text{sw}} = 21$ ns and comb bandwidth is fixed as $M\beta\omega_0 = 2\pi/\Delta t$.

The SGEM regime does not only allow an on-demand retrieval, but also demonstrates higher possible memory efficiency. From Fig. 6.3 (a), we see that the efficiency can be larger than the upper bound 54% of GFC regime. Indeed, as a discrete version of GEM, SGEM should achieve the same 100% efficiency in its continuous limit. This is confirmed by comparing the efficiency of GEM (red dashed line) with that of SGEM (contour plot) of Fig. 6.3 (a). We see that in this particular example by using 29 targets one can already achieve the GEM performance, which demonstrates 66% efficiency. Similar to GEM, by increasing the optical thickness, the fidelity drops because of the phase modulation and amplitude deformation (see Chap. IV for relevant discussions). The relatively low efficiency (66%) is mainly due to the decoherence effect in ^{57}Fe, which might be resolved by using some other much longer lived Mössbauer isotopes (see discussions in Sec. VI.2.2).

111

VI.2.2 Experimental consideration of Doppler frequency comb: GFC, SGEM, and γ photon time processing

The experimental demonstration of our quantum memory is straightforward. Here we show an example to illustrate the physical phenomena, where the parameters are chosen to facilitate the experimental requirements while still demonstrating significant quantum memory effect. Let us consider to store a single γ-photon of field duration $\Delta t = 23.3$ ns (intensity duration 16.5 ns) with central frequency on resonance with the 14.4 keV nuclear transition of ^{57}Fe. In Ref. [197], by tuning the Mössbauer absorber into proper vibrational sideband, a γ-ray waveform of a pulse train, each with intensity duration 18 ns, is produced out of a qusi-monochromatic γ-ray radiation from radioactive decay of ^{57}Co. Much shorter pulses can be prepared by increasing the absorber vibration amplitude and/or frequency.

The single photon arrives at $t_{\text{in}} = 0$ ns, and we store it in $M = 5$ ^{57}Fe-enriched stainless-steel foils with velocity spacing $\Delta v = 0.9$ mm/s (i.e., $v_{-2,-1,0,1,2} = -1.8, -0.9, 0, 0.9, 1.8$ mm/s). The polarization decay rate is $\Gamma/(2\pi) = 0.55$ MHz, corresponding to 141 ns excited state lifetime. This gives a comb finesse of $\mathcal{F} = 9.5$. The total optical density is chosen to be $\zeta = 60.45$, so that each stainless-steel foil has individual optical density $\zeta^0 = 12.1$. The rephasing time of the GFC signal is $T_0 = 95.7$ ns. The output intensity is plotted in Fig. 6.4. The peak G_0 corresponds to the leakage field passing through the medium directly without any interaction with the nuclei, taking away 15.3% of the single photon energy. This is because the optical density of each target covered by the frequency comb is only $\zeta^0/\mathcal{F} = 1.27$, not enough to absorb the entire input photon. However, notice
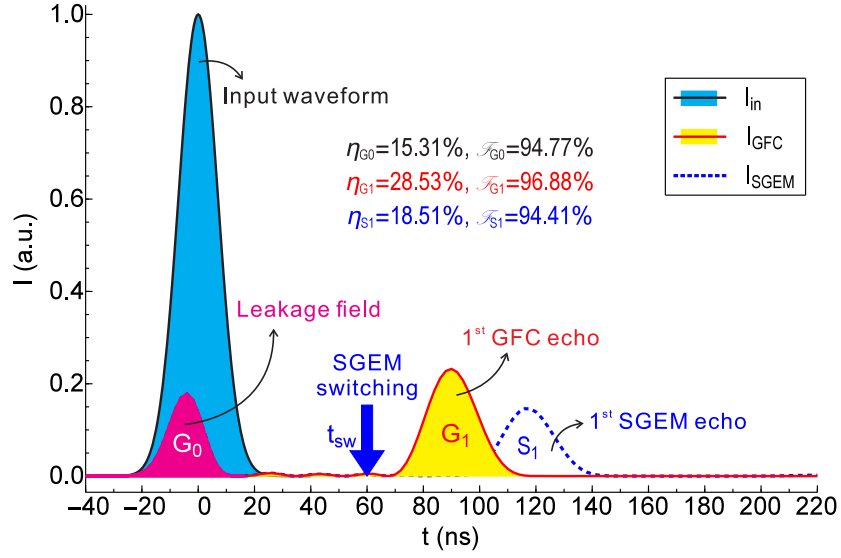
Figure 6.4: Input (black solid, cyan filled) and output GFC (red solid, yellow filled) and SGEM (blue dashed) echo intensities. The input field centers at $t_{in} = 0$ ns and has FWHM field duration 23.3 ns. The resonant medium consists of 5 identical ^{57}Fe-enriched stainless-steel foils, each with optical density $\zeta^0 = 12.1$. The rephasing time is $T_0 = 95.7$ ns, and the switching time is $t_{sw} = 60$ ns.

that from the retrieval optimization point of view, higher optical density is not beneficial for GFC scheme, although it helps to reduce the direct leakage. The peak G_1 is the first GFC echo, which contains 28.5% of the input energy. This retrieval signal preserves 96.9% of the input Gaussian shape and its phase.

In SGEM regime, the velocities are switched to the opposite at $T_{sw} = 60$ ns after t_{in}. T_{sw} is chosen to be larger than half of the input signal duration (11.7 ns) but smaller than the GFC rephasing time (95.7 ns), so that the SGEM echo is well separated in time from the input signal, and released before GFC echo can possibly be. As shown by the blue dashed line of Fig. 6.4, for SGEM scheme the leakage field is the same as in GFC scheme, while the first echo (peak S_1) emerges at the moment of time $2T_{sw} = 120$ ns after t_{in}. It contains 18.5% of the input energy, and preserves 94.4% of the original Gaussian shape

113
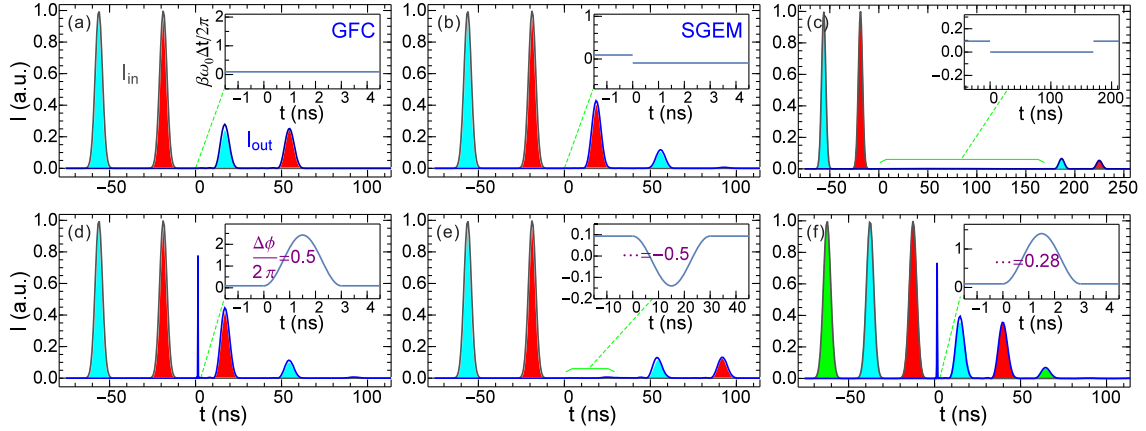
Figure 6.5: Single γ-photon processing. The solid gray (blue) lines are the multi-peak input (output) signals (leakage at $t < 0$ ns not plotted). The filled colors on top are the corresponding single-peak input (output) signals. The insets show the velocity modulation. Common parameters: $\Delta t = 7$ ns, $T_0 = 75$ ns, $\zeta = 200.6$ and $M = 13$. (a, b) GFC and SGEM echoes. (c) The echo is held by freezing the motion of all targets for 170 ns (> 141 ns excited state lifetime). (d) The targets' velocities are sinusoidally modulated during $t \in (0, 3)$ ns, producing a phase difference $\Delta\phi/(2\pi) = 0.5$. This switches the pulse order and acts as a NOT operation of a time-bin qubit. The narrow peak at $t \in (0, 3)$ ns is the loss during the modulation. (e) The modulation time T_{mod} is increased to 30 ns, during which the field is under destructive interference to suppress the loss. (f) Circular permutations of the input pulses.

and its phase.

Our scheme does not only store a single γ photon, but also perform a single-photon temporal processing. In Fig. 6.5, we show some of the photon processing functionalities with different parameters from Fig. 6.4. For instance, in SGEM regime a series of γ-ray signals is retrieved in a reversed order of the input [Fig. 6.5 (b)], which corresponds to a NOT operation of a time-bin qubit. In addition, more single-photon processing functionalities, such as a delayed and/or advanced signal retrieval, relative amplitude manipulation, signal temporal permutation, etc, can be achieved by a modulation of the targets' velocities before the emergence of the echo. For example, via freezing the motion of all

targets after absorption, we are able to hold the echo for arbitrary time allowed by the natural decoherence [Fig. 6.5 (c)]. By boosting the velocities of all the targets by the same ratio ($v_m = m\Delta v \rightarrow m\Delta v' \rightarrow m\Delta v$) during a time interval $t \in (t'_i, t'_f)$, we can impose additional phase difference of the polarizations between two adjacent targets compared with the absence of such modulation: $\Delta\phi = (\beta' - \beta)\omega_0 T'_{\text{mod}}$, where $T'_{\text{mod}} = t'_f - t'_i$ is the modulation time. As a result, the signal's first echo time is shifted to $t_{\text{in}} + \left(p - \frac{\Delta\phi}{2\pi}\right)T_0$, where $p = \left\lceil \frac{t'_f - t_{\text{in}}}{T_0} + \frac{\Delta\phi}{2\pi} \right\rceil$, $\lceil x \rceil$ represents the smallest integer greater than or equal to x. In this way we can address any individual signal peak among a series of them as we want. In fact, as long as the desired phase shift is produced, such modulation does not need to be square-shape [Fig. 6.5 (d, e-f)], neither necessarily to be of very high speed [Fig. 6.5 (e)]. Our scheme makes quantum information processing possible in the γ-ray regime, and can also be used for generating single γ photon on demand.

The above example are all based on ^{57}Fe. Longer photons with duration over a few nanoseconds can be efficiently stored in targets with longer lived Mössbauer nuclear transitions, such as 93.3 keV transition in ^{67}Zn with coherence time 13.6 μs [208]. Mössbauer transitions with lifetimes much longer than tens of microseconds, such as 12.4 keV transition in ^{45}Sc with lifetime 0.46 s and 88.0 keV transition in ^{109}Ag with lifetime 57.1 s [208], are typically inhomogeneously broadened due to magnetic dipole-dipole interactions [209]. Potentially, these interactions may be suppressed using techniques similar to those developed in nuclear magnetic resonance (see Ref. [210] and references therein), providing extraordinarily long storage time.

VI.3   Fast control of a γ photon's Bragg mode

We have suggested a way to manipulate the temporal mode of a single γ photon by a Doppler frequency comb. Next we discuss an all-optical method to control the Bragg mode of a γ-ray beam by nuclear vibration [211]. The fundamental principle of this method lies in the collective behavior of nuclear ensembles and a parametric coupling between different Bragg modes of the γ-ray field.

Collective spontaneous emission from atomic ensembles has been a subject of long standing interest since 1954 pioneering work of Dicke [92]. Collective nature of light interaction yields fascinating effects such as superradiance and radiation trapping even at the single-photon level. Recent studies focus on collective, virtual and nonlocal effects in such systems [93, 96, 98, 212--224].

Interaction of light with ordered arrays of nuclei in crystals offers new perspectives. For example, a photon collectively absorbed by a random medium (e.g. gas) will be reemitted in the same direction as the incident photon [98]. However, in the case of a crystal lattice, collective reemission can occur in several directions at Bragg angles.

Parametric process is a fascinating phenomenon which has been widely applied to nonlinear optical systems for the development of coherent light sources ranging from infrared to ultraviolet frequency regimes [225--227], especially at the spectral regions that lasers are difficult to operate. A typical example is optical parametric oscillator [228], which transfers energy from a driving optical electromagnetic wave to two other waves named as signal and idler. The frequency of these three waves are ν_d, ω_s and ω_i, respec-

tively, satisfying $v_d = \omega_s + \omega_i$. This is called sum combination resonance. Another type of two-mode parametric phenomenon is called difference combination resonance, where $v_d = |\omega_s - \omega_i|$. This is the mechanism of the recently proposed quantum amplification by superradiant emission of radiation [229], and parametric generation of high frequency coherent light in negative index materials and materials with strong anomalous dispersion [230]. All the above parametric resonances aim at reaching an instability of the system for the amplification of a signal wave. This is achieved with a symmetric coupling in the sum combination resonance or anti-symmetric coupling in the difference combination resonance. In the case when the symmetries of the coupling is reversed in these two types of parametric resonance, no instabilities can be developed. However, the time evolution of the system is dramatically changed because of the parametric processes. Here, in our case, we implement the difference combination resonance which does not amplify the input γ-ray wave but instead only modifies its time evolution of coupled spatial (Bragg) modes. This is suitable for quantum information application, where the amplification of an input photon is not permitted at the first place.

All these underlying physics are implemented by vibrating nuclear Mössbauer lattice. Nuclear vibrations can be generated by a driving laser field and can be turned on and off on a short time scale. γ-ray redirection, produced by parametric resonance, occurs on a time scale determined by the collective nuclear frequency Ω_a which typically lies in the terahertz region. This mechanism allows us to control propagation of high frequency γ photons by driving the system, e.g., with infrared laser.
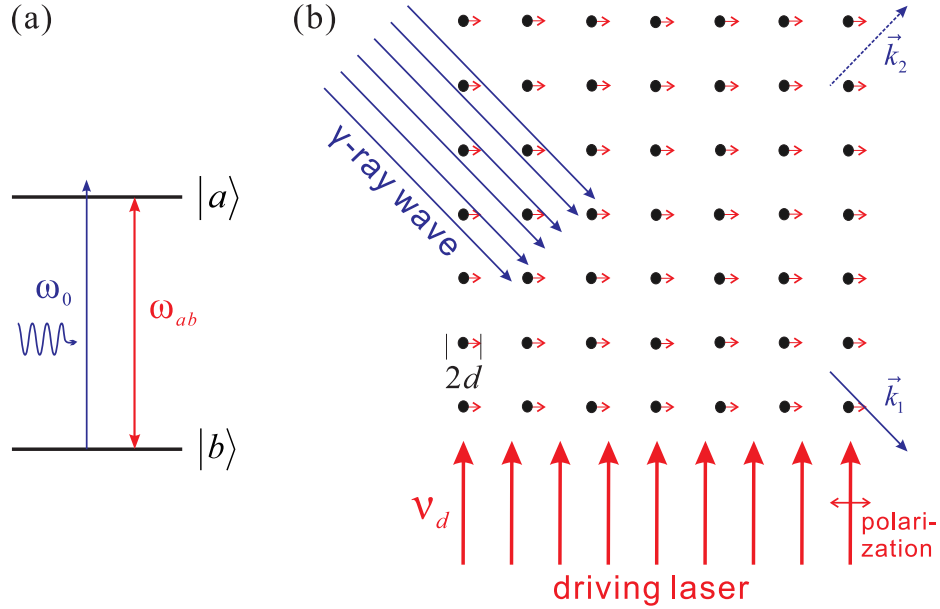
Figure 6.6: Illustration of superradiant control of a γ photon's propagation direction. (a) Energy diagram of the two-level nuclear system. (b) An incident γ-ray plane wave interacts collectively with a recoilless nuclear array, while the strong optical laser field produces coherent oscillations of the nuclei with amplitude d and frequency ν_d.

VI.3.1 Theoretical model for the interaction between γ ray and vibrating nuclear lattice

We consider a perfect crystal composed of two-level ($|a\rangle$ and $|b\rangle$) nuclei with transition frequency ω_{ab} as shown in Fig. 6.6 (a). Nuclear transition frequency ω_{ab} typically lies in the hard x-ray or γ-ray region. Nuclei are located at positions $\mathbf{r}_j$ and form a periodic lattice, where the index j labels different nuclei. In the high frequency region of γ transition, the inter nuclei spacing is much larger than the nuclear radiation wave length $\lambda_{ab} = 2\pi c/\omega_{ab}$.

We assume that lattice is coherently excited so that nuclei oscillate along the direction given by a unit vector $\hat{n}$ around their equilibrium positions $\mathbf{r}_j^0$. Oscillation frequency ν_d

lies in the infrared or visible region. In ionic crystals[4] such oscillations can be produced, e.g., by a strong linearly polarized driving laser with frequency ν_d. The motion of each nucleus j involved in the γ-ray-nuclei interaction is assumed to be

$$\mathbf{r}_j(t) = \mathbf{r}_j^0 + \hat{n}f(t), \tag{VI.15}$$

where $f(t) = d\sin(\nu_d t)$. Here $\nu_d \ll \omega_{ab}$ and $d \lesssim \lambda_{ab}$ is the amplitude of the laser induced nuclei oscillations.

In our model a weak plane linearly polarized γ-ray wave with the wave vector $\mathbf{k}_1$ and frequency $\omega_0 = ck_1$ detuned from the nuclear transition frequency ω_{ab} by an amount $\Delta \ll \omega_{ab}$ enters the crystal and collectively interacts with the oscillating recoilless nuclei [see Fig. 6.6 (b)]. For the sake of simplicity, we only consider the interaction of the wave with the nuclei and disregard its interaction with electrons. Processes such as internal conversion, photoelectric effect [232], electron Rayleigh scattering [233, 234], etc., are neglected.

We treat the problem in semiclassical formalism. Namely, electromagnetic field $E(t, \mathbf{r})$ of the γ-ray is described by classical Maxwell's equation:

$$\left(c^2\nabla^2 - \frac{\partial^2}{\partial t^2}\right)\Omega_\gamma(t,\mathbf{r}) = \frac{c^2\mu_0|d_{ab}|^2}{\hbar}\frac{\partial^2}{\partial t^2}\sum_j \left(\rho_{ab}^j + c.c.\right)\delta(\mathbf{r} - \mathbf{r}_j(t)), \tag{VI.16}$$

where μ_0 is the vacuum permeability, ρ_{ab}^j is the off-diagonal elements of the nuclear density matrix, d_{ab} is the nuclear transition matrix element, $\Omega_\gamma(t,\mathbf{r}) = d_{ab}E(t,\mathbf{r})/\hbar$ is the Rabi

---

[4]One example is potassium iodide KI crystal which has face-centered cubic unit cell of iodide ions with potassium ions in octahedral holes. By applying an external driving field one can make ions K^+ and I^- move in the opposite directions such that nuclei of the same species will oscillate in unison. Both K and I have Mössbauer isotopes. Namely, ^{40}K has Mössbauer transition with energy 29.4 keV and half lifetime 4.26 ns, while ^{127}I has transition with energy 57.6 keV and half lifetime 1.9 ns [231].

frequency of the γ-ray field. Eq. (VI.16) must be supplemented by the evolution equation for the nuclear density matrix

$$\frac{\partial \rho_{ab}^j(t)}{\partial t} = -i\omega_{ab}\rho_{ab}^j(t) + i\Omega_\gamma(t,\mathbf{r}_j(t))(1 - 2\rho_{aa}^j). \tag{VI.17}$$

We assume that nuclear excitation remains weak so that population of the excited state ρ_{aa}^j can be neglected. We look for solution in the form

$$\Omega_\gamma(t,\mathbf{r}) = \Omega(t,\mathbf{r})e^{-i\omega_{ab}t} + c.c., \tag{VI.18}$$

$$\rho_{ab}^j(t) = \rho^j(t)e^{-i\omega_{ab}t}, \tag{VI.19}$$

where $\Omega(t,\mathbf{r})$ and $\rho^j(t)$ are slowly varying functions of t as compared to the fast oscillating exponentials. In the slowly varying amplitude approximation, Eqs. (VI.16) and (VI.17) reduce to

$$\left(\frac{\partial}{\partial t} + \frac{c^2}{2i\omega_{ab}} \left[\left(\frac{\omega_{ab}}{c}\right)^2 + \nabla^2 \right] \right) \Omega(t,\mathbf{r}) = i\frac{\Omega_a^2}{N} \sum_j \rho^j(t)\delta(\mathbf{r} - \mathbf{r}_j(t)), \tag{VI.20}$$

$$\frac{\partial \rho^j(t)}{\partial t} = i\Omega(t,\mathbf{r}_j(t)), \tag{VI.21}$$

where $\Omega_a = \sqrt{c^2\mu_0|d_{ab}|^2\omega_{ab}N/(2\hbar)}$ is collective nuclei frequency proportional to the square root of the average nuclei density N. Physically, Ω_a determines the time scale of the collective resonant absorption of the incident photon by the medium [93, 224, 235] and typically is of the order of terahertz. For example, for the 29.4 keV transition of ^{40}K Mössbauer isotope with nuclei density $N = 8 \times 10^{21}$ cm^{-3}, the collective nuclei frequency is $\Omega_a \sim 3 \times 10^{11}$ s^{-1}.

In a crystal, the periodic arrangement of atoms (Bravais lattice) makes $\sum_j \delta\left(\mathbf{r} - \mathbf{r}_j(t)\right)$ a periodic function of $\mathbf{r}$. As a result, we have the following Fourier se-

ries:

$$\sum_j e^{i\mathbf{k}_1 \cdot \mathbf{r}_j^0} \delta(\mathbf{r} - \mathbf{r}_j(t)) = N \sum_m e^{i(\mathbf{k}_1 + \mathbf{K}_m) \cdot [\mathbf{r} - \hat{n}f(t)]}. \tag{VI.22}$$

If we look for $\rho^j(t)$ in the form

$$\rho^j(t) = \rho(t) e^{i\mathbf{k}_1 \cdot \mathbf{r}_j^0}, \tag{VI.23}$$

Eq. (VI.22) then enters the right hand side of Eq. (VI.20). In the Fourier series (VI.22) we are interested in terms that are in resonance with the left hand side of Eq. (VI.20). For simplicity we assume that only two vectors, namely, $\mathbf{k}_1$ and $\mathbf{k}_2 = \mathbf{k}_1 + \mathbf{K}_b$ have absolute values close to ω_{ab}/c, where $\mathbf{K}_b$ is a reciprocal lattice vector (see Fig. 6.7). The other terms in (VI.22) are off-resonant and, thus, can be disregarded. Therefore, one can approximately write

$$\sum_j e^{i\mathbf{k}_1 \cdot \mathbf{r}_j^0} \delta(\mathbf{r} - \mathbf{r}_j(t)) \approx N e^{-i\mathbf{k}_1 \cdot \hat{n}f(t)} e^{i\mathbf{k}_1 \cdot \mathbf{r}} + N e^{-i\mathbf{k}_2 \cdot \hat{n}f(t)} e^{i\mathbf{k}_2 \cdot \mathbf{r}}. \tag{VI.24}$$

This approximation implies that the incident wave $\mathbf{k}_1$ is coupled only with one Bragg wave $\mathbf{k}_2$.

Equation (VI.24) suggests to look for solution for $\Omega(t, \mathbf{r})$ in the form of a superposition of these coupled waves

$$\Omega(t, \mathbf{r}) = \Omega_1(t) e^{i\mathbf{k}_1 \cdot \mathbf{r}} + \Omega_2(t) e^{i\mathbf{k}_2 \cdot \mathbf{r}}. \tag{VI.25}$$

Then Eqs. (VI.20) and (VI.21) yield the following equations after eliminating the variable $\rho(t)$:

$$\left(\frac{\partial}{\partial t} + i\mathbf{k}_1 \cdot \hat{n}\dot{f}\right)\left(\frac{\partial}{\partial t} + i\Delta\right)\Omega_1 + \Omega_a^2 \left[\Omega_1 + \Omega_2 e^{-i(\mathbf{k}_1 - \mathbf{k}_2) \cdot \hat{n}f(t)}\right] = 0, \tag{VI.26}$$

$$\left(\frac{\partial}{\partial t} + i\mathbf{k}_2 \cdot \hat{n}\dot{f}\right)\left(\frac{\partial}{\partial t} + i\Delta\right)\Omega_2 + \Omega_a^2 \left[\Omega_2 + \Omega_1 e^{i(\mathbf{k}_1 - \mathbf{k}_2) \cdot \hat{n}f(t)}\right] = 0. \tag{VI.27}$$
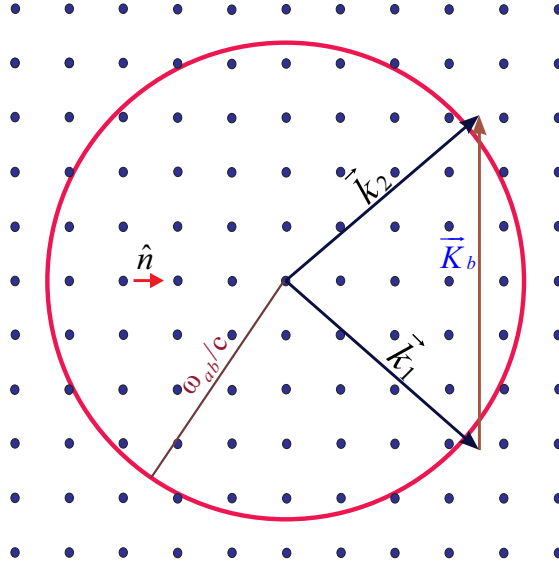
Figure 6.7: Two dimensional reciprocal lattice of the crystal is shown by dots. The incident γ-ray beam with the wave vector $\mathbf{k}_1$ is detuned from the nuclear transition frequency ω_{ab}. The incident wave is coupled with the Bragg wave that has wave vector $\mathbf{k}_2 = \mathbf{k}_1 + \mathbf{K}_b$, where $\mathbf{K}_b$ is a reciprocal lattice vector.

where $\Delta = c^2 k_{1,2}^2 - \omega_{ab}^2/(2\omega_{ab}) \approx \omega_0 - \omega_{ab}$ are detunings of the two coupled waves $\Omega_{1,2}$ from the nuclear transition frequency ω_{ab}.

Equations (VI.26) and (VI.27) describe two coupled harmonic oscillators whose parameters periodically change in time. The variation of the parameters sitting in $f(t)$ drives the system dynamically. Namely, nuclei vibrations modulate the coupling (which is $\Omega_a^2 e^{\pm i(\mathbf{k}_1 - \mathbf{k}_2) \cdot \hat{n} f(t)}$) between two oscillators, and, in addition change their frequencies by means of the Doppler shift (described by $i\mathbf{k}_{1,2} \cdot \hat{n} \dot{f}$). The presence of modulations on both coupling constant and eigen frequencies ensures an energy conservation of the γ-ray-nuclei system, prohibiting a power flow coming from the lattice vibration [211]. The energy conversion between the two Bragg modes of the γ-ray field [or the two harmonic oscillators as seen from Eqs. (VI.26) and (VI.27)], however, constantly happens with its dynamics

122

modified by the parametric driving. This allows a fast switch of γ-ray propagation.

VI.3.2 γ-ray beam deflection by coherent nuclear lattice vibration

From now on we consider the system with initial condition $\Omega_1(0) = A$, $\Omega_2(0) = 0$ and $\rho(0) = 0$. Then it is straightforward to find the analytical solution of Eqs. (VI.26) and (VI.27) in the case of static lattice ($f = 0$), which is reads:

$$\Omega_1(t) = \frac{Ae^{-i\Delta t}}{2} \left[\frac{\omega_+ e^{i\omega_- t} - \omega_- e^{i\omega_+ t}}{\sqrt{\Delta^2 + 8\Omega_a^2}} + 1 \right], \tag{VI.28}$$

$$\Omega_2(t) = \frac{Ae^{-i\Delta t}}{2} \left[\frac{\omega_+ e^{i\omega_- t} - \omega_- e^{i\omega_+ t}}{\sqrt{\Delta^2 + 8\Omega_a^2}} - 1 \right], \tag{VI.29}$$

where $\omega_\pm = \left(\Delta \pm \sqrt{\Delta^2 + 8\Omega_a^2} \right) \Big/ 2$.

The solution (VI.28) - (VI.29) shows that the input energy is periodically transferred back and forth between two coupled waves on a time scale determined by the collective nuclear frequency Ω_a and photon detuning Δ. Specifically, let us consider an off-resonant interaction $\Delta \ll \Omega_a$, then this energy transformation between beams Ω_1 and Ω_2 occurs during a time

$$t_{\text{tr}}^0 = \frac{\pi}{|\omega_-|} \approx \frac{\pi|\Delta|}{2\Omega_a^2}. \tag{VI.30}$$

If we turn on the driving laser to vibrate the lattice, this transformation time changes. We assume that nuclei vibrate with amplitude d along the direction $\hat{n}$ perpendicular to $\mathbf{k}_1 - \mathbf{k}_2$, so that $\mathbf{k}_1 \cdot \hat{n} = \mathbf{k}_2 \cdot \hat{n}$, as indicated in Fig. 6.7. In the following we introduce a

dimensionless modulation amplitude[5]

$$\kappa = d\mathbf{k}_1 \cdot \hat{n}. \tag{VI.31}$$

In the case of when driving frequency matches the γ-ray photon detuning $\nu_d = \Delta$, Eqs. (VI.26) and (VI.27) can be approximately solved as (see Appendix E):

$$\Omega_1 = A e^{-i\Delta t} \cos^2 \left(\frac{J_1(\kappa)}{\sqrt{2}} \Omega_a t \right), \tag{VI.32}$$

$$\Omega_2 = -A e^{-i\Delta t} \sin^2 \left(\frac{J_1(\kappa)}{\sqrt{2}} \Omega_a t \right). \tag{VI.33}$$

Equations (E.15) and (E.16) show that the rate of energy transfer between two coupled waves depends on the amplitude of the nuclear vibrations. The optimum value of the modulation amplitude κ corresponds to maximum of $J_1(\kappa)$, that is $\kappa = 1.841$ which gives $J_1(\kappa)/\sqrt{2} = 0.411$. For larger κ the transfer rate oscillates following $J_1(\kappa)$.

For $\kappa \ll 1$ one can use expansion $J_1(\kappa) \approx \kappa/2$. Then from Eq. (E.16), the energy transfer time between two waves becomes

$$t_{\text{tr}} = \frac{\sqrt{2}\pi}{\kappa \Omega_a}. \tag{VI.34}$$

Comparing Eq. (VI.30) with Eq. (VI.34), it is seen that when the incident γ-ray wave Ω_1 is off-resonant with the nuclear transition, the time it takes for the energy to transfer from Ω_1 into the deflected wave Ω_2 can substantially vary with or without nuclear vibrations. In the regime $\kappa\Delta \gg \Omega_a$ and $\nu_d = \Delta$, this realizes a fast switching of the wave propagation.

As an example, in Fig. 6.8 we demonstrate the switching effect for a medium with

---

[5]In practical implantation, the amplitude of the nuclei vibrations d is much smaller than spacing a between nuclei. However, since the wave length of the nuclear transition is also small compared to a the modulation amplitude κ could be of the order of 1.
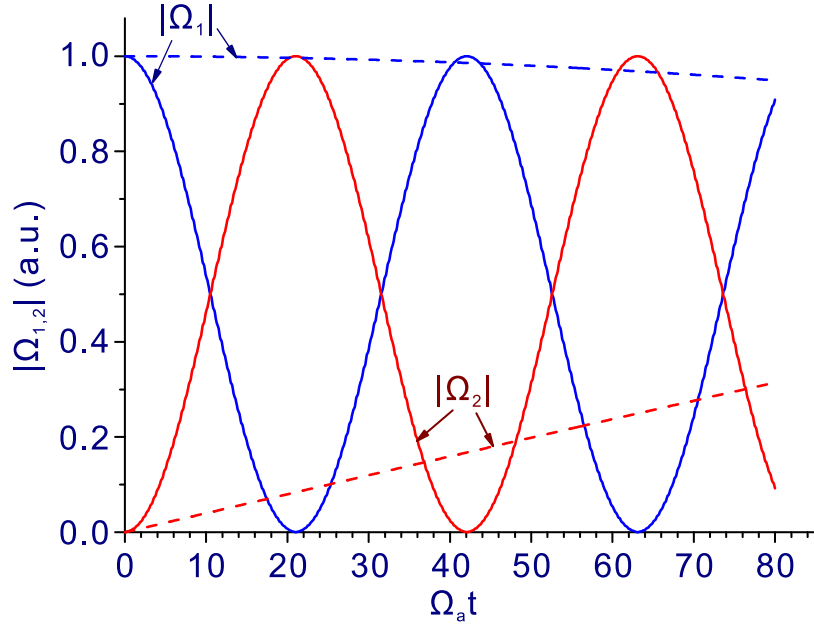
Figure 6.8: Illustration of the fast γ-ray switch operation. The incident γ-ray mode Ω_1 is detuned from the nuclear transition by $\Delta = 250\Omega_a$. Dash lines show transformation of mode Ω_1 into Ω_2 in a static crystal, while solid lines show such transformation in a nuclear array vibrating with frequency $\nu_d = \Delta$ and modulation amplitude $\kappa = 0.21$.

$\Omega_a = 0.8$ THz assuming that the incident wave is detuned from the nuclear transition by $\Delta = 250\Omega_a$. For a static crystal the amplitude of γ-ray modes Ω_1 and Ω_2 are plotted by dash lines in the figure. Without nuclear vibrations it takes $t_{\text{tr}}^0 = 491$ ps for the wave Ω_1 to convert into Ω_2. This means that if the crystal size is smaller than $ct_{\text{tr}}^0 = 15$ cm, the incident wave passes through. However, if the nuclear array vibrates with modulation frequency $\nu_d = \Delta$ and amplitude $\kappa = 0.21$, the transformation time becomes $t_{\text{tr}} = 26$ ps, therefore the wave will be deflected at a length of 0.8 cm (shown by solid lines in Fig. 6.8). In the case of ^{40}K, such modulation strength corresponds to an amplitude $d = 1.3 \times 10^{-3}$ nm.

Thus we show that one can redirect a γ-ray beam by making the crystal lattice coherently vibrate with frequency Δ which lies, e.g., in the infrared region. Such lattice vi-

125

brations are in the parametric resonance with the frequency difference between two eigen-modes of the coupled γ-ray-nuclei system, and modify the fields' collective absorption and reemission among many nuclei. This results in a resonant energy transfer from the incident γ-ray field to the wave propagating at the Bragg angle. Our findings could be used for manipulation of the propagation direction of γ photons on a picosecond time scale.

VI.4   Conclusion

In this chapter, we first propose a scheme to achieve quantum storage and time processing of a single γ photon by using Doppler frequency comb, and then suggest a method to realize the fast control of the propagation direction of input γ-ray field using vibrating nuclear lattice. These schemes are important for quantum information processing in the γ-ray regime.

With this we can envision some quantum computing applications based on the recent studies on time-bin qubit and quantum memory. Quantum memory can be used for building logical gates [17], where the required frequency-multiplexing might be realized by a velocity offset of the Mössbauer targets in γ-ray regime. Also, the single-spatial mode time-bin qubit can be used to perform linear optical quantum computing [27], in which the ingredient of polarization manipulation may be achieved in Mössbauer solid of iron borate (instead of the present two-level system in stainless steel) controlled by weak magnetic field [196, 205, 236].

For direct applications, our storage scheme can be used as a way to prepare and pro-

cess on-demand single photons, or synchronize multiple photons in γ-ray regime. The fast switching scheme further adds more controllability to these functionalities. The coherence of these photons depends on the source. If radioactive source is used, these photons will be inchoerent. The coherent sources are still being developed. The x-ray parametric down conversion [193] is experimentally demonstrated but currently still operated at very low efficiency. A tabletop creation of entangled keV photon pairs is theoretically suggested [237] using Unruh effect. In principle, the γ-ray source by x-ray free electron laser that is delivering ~ 10 coherent γ photons within the absorption bandwidth of ^{57}Fe may facilitate the development of entangled γ photons.

Doppler frequency comb can also prepare a single-peak γ photon into a time-bin waveforms by optimizing the leakage field and the first echo (though does not explore the whole Bloch sphere due to fixed phase relation between different peaks of the output waveform). As in AFC, a double gradient frequency comb can be used to implement an in-medium interferometer, which, in general, could be very useful since γ-ray interferometer is more difficult to build than in optical range. Vibrating nuclear array, on the other hand, combines rich physical phenomena of Dicke superradiance, Bragg diffraction and parametric resonance. It holds promise for being engineered into an interesting and important tool for γ photon manipulation.

CHAPTER VII

CONCLUSIONS

Quantum information, such as quantum computing and quantum communication, has attracted lots of attention since being suggested in the 1980s, and was vastly developed over the last twenty years. Many different architectures and quantum interfaces were intensively studied in different areas of physics, including ion trap, superconducting qubit, nuclear magnetic resonance, quantum dots, etc. Optical system is one of the major promising candidates for the implementation of quantum information processing, ranging from long-distance quantum key distribution to local quantum calculation. In such a system, optical quantum memory plays a crucial role in a quantum computing or quantum communicating machine.

In the optical realization of quantum memory, the study of light-matter-ensemble interface is essential for the development of building blocks of quantum information processing devices. From this point of view, there are several important theoretical tasks one needs to consider, including: Deriving mathematical formulism that easily treats such a complicated full-quantum-mechanical single-photon problem; developing new quantum interface that resolves many disadvantages of the existing ones; designing new schemes based on these interfaces for different functionalities in the real-world quantum information applications.

The mathematical formulation was developed for ensemble-based quantum memo-

ries and various related problems in many literatures, such as Refs. [101, 238]. Recently we showed that the full quantum mechanical problem of single-photon superradiance can be treated in the semi-classical approach of Maxwell-bloch formulism [97]. In this dissertation we primarily adopt Maxwell-bloch equation to describe our system.

The quantum interfaces we treated and proposed fall into two categories: optical-electronic interface and γ-ray-nuclear interface. The theoretical treatments are analogous, but the physical features are substantially different. The discussion of the former includes cold rubidium gas system and solid state system such as nitrogen-vacancy centers in diamond, silicon-vacancy centers in diamond, and rare-earth-doped crystals. The corresponding photons is at ~ 1 eV level. Current studies of optical quantum information all belong to this optical frequency regime. In order to resolve some of the difficulties in the optical-electronic platform, we propose the latter interface for quantum information operating at ~ 10 - 100 keV. The discussion of this interface focuses on Mösbauer solid, in pedicular, ^{57}Fe enriched stainless-steel foils [207]. In addition to the quantum memory and processing of the γ photon's temporal mode, we also proposed a laser-controlled picosecond switch of its Bragg mode using superradiant and parametric effect [211]. Each of the atomic and nuclear systems demonstrates its own advantages for quantum information.

On the proposed quantum interfaces, we designed new schemes for optical quantum memory based on the collective interaction between a single photon and an atomic ensemble. Generally speaking, we are seeking for quantum storage methods that on-demand and standby recover and processe single-photon temporal waveform with high efficiency and

fidelity, which are implementable in as many systems as possible without relying on complicated preparation techniques. So we proposed several schemes satisfying these requirements, including quantum memories based on phase matching control [88, 90], control field spatial chirp [91] and its discrete version [173, 176], and Doppler frequency comb [207] in nuclear system. We also discovered that the natural decay of atomic excitation due to its interaction with the environment could be completely suppressed in atomic shell configuration [239], which leads to a radiation trapping in such a system and, in principle, could allow an extraordinarily long storage time of a photon.

We hope these quantum memory schemes will facilitate the advancing of optical quantum information science and technology, and the corresponding theoretical treatment can help the understanding of light-matter interaction in general.

REFERENCES

[1] D. P. DiVincenzo, Fortschr. Phys. **48**, 771 (2000).

[2] R. P. Feynman, Int. J. Theor. Phys. **21**, 467 (1982).

[3] D. Deutsch, Proc. R. Soc. London, Ser. A **400**, 97 (1985).

[4] M. Genovese, Phys. Reports-Review Sect. Phys. Lett. **413**, 319 (2005).

[5] N. Brunner, D. Cavalcanti, S. Pironio, V. Scarani, and S. Wehner, Rev. Mod. Phys. **86**, 419 (2014).

[6] X.-S. Ma, T. Herbst, T. Scheidl, D. Wang, S. Kropatschek, W. Naylor, B. Wittmann, A. Mech, J. Kofler, E. Anisimova, V. Makarov, T. Jennewein, R. Ursin, and A. Zeilinger, Nat. **489**, 269 (2012).

[7] A. Rubenok, J. A. Slater, P. Chan, I. Lucio-Martinez, and W. Tittel, Phys. Rev. Lett. **111**, 130501 (2013).

[8] Y.-L. Tang, H.-L. Yin, S.-J. Chen, Y. Liu, W.-J. Zhang, X. Jiang, L. Zhang, J. Wang, L.-X. You, J.-Y. Guan, D.-X. Yang, Z. Wang, H. Liang, Z. Zhang, N. Zhou, X. Ma, T.-Y. Chen, Q. Zhang, and J.-W. Pan, Phys. Rev. Lett. **113**, 190501 (2014).

[9] A. I. Lvovsky, B. C. Sanders, and W. Tittel, Nat. Photonics **3**, 706 (2009).

[10] C. Simon, M. Afzelius, J. Appel, A. B. de la Giroday, S. J. Dewhurst, N. Gisin, C. Y. Hu, F. Jelezko, S. Kröll, J. H. Müller, J. Nunn, E. S. Polzik, J. G. Rarity,

H. De Riedmatten, W. Rosenfeld, A. J. Shields, N. Sköld, R. M. Stevenson, R. Thew, I. A. Walmsley, M. C. Weber, H. Weinfurter, J. Wrachtrup, and R. J. Young, Eur. Phys. J. D **58**, 1 (2010).

[11] W. Tittel, M. Afzelius, T. Chanelière, R. L. Cone, S. Kröll, S. A. Moiseev, and M. Sellars, Laser & Photonics Rev. **4**, 244 (2010).

[12] N. Sangouard, C. Simon, H. de Riedmatten, and N. Gisin, Rev. Mod. Phys. **83**, 33 (2011).

[13] F. Bussières, N. Sangouard, M. Afzelius, H. de Riedmatten, C. Simon, and W. Tittel, J. Mod. Opt. **60**, 1519 (2013).

[14] M. Afzelius, N. Gisin, and H. de Riedmatten, Phys. Today **68**, 42 (2015).

[15] H. J. Briegel, W. Dür, J. I. Cirac, and P. Zoller, Phys. Rev. Lett. **81**, 5932 (1998).

[16] C. A. Pérez-Delgado and P. Kok, Phys. Rev. A **83**, 012303 (2011).

[17] G. T. Campbell, O. Pinel, M. Hosseini, T. C. Ralph, B. C. Buchler, and P. K. Lam, Phys. Rev. Lett. **113**, 063601 (2014).

[18] A. Imamoḡlu, Phys. Rev. Lett. **89**, 163602 (2002).

[19] D. F. V. James and P. G. Kwiat, Phys. Rev. Lett. **89**, 183601 (2002).

[20] K. Honda, D. Akamatsu, M. Arikawa, Y. Yokoi, K. Akiba, S. Nagatsuka, T. Tanimura, A. Furusawa, and M. Kozuma, Phys. Rev. Lett. **100**, 093601 (2008).

[21] J. Appel, E. Figueroa, D. Korystov, M. Lobino, and A. I. Lvovsky, Phys. Rev. Lett. **100**, 093602 (2008).

[22] J. Appel, P. J. Windpassinger, D. Oblak, U. B. Hoff, N. Kjaergaard, and E. S. Polzik, Proc. Natl. Acad. Sci. United States Am. **106**, 10960 (2009).

[23] D. L. McAuslan, L. R. Taylor, and J. J. Longdell, Appl. Phys. Lett. **101**, 191112 (2012).

[24] A. V. Tsukanov, Russ. Microelectron. **42**, 127 (2013).

[25] N. Gisin, J. P. V. d. Weid, and J. P. Pellaux, J. Light. Technol. **9**, 821 (1991).

[26] J. Brendel, N. Gisin, W. Tittel, and H. Zbinden, Phys. Rev. Lett. **82**, 2594 (1999).

[27] P. C. Humphreys, B. J. Metcalf, J. B. Spring, M. Moore, X. M. Jin, M. Barbieri, W. S. Kolthammer, and I. A. Walmsley, Phys. Rev. Lett. **111**, 150501 (2013).

[28] J. I. Cirac, P. Zoller, H. J. Kimble, and H. Mabuchi, Phys. Rev. Lett. **78**, 3221 (1997).

[29] A. D. Boozer, A. Boca, R. Miller, T. E. Northup, and H. J. Kimble, Phys. Rev. Lett. **98**, 193601 (2007).

[30] H. P. Specht, C. Nölleke, A. Reiserer, M. Uphoff, E. Figueroa, S. Ritter, and G. Rempe, Nat. **473**, 190 (2011).

[31] K. Hammerer, A. S. Sørensen, and E. S. Polzik, Rev. Mod. Phys. **82**, 1041 (2010).

[32] T. Chanelière, D. N. Matsukevich, S. D. Jenkins, S. Y. Lan, T. A. B. Kennedy, and A. Kuzmich, Nat. **438**, 833 (2005).

[33] M. D. Eisaman, A. André, F. Massou, M. Fleischhauer, A. S. Zibrov, and M. D. Lukin, Nat. **438**, 837 (2005).

[34] I. Novikova, A. V. Gorshkov, D. F. Phillips, A. S. Sørensen, M. D. Lukin, and R. L. Walsworth, Phys. Rev. Lett. **98**, 243602 (2007).

[35] K. S. Choi, H. Deng, J. Laurat, and H. J. Kimble, Nat. **452**, 67 (2008).

[36] G. Heinze, C. Hubrich, and T. Halfmann, Phys. Rev. Lett. **111**, 033601 (2013).

[37] Y.-H. Chen, M.-J. Lee, I. C. Wang, S. Du, Y.-F. Chen, Y.-C. Chen, and I. A. Yu, Phys. Rev. Lett. **110**, 083601 (2013).

[38] K. F. Reim, J. Nunn, V. O. Lorenz, B. J. Sussman, K. C. Lee, N. K. Langford, D. Jaksch, and I. A. Walmsley, Nat. Photonics **4**, 218 (2010).

[39] K. F. Reim, P. Michelberger, K. C. Lee, J. Nunn, N. K. Langford, and I. A. Walmsley, Phys. Rev. Lett. **107**, 053603 (2011).

[40] K. F. Reim, J. Nunn, X. M. Jin, P. S. Michelberger, T. F. M. Champion, D. G. England, K. C. Lee, W. S. Kolthammer, N. K. Langford, and I. A. Walmsley, Phys. Rev. Lett. **108**, 263602 (2012).

[41] P. J. Bustard, R. Lausten, D. G. England, and B. J. Sussman, Phys. Rev. Lett. **111**, 083901 (2013).

[42] D. G. England, P. J. Bustard, J. Nunn, R. Lausten, and B. J. Sussman, Phys. Rev. Lett. **111**, 243601 (2013).

[43] A. Hayat, X. X. Xing, A. Feizpour, and A. M. Steinberg, Opt. Express **20**, 29174 (2012).

[44] G. Hétet, J. J. Longdell, M. J. Sellars, P. K. Lam, and B. C. Buchler, Phys. Rev. Lett. **101**, 203601 (2008).

[45] S. A. Moiseev and S. Kröll, Phys. Rev. Lett. **87**, 173601 (2001).

[46] W.-T. Liao, C. H. Keitel, and A. Pálffy, Phys. Rev. Lett. **113**, 123602 (2014).

[47] M. Afzelius, C. Simon, H. de Riedmatten, and N. Gisin, Phys. Rev. A **79**, 052329 (2009).

[48] G. Hétet, J. J. Longdell, A. L. Alexander, P. K. Lam, and M. J. Sellars, Phys. Rev. Lett. **100**, 023601 (2008).

[49] M. P. Hedges, J. J. Longdell, Y. M. Li, and M. J. Sellars, Nat. **465**, 1052 (2010).

[50] B. Lauritzen, J. Minář, H. de Riedmatten, M. Afzelius, N. Sangouard, C. Simon, and N. Gisin, Phys. Rev. Lett. **104**, 080502 (2010).

[51] G. Hétet, M. Hosseini, B. M. Sparkes, D. Oblak, P. K. Lam, and B. C. Buchler, Opt. Lett. **33**, 2323 (2008).

[52] M. Hosseini, B. M. Sparkes, G. Hétet, J. J. Longdell, P. K. Lam, and B. C. Buchler, Nat. **461**, 241 (2009).

[53] M. Hosseini, B. M. Sparkes, G. Campbell, P. K. Lam, and B. C. Buchler, Nat. Commun. **2**, 174 (2011).

[54] D. B. Higginbottom, B. M. Sparkes, M. Rancic, O. Pinel, M. Hosseini, P. K. Lam, and B. C. Buchler, Phys. Rev. A **86**, 023801 (2012).

[55] Q. Glorieux, J. B. Clark, A. M. Marino, Z. F. Zhou, and P. D. Lett, Opt. Express **20**, 12350 (2012).

[56] B. M. Sparkes, J. Bernu, M. Hosseini, J. Geng, Q. Glorieux, P. Altin, P. K. Lam, N. P. Robins, and B. C. Buchler, New J. Phys. **15**, 085027 (2013).

[57] H. de Riedmatten, M. Afzelius, M. U. Staudt, C. Simon, and N. Gisin, Nat. **456**, 773 (2008).

[58] T. Chanelière, J. Ruggiero, M. Bonarota, M. Afzelius, and J.-L. L. Gouët, New J. Phys. **12**, 023025 (2010).

[59] M. Sabooni, F. Beaudoin, A. Walther, N. Lin, A. Amari, M. Huang, and S. Kröll, Phys. Rev. Lett. **105**, 060501 (2010).

[60] M. Afzelius, I. Usmani, A. Amari, B. Lauritzen, A. Walther, C. Simon, N. Sangouard, J. Minář, H. de Riedmatten, N. Gisin, and S. Kröll, Phys. Rev. Lett. **104**, 040503 (2010).

[61] I. Usmani, M. Afzelius, H. de Riedmatten, and N. Gisin, Nat. Commun. **1**, 1 (2010).

[62] M. Bonarota, J. Ruggiero, J. L. L. Gouët, and T. Chanelière, Phys. Rev. A **81**, 033803 (2010).

[63] M. Bonarota, J.-L. Le Gouët, and T. Chanelière, New J. Phys. **13**, 013013 (2011).

[64] E. Saglamyurek, N. Sinclair, J. Jin, J. A. Slater, D. Oblak, F. Bussières, M. George, R. Ricken, W. Sohler, and W. Tittel, Nat. **469**, 512 (2011).

[65] C. Clausen, I. Usmani, F. Bussières, N. Sangouard, M. Afzelius, H. de Riedmatten, and N. Gisin, Nat. **469**, 508 (2011).

[66] B. Lauritzen, J. Minář, H. de Riedmatten, M. Afzelius, and N. Gisin, Phys. Rev. A **83**, 012318 (2011).

[67] C. Clausen, F. Bussières, M. Afzelius, and N. Gisin, Phys. Rev. Lett. **108**, 190503 (2012).

[68] E. Saglamyurek, N. Sinclair, J. Jin, J. A. Slater, D. Oblak, F. Bussières, M. George, R. Ricken, W. Sohler, and W. Tittel, Phys. Rev. Lett. **108**, 083602 (2012).

[69] N. Timoney, B. Lauritzen, I. Usmani, M. Afzelius, and N. Gisin, J. Phys. B: At. Mol. Opt. Phys. **45**, 124001 (2012).

[70] M. Gündoğan, P. M. Ledingham, A. Almasi, M. Cristiani, and H. de Riedmatten, Phys. Rev. Lett. **108**, 190504 (2012).

[71] I. Usmani, C. Clausen, F. Bussieres, N. Sangouard, M. Afzelius, and N. Gisin, Nat. Photonics **6**, 234 (2012).

[72] R. A. Akhmedzhanov, A. A. Bondartsev, L. A. Gushchin, I. V. Zelensky, A. G. Litvak, and D. A. Sobgaida, Opt. Spectrosc. **115**, 320 (2013).

[73] M. Sabooni, Q. Li, S. Kröll, and L. Rippe, Phys. Rev. Lett. **110**, 133604 (2013).

[74] N. Timoney, I. Usmani, P. Jobez, M. Afzelius, and N. Gisin, Phys. Rev. A **88**, 022324 (2013).

[75] J. Jin, J. A. Slater, E. Saglamyurek, N. Sinclair, M. George, R. Ricken, D. Oblak, W. Sohler, and W. Tittel, Nat. Commun. **4**, 2386 (2013).

[76] Z. Q. Zhou, J. Wang, C. F. Li, and G. C. Guo, Sci. Reports **3**, 2754 (2013).

[77] C. Clausen, F. Bussières, A. Tiranov, H. Herrmann, C. Silberhorn, W. Sohler, M. Afzelius, and N. Gisin, New J. Phys. **16**, 093058 (2014).

[78] N. Sinclair, E. Saglamyurek, H. Mallahzadeh, J. A. Slater, M. George, R. Ricken, M. P. Hedges, D. Oblak, C. Simon, W. Sohler, and W. Tittel, Phys. Rev. Lett. **113**, 053603 (2014).

[79] D. Rieländer, K. Kutluer, P. M. Ledingham, M. Gündoğan, J. Fekete, M. Mazzera, and H. de Riedmatten, Phys. Rev. Lett. **112**, 040504 (2014).

[80] E. Saglamyurek, N. Sinclair, J. A. Slater, K. Heshami, D. Oblak, and W. Tittel, New J. Phys. **16**, 065019 (2014).

[81] P. Jobez, I. Usmani, N. Timoney, C. Laplane, N. Gisin, and M. Afzelius, New J. Phys. **16**, 083005 (2014).

[82] P. Jobez, C. Laplane, N. Timoney, N. Gisin, A. Ferrier, P. Goldner, and M. Afzelius, Phys. Rev. Lett. **114**, 230502 (2015).

[83] M. Gündoğan, P. M. Ledingham, K. Kutluer, M. Mazzera, and H. de Riedmatten, Phys. Rev. Lett. **114**, 230501 (2015).

[84] E. Saglamyurek, J. Jin, V. B. Verma, M. D. Shaw, F. Marsili, S. W. Nam, D. Oblak, and W. Tittel, Nat Photon **9**, 83 (2015).

[85] A. Kalachev and O. Kocharovskaya, Phys. Rev. A **83**, 053849 (2011).

[86] A. Kalachev and O. Kocharovskaya, J. Mod. Opt. **58**, 1971 (2011).

[87] J. Clark, K. Heshami, and C. Simon, Phys. Rev. A **86**, 013833 (2012).

[88] X. Zhang, A. Kalachev, and O. Kocharovskaya, Phys. Rev. A **87**, 013811 (2013).

[89] A. Kalachev and O. Kocharovskaya, Phys. Rev. A **88**, 033846 (2013).

[90] X.-W. Zhang, A. Kalachev, P. Hemmer, M. O. Scully, and O. Kocharovskaya, Laser Phys. **24**, 094016 (2014).

[91] X. Zhang, A. Kalachev, and O. Kocharovskaya, Phys. Rev. A **90**, 052322 (2014).

[92] R. H. Dicke, Phys. Rev. **93**, 99 (1954).

[93] A. A. Svidzinsky, J. T. Chang, and M. O. Scully, Phys. Rev. Lett. **100**, 160504 (2008).

[94] M. O. Scully, Phys. Rev. Lett. **102**, 143601 (2009).

[95] R. Röhlsberger, K. Schlage, B. Sahoo, S. Couet, and R. Rüffer, Sci. **328**, 1248 (2010).

[96] A. A. Svidzinsky, J.-T. Chang, and M. O. Scully, Phys. Rev. A **81**, 053821 (2010).

[97] A. A. Svidzinsky, X. Zhang, and M. O. Scully, Phys. Rev. A **92**, 013801 (2015).

[98] M. O. Scully, E. S. Fry, C. H. R. Ooi, and K. Wódkiewicz, Phys. Rev. Lett. **96**, 010501 (2006).

[99] B. W. Adams, J. Mod. Opt. **58**, 1638 (2011).

[100] A. V. Gorshkov, A. André, M. D. Lukin, and A. S. Sørensen, Phys. Rev. A **76**, 033804 (2007).

[101] A. V. Gorshkov, A. André, M. D. Lukin, and A. S. Sørensen, Phys. Rev. A **76**, 033805 (2007).

[102] C. W. Thiel, Y. Sun, R. M. MacFarlane, T. Böttger, and R. L. Cone, J. Phys. B: At. Mol. Opt. Phys. **45**, 124013 (2012).

[103] J. J. Longdell, G. Hétet, P. K. Lam, and M. J. Sellars, Phys. Rev. A **78**, 032337 (2008).

[104] S. A. Moiseev and N. M. Arslanov, Phys. Rev. A **78**, 023803 (2008).

[105] M. Nilsson and S. Kröll, Opt. Commun. **247**, 393 (2005).

[106] K. Surmacz, J. Nunn, K. Reim, K. C. Lee, V. O. Lorenz, B. Sussman, I. A. Walmsley, and D. Jaksch, Phys. Rev. A **78**, 033806 (2008).

[107] F. Jelezko and J. Wrachtrup, Phys. Status Solidi a-Applications Mater. Sci. **203**, 3207 (2006).

[108] G. Balasubramanian, P. Neumann, D. Twitchen, M. Markham, R. Kolesov, N. Mizuochi, J. Isoya, J. Achard, J. Beck, J. Tissler, V. Jacques, P. R. Hemmer, F. Jelezko, and J. Wrachtrup, Nat. Mater. **8**, 383 (2009).

[109] P. R. Hemmer, A. V. Turukhin, M. S. Shahriar, and J. A. Musser, Opt. Lett. **26**, 361 (2001).

[110] C. Santori, P. Tamarat, P. Neumann, J. Wrachtrup, D. Fattal, R. G. Beausoleil, J. Rabeau, P. Olivero, A. D. Greentree, S. Prawer, F. Jelezko, and P. Hemmer, Phys. Rev. Lett. **97**, 247401 (2006).

[111] C. Santori, D. Fattal, S. M. Spillane, M. Fiorentino, R. G. Beausoleil, A. D. Greentree, P. Olivero, M. Draganski, J. R. Rabeau, P. Reichart, B. C. Gibson, S. Rubanov, D. N. Jamieson, and S. Prawer, Opt. Express **14**, 7986 (2006).

[112] G. de Lange, Z. H. Wang, R. D., V. V. Dobrovitski, and R. Hanson, Sci. **330**, 60 (2010).

[113] C. A. Ryan, J. S. Hodges, and D. G. Cory, Phys. Rev. Lett. **105**, 200402 (2010).

[114] B. Naydenov, F. Dolde, L. T. Hall, C. Shin, H. Fedder, L. C. L. Hollenberg, F. Jelezko, and J. Wrachtrup, Phys. Rev. B **83**, 081201 (2011).

[115] M. V. G. Dutt, L. Childress, L. Jiang, E. Togan, J. Maze, F. Jelezko, A. S. Zibrov, P. R. Hemmer, and M. D. Lukin, Sci. **316**, 1312 (2007).

[116] P. C. Maurer, G. Kucsko, C. Latta, L. Jiang, N. Y. Yao, S. D. Bennett, F. Pastawski, D. Hunger, N. Chisholm, M. Markham, D. J. Twitchen, J. I. Cirac, and M. D. Lukin, Sci. **336**, 1283 (2012).

[117] U. Schnorrberger, J. D. Thompson, S. Trotzky, R. Pugatch, N. Davidson, S. Kuhr, and I. Bloch, Phys. Rev. Lett. **103**, 033003 (2009).

[118] Y. O. Dudin, R. Zhao, T. A. B. Kennedy, and A. Kuzmich, Phys. Rev. A **81**, 041805 (2010).

[119] J. Nunn, U. Dorner, P. Michelberger, K. F. Reim, K. C. Lee, N. K. Langford, I. A. Walmsley, and D. Jaksch, Phys. Rev. A **82**, 022327 (2010).

[120] P. K. Vudyasetu, R. M. Camacho, and J. C. Howell, Phys. Rev. Lett. **100**, 123903 (2008).

[121] M. Shuker, O. Firstenberg, R. Pugatch, A. Ron, and N. Davidson, Phys. Rev. Lett. **100**, 223601 (2008).

[122] G. Heinze, A. Rudolf, F. Beil, and T. Halfmann, Phys. Rev. A **81**, 011401 (2010).

[123] D.-S. Ding, J.-H. Wu, Z.-Y. Zhou, Y. Liu, B.-S. Shi, X.-B. Zou, and G.-C. Guo, Phys. Rev. A **87**, 013835 (2013).

[124] J. Minář, N. Sangouard, M. Afzelius, H. de Riedmatten, and N. Gisin, Phys. Rev. A **82**, 042309 (2010).

[125] E. Narevicius, C. G. Parthey, A. Libson, J. Narevicius, I. Chavez, U. Even, and M. G. Raizen, New J. Phys. **9** (2007).

[126] B. M. Sparkes, M. Hosseini, G. Hétet, P. K. Lam, and B. C. Buchler, Phys. Rev. A **82**, 043847 (2010).

[127] A. Lyachev, I. O. Musgrave, Y. Tang, C. Hernandez-Gomez, I. N. Ross, M. Galimberti, O. V. Chekhlov, and J. Collier, Opt. Express **19**, 15824 (2011).

[128] F. Raoult, A. C. L. Boscheron, D. Husson, C. Sauteret, A. Modena, V. Malka, F. Dorchies, and A. Migus, Opt. Lett. **23**, 1117 (1998).

[129] A. Kanno, S. Honda, R. Yamanaka, H. Sotobayashi, and T. Kawanishi, Opt. Lett. **35**, 4160 (2010).

[130] K. W. Holman, D. G. Kocher, and S. Kaushik, in *Conference on Lasers and Electro-Optics & Quantum Electronics and Laser Science, Vols 1-9* (IEEE, New York, 2008) pp. 1268--1269.

[131] C. E. Rogers III, M. J. Wright, J. L. Carini, J. A. Pechkis, and P. L. Gould, J. Opt. Soc. Am. B **24**, 1249 (2007).

[132] E. S. Moiseev and S. A. Moiseev, New J. Phys. **15**, 105005 (2013).

[133] V. M. Acosta, K. Jensen, C. Santori, D. Budker, and R. G. Beausoleil, Phys. Rev. Lett. **110**, 213605 (2013).

[134] K. Heshami, C. Santori, B. Khanaliloo, C. Healey, V. M. Acosta, P. E. Barclay, and C. Simon, Phys. Rev. A **89**, 040301 (2014).

[135] P. Neumann, R. Kolesov, V. Jacques, J. Beck, J. Tisler, A. Batalov, L. Rogers, N. B. Manson, G. Balasubramanian, F. Jelezko, and J. Wrachtrup, New J. Phys. **11**, 013017 (2009).

[136] X. F. He, N. B. Manson, and P. T. H. Fisk, Phys. Rev. B **47**, 8809 (1993).

[137] C. Hepp, T. Müller, V. Waselowski, J. N. Becker, B. Pingault, H. Sternschulte, D. Steinmüller-Nethl, A. Gali, J. R. Maze, M. Atatüre, and C. Becher, Phys. Rev. Lett. **112**, 036405 (2014).

[138] E. Neu, D. Steinmetz, J. Riedrich-Möller, S. Gsell, M. Fischer, M. Schreck, and C. Becher, New J. Phys. **13**, 025012 (2011).

[139] M. W. Doherty, N. B. Manson, P. Delaney, F. Jelezko, J. Wrachtrup, and L. C. L. Hollenberg, Phys. Reports **528**, 1 (2013).

[140] A. Batalov, V. Jacques, F. Kaiser, P. Siyushev, P. Neumann, L. J. Rogers, R. L. Mc-Murtrie, N. B. Manson, F. Jelezko, and J. Wrachtrup, Phys. Rev. Lett. **102**, 195506 (2009).

[141] M. S. Shahriar, P. Kumar, and P. R. Hemmer, J. Phys. B: At. Mol. Opt. Phys. **45**, 124018 (2012).

[142] N. Bar-Gill, L. M. Pham, A. Jarmola, D. Budker, and R. L. Walsworth, Nat. Commun. **4**, 1743 (2013).

[143] T. M. Babinec, B. J. M. Hausmann, M. Khan, Y. A. Zhang, J. R. Maze, P. R. Hemmer, and M. Lončar, Nat. Nanotechnol. **5**, 195 (2010).

[144] L. Childress, M. V. G. Dutt, J. M. Taylor, A. S. Zibrov, F. Jelezko, J. Wrachtrup, P. R. Hemmer, and M. D. Lukin, Sci. **314**, 281 (2006).

[145] P. Neumann, R. Kolesov, B. Naydenov, J. Beck, F. Rempp, M. Steiner, V. Jacques, G. Balasubramanian, M. L. Markham, D. J. Twitchen, S. Pezzagna, J. Meijer, J. Twamley, F. Jelezko, and J. Wrachtrup, Nat. Phys. **6**, 249 (2010).

[146] E. Togan, Y. Chu, A. S. Trifonov, L. Jiang, J. Maze, L. Childress, M. V. G. Dutt, A. S. Sørensen, P. R. Hemmer, A. S. Zibrov, and M. D. Lukin, Nat. **466**, 730 (2010).

[147] Y. Kubo, F. R. Ong, P. Bertet, D. Vion, V. Jacques, D. Zheng, A. Dréau, J. F. Roch, A. Auffeves, F. Jelezko, J. Wrachtrup, M. F. Barthe, P. Bergonzo, and D. Esteve, Phys. Rev. Lett. **105**, 140502 (2010).

[148] K. C. Lee, B. J. Sussman, M. R. Sprague, P. Michelberger, K. F. Reim, J. Nunn, N. K. Langford, P. J. Bustard, D. Jaksch, and I. A. Walmsley, Nat. Photonics **6**, 41 (2012).

[149] P. Tamarat, N. B. Manson, J. P. Harrison, R. L. McMurtrie, A. Nizovtsev, C. Santori, R. G. Beausoleil, P. Neumann, T. Gaebel, F. Jelezko, P. Hemmer, and J. Wrachtrup, New J. Phys. **10**, 045004 (2008).

[150] C. Santori, P. E. Barclay, K. M. C. Fu, R. G. Beausoleil, S. Spillane, and M. Fisch, Nanotechnol. **21**, 274008 (2010).

[151] A. Gali and J. R. Maze, Phys. Rev. B **88**, 235205 (2013).

[152] L. J. Rogers, K. D. Jahnke, M. W. Doherty, A. Dietrich, L. P. McGuinness, C. Müller, T. Teraji, H. Sumiya, J. Isoya, N. B. Manson, and F. Jelezko, Phys. Rev. B **89**, 235101 (2014).

[153] T. Müller, C. Hepp, B. Pingault, E. Neu, S. Gsell, M. Schreck, H. Sternschulte, D. Steinmüller-Nethl, C. Becher, and M. Atatüre, Nat. Commun. **5** (2014).

[154] E. Neu, C. Hepp, M. Hauschild, S. Gsell, M. Fischer, H. Sternschulte, D. Steinmüller-Nethl, M. Schreck, and C. Becher, New J. Phys. **15**, 043005 (2013).

[155] L. J. Rogers, K. D. Jahnke, M. H. Metsch, A. Sipahigil, J. M. Binder, T. Teraji, H. Sumiya, J. Isoya, M. D. Lukin, P. Hemmer, and F. Jelezko, Phys. Rev. Lett. **113**, 263602 (2014).

[156] L. J. Rogers, K. D. Jahnke, T. Teraji, L. Marseglia, C. Müller, B. Naydenov, H. Schauffert, C. Kranz, J. Isoya, L. P. McGuinness, and F. Jelezko, Nat. Commun. **5**, 4739 (2014).

[157] J. P. Heritage, A. M. Weiner, and R. N. Thurston, Opt. Lett. **10**, 609 (1985).

[158] G. H. Zhu, J. van Howe, M. Durst, W. Zipfel, and C. Xu, Opt. Express **13**, 2153 (2005).

[159] D. Oron, E. Tal, and Y. Silberberg, Opt. Express **13**, 1468 (2005).

[160] D. N. Vitek, D. E. Adams, A. Johnson, P. S. Tsai, S. Backus, C. G. Durfee, D. Kleinfeld, and J. A. Squier, Opt. Express **18**, 18086 (2010).

[161] C. G. Durfee, M. Greco, E. Block, D. Vitek, and J. A. Squier, Opt. Express **20**, 14244 (2012).

[162] G. Futia, P. Schlup, D. G. Winters, and R. A. Bartels, Opt. Express **19**, 1626 (2011).

[163] X. Gu, S. Akturk, and R. Trebino, Opt. Commun. **242**, 599 (2004).

[164] M. E. Durst, G. Zhu, and C. Xu, Opt. Commun. **281**, 1796 (2008).

[165] M. M. Wefers and K. A. Nelson, J. Opt. Soc. Am. B-Optical Phys. **12**, 1343 (1995).

[166] J. S. Sanders, R. G. Driggers, C. E. Halford, and S. T. Griffin, Opt. Eng. **30**, 1720 (1991).

[167] M. G. Raymer and J. Mostowski, Phys. Rev. A **24**, 1980 (1981).

[168] J. Ruggiero, J. L. Le Gouët, C. Simon, and T. Chanelière, Phys. Rev. A **79**, 053851 (2009).

[169] V. Damon, M. Bonarota, A. Louchet-Chauvet, T. Chaneliere, and J. L. Le Gouët, New J. Phys. **13**, 093031 (2011).

[170] N. Sangouard, C. Simon, M. Afzelius, and N. Gisin, Phys. Rev. A **75**, 032327 (2007).

[171] S. A. Moiseev and W. Tittel, New J. Phys. **13**, 063035 (2011).

[172] M. R. Hush, A. R. R. Carvalho, M. Hedges, and M. R. James, New J. Phys. **15**, 085020 (2013).

[173] X. Zhang, "Exact solution of gradient echo memory and analytical treatment of gradient frequency comb," (2016), arXiv:1602.05115.

[174] B. C. Buchler, M. Hosseini, G. Hétet, B. M. Sparkes, and P. K. Lam, Opt. Lett. **35**, 1091 (2011).

[175] B. M. Sparkes, M. Hosseini, C. Cairns, D. Higginbottom, G. T. Campbell, P. K. Lam, and B. C. Buchler, Phys. Rev. X **2**, 021011 (2012).

[176] X. Zhang, A. Kalachev, P. Hemmer, and O. Kocharovskaya, "Quantum storage based on controllable frequency comb," (2016), arXiv:1602.02322.

[177] P. W. Milonni, J. Mod. Opt. **42**, 1991 (1995).

[178] B. Zhao, Y. A. Chen, X. H. Bao, T. Strassel, C. S. Chuu, X. M. Jin, J. Schmiedmayer, Z. S. Yuan, S. Chen, and J. W. Pan, Nat. Phys. **5**, 95 (2008).

[179] M. D. Eisaman, J. Fan, A. Migdall, and S. V. Polyakov, Rev. Sci. Instruments **82**, 071101 (2011).

[180] N. Rohringer, D. Ryan, R. A. London, M. Purvis, F. Albert, J. Dunn, J. D. Bozek, C. Bostedt, A. Graf, R. Hill, S. P. Hau-Riege, and J. J. Rocca, Nat. **481**, 488 (2012).

[181] T. Popmintchev, M. C. Chen, D. Popmintchev, P. Arpin, S. Brown, S. Ališauskas, G. Andriukaitis, T. Balciunas, O. D. Mücke, A. Pugzlys, A. Baltuška, B. Shim, S. E. Schrauth, A. Gaeta, C. Hernández-García, L. Plaja, A. Becker, A. Jaron-Becker, M. M. Murnane, and H. C. Kapteyn, Sci. **336**, 1287 (2012).

[182] J. Amann, W. Berg, V. Blank, F. J. Decker, Y. Ding, P. Emma, Y. Feng, J. Frisch, D. Fritz, J. Hastings, Z. Huang, J. Krzywinski, R. Lindberg, H. Loos, A. Lutman, H. D. Nuhn, D. Ratner, J. Rzepiela, D. Shu, Y. Shvyd'ko, S. Spampinati, S. Stoupin, S. Terentyev, E. Trakhtenberg, D. Walz, J. Welch, J. Wu, A. Zholents, and D. Zhu, Nat. Photonics **6**, 693 (2012).

[183] Y. Shvyd'ko, S. Stoupin, V. Blank, and S. Terentyev, Nat. Photonics **5**, 539 (2011).

[184] J. Chen, I. V. Tomov, A. O. Er, and P. M. Rentzepis, Appl. Phys. Lett. **102**, 174101 (2013).

[185] R. Coussement, Y. Rostovtsev, J. Odeurs, G. Neyens, H. Muramatsu, S. Gheysen, R. Callens, K. Vyvey, G. Kozyreff, P. Mandel, R. Shakhmuratov, and O. Kocharovskaya, Phys. Rev. Lett. **89**, 107601 (2002).

[186] R. Röhlsberger, H. C. Wille, K. Schlage, and B. Sahoo, Nat. **482**, 199 (2012).

[187] H. P., I. Tittonen, M. Lippmaa, and T. Katila, Phys. Rev. Lett. **66**, 2037 (1991).

[188] G. V. Smirnov, U. van Bürck, J. Arthur, S. L. Popov, A. Q. R. Baron, A. I. Chumakov, S. L. Ruby, W. Potzel, and G. S. Brown, Phys. Rev. Lett. **77**, 183 (1996).

[189] R. N. Shakhmuratov, F. Vagizov, and O. Kocharovskaya, Phys. Rev. A **84**, 043820 (2011).

[190] R. N. Shakhmuratov, F. Vagizov, and O. Kocharovskaya, Phys. Rev. A **87**, 013807 (2013).

[191] R. Röhlsberger, T. S. Toellner, W. Sturhahn, K. W. Quast, E. E. Alp, A. Bernhard, E. Burkel, O. Leupold, and E. Gerdau, Phys. Rev. Lett. **84**, 1007 (2000).

[192] K. P. Heeg, H. C. Wille, K. Schlage, T. Guryeva, D. Schumacher, I. Uschmann, K. S. Schulze, B. Marx, T. Kämpfer, G. G. Paulus, R. Röhlsberger, and J. Evers, Phys. Rev. Lett. **111**, 073601 (2013).

[193] S. Shwartz, R. N. Coffee, J. M. Feldkamp, Y. Feng, J. B. Hastings, G. Y. Yin, and S. E. Harris, Phys. Rev. Lett. **109**, 013602 (2012).

[194] S. Shwartz, M. Fuchs, J. B. Hastings, Y. Inubushi, T. Ishikawa, T. Katayama, D. A. Reis, T. Sato, K. Tono, M. Yabashi, S. Yudovich, and S. E. Harris, Phys. Rev. Lett. **112**, 163901 (2014).

[195] W. T. Liao, A. Pálffy, and C. H. Keitel, Phys. Lett. B **705**, 134 (2011).

150

[196] A. Pálffy, C. H. Keitel, and J. Evers, Phys. Rev. Lett. **103**, 017401 (2009).

[197] F. Vagizov, V. Antonov, Y. V. Radeonychev, R. N. Shakhmuratov, and O. Kocharovskaya, Nat. **508**, 80 (2014).

[198] Y. V. Shvyd'ko, S. L. Popov, and G. V. Smirnov, J. Physics: Condens. Matter **5**, 1557 (1993).

[199] Y. V. Shvyd'ko, A. I. Chumakov, G. V. Smirnov, T. Hertrich, U. Van Bürck, H. D. Rüter, O. Leupold, J. Metge, and E. Gerdau, Europhys. Lett. **26**, 215 (1994).

[200] P. H. Bucksbaum and R. Merlin, Solid State Commun. **111**, 535 (1999).

[201] M. F. DeCamp, D. A. Reis, P. H. Bucksbaum, B. Adams, J. M. Caraher, R. Clarke, C. W. S. Conover, E. M. Dufresne, R. Merlin, V. Stoica, and J. K. Wahlstrand, Nat. **413**, 825 (2001).

[202] M. Herzog, W. Leitenberger, R. Shayduk, R. M. Van Der Veen, C. J. Milne, S. L. Johnson, I. Vrejoiu, M. Alexe, D. Hesse, and M. Bargheer, Appl. Phys. Lett. **96**, 161906 (2010).

[203] G. V. Smirnov, Y. V. Shvyd'ko, O. S. Kolotov, V. A. Pogozhev, M. Kotrbova, S. Kadeckova, and J. Novak, Zh. Eksp. Teor. Fiz. **86**, 1495 (1984).

[204] Y. V. Shvyd'ko, G. V. Smirnov, S. L. Popov, and T. Hertrich, Pis'ma Zh. Eksp. Teor. Fiz. [JETP Lett.] **53**, 69 (1991).

[205] Y. V. Shvyd'ko, T. Hertrich, U. van Bürck, E. Gerdau, O. Leupold, J. Metge, H. D. Rüter, S. Schwendy, G. V. Smirnov, W. Potzel, and P. Schindelmann, Phys. Rev. Lett. **77**, 3232 (1996).

[206] W. T. Liao, A. Pálffy, and C. H. Keitel, Phys. Rev. Lett. **109**, 197403 (2012).

[207] X. Zhang, W.-T. Liao, A. Kalachev, R. Shakhmuratov, M. Scully, and O. Kocharovskaya, "Nuclear quantum memory and time sequencing of a single γ photon," (2016), to be published.

[208] Y. V. Shvyd'ko and G. V. Smirnov, Nucl. Instrum. Methods Phys. Res. B **51**, 452 (1990).

[209] P. Boolchand, J. Quant. Spectrosc. & Radiat. Transf. **40**, 777 (1988).

[210] P. Anisimov, Y. Rostovtsev, and O. Kocharovskaya, Phys. Rev. B **76**, 094422 (2007).

[211] X. Zhang and A. A. Svidzinsky, Phys. Rev. A **88**, 033854 (2013).

[212] J. H. Eberly, J. Phys. B: At. Mol. Opt. Phys. **39**, S599 (2006).

[213] I. E. Mazets and G. Kurizki, J. Phys. B: At. Mol. Opt. Phys. **40**, F105 (2007).

[214] A. A. Svidzinsky and J. T. Chang, Phys. Rev. A **77**, 043833 (2008).

[215] R. Friedberg and J. T. Manassah, Phys. Lett. A **372**, 2514 (2008).

[216] R. Friedberg and J. T. Manassah, Phys. Lett. A **372**, 6833 (2008).

[217] D. Porras and J. I. Cirac, Phys. Rev. A **78**, 053816 (2008).

[218] M. O. Scully and A. A. Svidzinsky, Sci. **325**, 1510 (2009).

[219] L. H. Pedersen and K. Mølmer, Phys. Rev. A **79**, 012320 (2009).

[220] A. A. Svidzinsky and M. O. Scully, Opt. Commun. **282**, 2894 (2009).

[221] A. A. Svidzinsky and M. O. Scully, Opt. Commun. **283**, 753 (2010).

[222] R. Friedberg, Annals Phys. **325**, 345 (2010).

[223] P. R. Berman and J. L. Le Gouët, Phys. Rev. A **83**, 035804 (2011).

[224] A. A. Svidzinsky, Phys. Rev. A **85**, 013821 (2012).

[225] Q. Fu, G. Mak, and H. M. Vandriel, Opt. Lett. **17**, 1006 (1992).

[226] R. J. Ellingson and C. L. Tang, Opt. Lett. **18**, 438 (1993).

[227] M. Ghotbi, A. Esteban-Martin, and M. Ebrahim-Zadeh, Opt. Lett. **33**, 345 (2008).

[228] R. H. Kingston, Proc. IRE **50**, 472 (1962).

[229] A. A. Svidzinsky, L. Yuan, and M. O. Scully, Phys. Rev. X **3**, 041001 (2013).

[230] A. A. Svidzinsky, X. Zhang, L. Wang, and J. Wang, Coherent Phenom. **2**, 19 (2015).

[231] U. Gonser, *Mössbauer Spectroscopy*, Topics in Applied Physics (Springer Berlin Heidelberg, New York, 1975).

[232] D. V. Borobchenko, I. I. Lukashevich, V. V. Sklyarevskii, and N. I. Filippov, Sov. Phys. JETP Lett. **9**, 139 (1969).

[233] P. J. Black and I. P. Duerdoth, Proc. Phys. Soc. **84**, 169 (1964).

[234] E. P. Stepanov, A. N. Artem'ev, I. P. Perstnev, V. V. Sklyarevskii, and G. V. Smirnov, Sov. Phys. JETP **39**, 562 (1974).

[235] D. C. Burnham and R. Y. Chiao, Phys. Rev. **188**, 667 (1969).

[236] W.-T. Liao and A. Pálffy, Phys. Rev. Lett. **112**, 057401 (2014).

[237] R. Schützhold, G. Schaller, and D. Habs, Phys. Rev. Lett. **100**, 091301 (2008).

[238] A. V. Gorshkov, A. André, M. Fleischhauer, A. S. Sørensen, and M. D. Lukin, Phys. Rev. Lett. **98**, 123601 (2007).

[239] A. A. Svidzinsky, F. Li, H. Li, X. Zhang, C. H. R. Ooi, and M. O. Scully, Phys. Rev. A **93**, 043830 (2016).

[240] A. P. Prudnikov, U. A. Bryčkov, and O. I. Marichev, *Integrals and series. Volume 5, Inverse Laplace transforms* (Gordon and Breach science publication, Amsterdam, 1992).

[241] J. Choi and A. Hasanov, Comput. & Math. with Appl. **61**, 663 (2011).

[242] V. V. Manako, Integral Transform. Special Funct. **23**, 503 (2011).

[243] A. K. Rathie, "On a representation of Humbert's double hypergeometric series in a series of Gauss's $_2F_1$ function," (2013), arXiv:1312.0064.

[244] J. Choi and A. K. Rathie, Commun. Korean Math. Soc. **30**, 439 (2015).

[245] H. Stehfest, Commun. Acm **13**, 47 (1970).

[246] P. P. Valkó and J. Abate, Comput. & Math. with Appl. **48**, 629 (2004).

APPENDIX A

EVOLUTION EQUATIONS OF QUANTUM MEMORY BASED ON

PHASE MATCHING CONTROL[*]

In this appendix[1], we provide the derivation of the equations of motion (II.5), (II.6). Let us start with the one-dimensional Maxwell equation for the signal field

$$\left(\frac{\partial^2}{\partial z^2} - \frac{1}{c^2}\frac{\partial^2}{\partial t^2}\right)E_s(\mathbf{r},t) = \mu_0 \frac{\partial^2 P(\mathbf{r},t)}{\partial t^2}, \tag{A.1}$$

where μ_0 is the vacuum permeability, and define slow varying amplitudes of the electric field, $\mathcal{E}(\mathbf{r},t)$, and atomic polarization density, $p(\mathbf{r},t)$, via relations

$$E_s(\mathbf{r},t) = \mathcal{E}(\mathbf{r},t)\,e^{ik_s z - i\omega_s t} + \text{c.c.}, \tag{A.2}$$

$$P(\mathbf{r},t) = Nd_{12}\,p(\mathbf{r},t)\,e^{ik_s z - i\omega_s t} + \text{c.c.} \tag{A.3}$$

Then inserting (A.2), (A.3) into (A.1), and neglecting second derivatives of the slowly varying amplitudes, we obtain

$$\left(\frac{\partial}{\partial z} + \frac{\omega_s}{c^2 k_s}\frac{\partial}{\partial t} + \frac{\omega_s^2/c^2 - k_s^2}{2ik_s}\right)\mathcal{E}(\mathbf{r},t) = \frac{i\omega_s^2 N d_{12}}{2\varepsilon_0 c^2 k_s}p(\mathbf{r},t) - \frac{\omega_s N d_{12}}{\varepsilon_0 c^2 k_s}\frac{\partial p(\mathbf{r},t)}{\partial t}. \tag{A.4}$$

If we take $k_s = \omega_s/c$ and neglect the first derivative of polarization, we come to the standard propagation equation, where dispersive effects are not present explicitly. To reveal them we take into account the equations of motion for the slowly varying amplitudes of polarization

---

[1]Some notations in this appendix, such as the optical coherence dephasing rate Γ, functions of F and η, are different from that in the main text of Chaps. II - VI. The validity of these notations stay only in this appendix.

and spin coherence densities, which describe interaction of three-level atoms with the weak

signal and strong control fields:

$$\frac{d}{dt}p(\mathbf{r},t) = (-\Gamma + i\Delta)p(\mathbf{r},t) + \frac{id_{21}}{\hbar}\mathcal{E}(\mathbf{r},t) + i\Omega s(\mathbf{r},t)\,e^{i\phi(\mathbf{r},t)}, \tag{A.5}$$

$$\frac{d}{dt}s(\mathbf{r},t) = (-\gamma + i\delta)s(\mathbf{r},t) + i\Omega^* p(\mathbf{r},t)\,e^{-i\phi(\mathbf{r},t)}. \tag{A.6}$$

where $\Delta = \omega_s - \omega_2$, $\delta = \omega_s - \omega_c - \omega_3$, Γ and γ are dephasing rates for optical and spin

transitions, respectively, $\Omega = d_{23}E_0/\hbar$ is the Rabi frequency of the control field, and $\phi(\mathbf{r},t)$

is the phase shift due to the angular or frequency manipulation with the control field. When

considering off-resonance Raman interaction ($|\Delta| \gg \Gamma$) and doing adiabatic elimination of

the polarization, we usually set time derivative $\dot{p}(z,t)$ equal to zero and then express the

polarization amplitude through the field one. But this procedure does not take into account

dispersion. To do this we can take advantage of the frequency domain:

$$-i\omega p(\mathbf{r},\omega) = (-\Gamma + i\Delta)p(\mathbf{r},\omega) + \frac{id_{21}}{\hbar}\mathcal{E}(\mathbf{r},\omega) + i\Omega F(\mathbf{r},\omega), \tag{A.7}$$

where $F(\mathbf{r},\omega)$ stands for the Fourier transform of $s(\mathbf{r},t)\,e^{i\phi(\mathbf{r},t)}$. Then

$$p(\mathbf{r},\omega) = \frac{1}{(\Gamma - i\Delta - i\omega)}\frac{id_{21}}{\hbar}\mathcal{E}(\mathbf{r},\omega) + \frac{i\Omega F(\mathbf{r},\omega)}{(\Gamma - i\Delta - i\omega)} \tag{A.8}$$

$$\equiv \varepsilon_0 \bar{\chi}(\omega_s + \omega)\mathcal{E}(\mathbf{r},\omega) + \eta(\omega_s + \omega)F(\mathbf{r},\omega). \tag{A.9}$$

Now we expand $\bar{\chi}(\omega_s + \omega)$ and $\eta(\omega_s + \omega)$ in a series around the point ω_s:

$$\bar{\chi}(\omega_s + \omega) = \bar{\chi}(\omega_s) + \frac{\partial \bar{\chi}}{\partial \omega}\bigg|_{\omega_s}\omega + \dots, \tag{A.10}$$

$$\eta(\omega_s + \omega) = \eta(\omega_s) + \frac{\partial \eta}{\partial \omega}\bigg|_{\omega_s}\omega + \dots, \tag{A.11}$$

and return to the time domain:

$$p(\mathbf{r},t) = \varepsilon_0 \bar{\chi}(\omega_s)\mathcal{E}(\mathbf{r},t) + i\varepsilon_0 \frac{\partial \bar{\chi}}{\partial \omega}\bigg|_{\omega_s} \frac{\partial \mathcal{E}(\mathbf{r},t)}{\partial t} + \eta(\omega_s)s(\mathbf{r},t)\,e^{i\phi(\mathbf{r},t)} + \ldots \qquad (A.12)$$

Then from (A.4) and (A.6) we have

$$\left(\frac{\partial}{\partial z} + \frac{1}{v_{gs}}\frac{\partial}{\partial t}\right)\mathcal{E}(\mathbf{r},t) = \frac{i\omega_s N d_{12}}{2\varepsilon_0 c n_s}\eta(\omega_s)s(\mathbf{r},t)\,e^{i\phi(\mathbf{r},t)}, \qquad (A.13)$$

$$\frac{d}{dt}s(\mathbf{r},t) = (-\gamma + i\delta)s(\mathbf{r},t) + i\Omega^*\left[\varepsilon_0\bar{\chi}(\omega_s)\mathcal{E}(\mathbf{r},t)\,e^{-i\phi(\mathbf{r},t)} + \eta(\omega_s)s(\mathbf{r},t)\right], \qquad (A.14)$$

provided that $k_s = n_s\omega_s/c$, where $n_s = \sqrt{1+\chi(\omega_s)}$ is the refractive index and $\chi = N d_{12}\bar{\chi}$

is the linear susceptibility of the atomic system, and

$$\frac{1}{v_{gs}} = \frac{n_s}{c} + \frac{\omega_s}{2cn_s}\frac{\partial \chi}{\partial \omega}\bigg|_{\omega_s} \qquad (A.15)$$

is the reciprocal of group velocity. Taking into account that

$$\varepsilon_0\bar{\chi}(\omega_s) = \frac{id_{21}}{\hbar(\Gamma - i\Delta)}, \quad \eta(\omega_s) = \frac{i\Omega}{\Gamma - i\Delta}, \qquad (A.16)$$

$$\varepsilon_0\frac{\partial \bar{\chi}}{\partial \omega}\bigg|_{\omega_s} = -\frac{d_{21}}{\hbar(\Gamma - i\Delta)^2}, \qquad (A.17)$$

and considering the limit $|\Delta| \gg \Gamma$, we obtain

$$\left(\frac{\partial}{\partial z} + \frac{1}{v_{gs}}\frac{\partial}{\partial t}\right)\mathcal{E}(\mathbf{r},t) = -\frac{i\hbar\omega_s N}{2\varepsilon_0 c n_s}\frac{d_{12}\Omega}{\hbar\Delta}s(\mathbf{r},t)\,e^{i\phi(\mathbf{r},t)}, \qquad (A.18)$$

$$\frac{d}{dt}s(\mathbf{r},t) = \left(-\gamma - \frac{|\Omega|^2\Gamma}{\Delta^2} + i\left[\delta - \frac{|\Omega|^2}{\Delta}\right]\right)s(\mathbf{r},t) - i\frac{d_{21}\Omega^*}{\hbar\Delta}\mathcal{E}(\mathbf{r},t)\,e^{-i\phi(\mathbf{r},t)}, \qquad (A.19)$$

where

$$\frac{1}{v_{gs}} = \frac{n_s}{c} + \frac{\omega_s}{2\varepsilon_0\hbar cn_s}\frac{N|d|^2}{\Delta^2}. \qquad (A.20)$$

Finally, in terms of the slowly varying annihilation operator we have

$$\mathcal{E}(\mathbf{r},t) = i\sqrt{\frac{\hbar\omega_s}{2\varepsilon_0 cn_s}}\,a(\mathbf{r},t), \qquad (A.21)$$

which gives

$$\left(\frac{\partial}{\partial z} + \frac{1}{v_{gs}}\frac{\partial}{\partial t}\right)a(\mathbf{r},t) = -g^* N s(\mathbf{r},t)\,e^{i\phi(\mathbf{r},t)}, \tag{A.22}$$

$$\frac{\partial}{\partial t}s(\mathbf{r},t) = (-\gamma + i\delta)s(\mathbf{r},t) + g\,a(\mathbf{r},t)\,e^{-i\phi(\mathbf{r},t)}, \tag{A.23}$$

where

$$g = \frac{d_{21}\Omega^*}{\Delta}\sqrt{\frac{\omega_s}{2\varepsilon_0\hbar c n_s}}, \tag{A.24}$$

the dephasing rate γ is redefined so that it includes $|\Omega|^2\Gamma/\Delta^2$, while excitation induced frequency shift $|\Omega|^2/\Delta$ is compensated by tuning the coupling field frequency. The annihilation operator is normalized so that $a^\dagger(\mathbf{r},t)a(\mathbf{r},t)$ corresponds to the photon flux density in the dispersive medium.

APPENDIX B

ANALYTICAL SOLUTION OF GRADIENT ECHO MEMORY[*]

The equations we are solving in this appendix are Eqs. (IV.7) and (IV.8) in Chap. IV:

$$\frac{\partial}{\partial z}a(z,t) = g^*Ns(z,t)e^{i\beta tz}e^{-i(\beta\frac{L}{2}-\omega_m)t}, \tag{B.1}$$

$$\frac{\partial}{\partial t}s(z,t) = -\gamma s(z,t) - ga(z,t)e^{-i\beta tz}e^{i(\beta\frac{L}{2}-\omega_m)t}. \tag{B.2}$$

with $t \in [-T,0]$ for storage, $t \in [0,T]$ for retrieval, and $z \in [0,L]$. Eqs. (B.1) and (B.2) describe the field-atom evolution of quantum memory based on GEM, PMC and control field spatial chirp with continuous frequency gradient in space. These evolution equations can be solved exactly without assumptions on the parameters, not only for storage but also for retrieval. The exact solution of Eqs. (B.1) and (B.2) for $t \in [t_i, t_f]$ is derived in the following in Laplace domain of space variable z, with boundary condition $a(0,t)$ and initial condition $s(z,t_i)$. Here t_i (t_f) represents the initial (final) time with meaning depending on the context.

B.1   General solution of GEM in Laplace domain

First let us take the spatial derivative of Eq. (B.2):

$$\frac{\partial}{\partial z}\frac{\partial}{\partial t}s(z,t) = -\gamma\frac{\partial}{\partial z}s(z,t) - |g|^2Ns(z,t) - i\beta t\left[\frac{\partial}{\partial t}s(z,t) + \gamma s(z,t)\right]. \tag{B.3}$$

---

[*]The preprint of the related work "Exact solution of gradient echo memory and analytical treatment of gradient frequency comb" by Xiwen Zhang is available on arXiv:1602.05115 (2016), and will be submitted to journal publication soon.

So Eqs. (B.1) and (B.2) become

$$\frac{\partial}{\partial z}a(z,t) = g^*Ns(z,t)e^{i\beta tz}e^{-i\left(\beta\frac{L}{2}-\omega_m\right)t}, \tag{B.4}$$

$$\left(\frac{\partial}{\partial z}+i\beta t\right)\frac{\partial}{\partial t}s(z,t) = -\gamma\frac{\partial}{\partial z}s(z,t) - \left(|g|^2N+i\beta t\gamma\right)s(z,t), \tag{B.5}$$

with boundary condition built in through Eq. (B.2):

$$\frac{\partial}{\partial t}s(0,t) = -\gamma s(0,t) - ga(0,t)e^{i\left(\beta\frac{L}{2}-\omega_m\right)t}. \tag{B.6}$$

After taking the Laplace transformation of Eqs. (B.4) and (B.5) and substituting the boundary condition (B.6), we have:

$$pa(p,t) - a(0,t) = g^*Ns(p-i\beta t,t)e^{-i\left(\beta\frac{L}{2}-\omega_m\right)t}, \tag{B.7}$$

$$(p+i\beta t)\frac{\partial}{\partial t}s(p,t) + \left(|g|^2N+p\gamma+i\beta t\gamma\right)s(p,t) = -ga(0,t)e^{i\left(\beta\frac{L}{2}-\omega_m\right)t}. \tag{B.8}$$

Solving Eq. (B.8) with the initial condition $s(p,t_i)$ in Laplace domain, one has

$$s(p,t) = s(p,t_i)\exp\left[-\int_{t_i}^t d\tau\left(\frac{|g|^2N}{p+i\beta\tau}+\gamma\right)\right] + \int_{t_i}^t d\tau\frac{-g}{p+i\beta\tau}a(0,\tau)e^{i\left(\beta\frac{L}{2}-\omega_m\right)\tau}\times$$
$$\exp\left[-\int^t d\tau''\left(\frac{|g|^2N}{p+i\beta\tau''}+\gamma\right)\right]\exp\left[\int^\tau d\tau''\left(\frac{|g|^2N}{p+i\beta\tau''}+\gamma\right)\right]. \tag{B.9}$$

Up to Eq. (B.9), $s(p,t)$ is valid for arbitrary time dependent frequency gradient $\beta = \beta(t)$. Explicit solution is possible as long as the inverse Laplace transformation can be calculated. In general this is difficult, but for a constant frequency gradient β (during storage or retrieval), the exact solution can be found. In such a case, substituting the result of Eq. (B.9) into Eq. (B.7), we have the solution for non-vanishing frequency gradient $\beta \neq 0$ given by Eqs. (B.15) and (B.16).

For a flat single-frequency absorption, the frequency gradient $\beta = 0$. The corre-

sponding evolution equation is simpler:

$$\frac{\partial}{\partial z}a(z,t) = g^*Ns(z,t)e^{i\omega_m t}, \tag{B.10}$$

$$\frac{\partial}{\partial t}s(z,t) = -\gamma s(z,t) - ga(z,t)e^{-i\omega_m t}. \tag{B.11}$$

The Laplace transformation of Eqs. (B.10) and (B.11) are:

$$a(p,t) = \frac{1}{p}a(0,t) + \frac{g^*N}{p}s(p,t)e^{i\omega_m t}, \tag{B.12}$$

$$\frac{\partial}{\partial t}s(p,t) = -\gamma s(p,t) - ga(p,t)e^{-i\omega_m t}. \tag{B.13}$$

Equations (B.12) and (B.13) are reduced to

$$\frac{\partial}{\partial t}s(p,t) + \left(\gamma + \frac{|g|^2N}{p}\right)s(p,t) = -\frac{1}{p}a(0,t)ge^{-i\omega_m t}. \tag{B.14}$$

Solving for Eq. (B.14) with initial condition $s(p,t_i)$ and boundary condition $a(0,t)$, and substituting the result into Eq. (B.12), we obtain the solution (B.17) and (B.18) of a flat single-frequency absorption.

The solution of Eqs. (B.1) and (B.2) in Laplace domain are summarized as follows:

$$a^{(\beta\neq0)}(p,t) = \frac{1}{p}a(0,t) - |g|^2N\int_{t_i}^t d\tau a(0,\tau)e^{-i\left(\beta\frac{L}{2}-\omega_m\right)(t-\tau)}e^{-\gamma(t-\tau)} \times$$

$$\frac{p^{i\mu-1}}{[p-i\beta(t-\tau)]^{i\mu+1}} + g^*Ns(p-i\beta t,t_i)\frac{p^{i\mu-1}}{[p-i\beta(t-t_i)]^{i\mu}}e^{-\gamma(t-t_i)}e^{-i\left(\beta\frac{L}{2}-\omega_m\right)t},$$

$$\tag{B.15}$$

$$s^{(\beta\neq0)}(p,t) = s(p,t_i)\left(\frac{p+i\beta t}{p+i\beta t_i}\right)^{i\mu}e^{-\gamma(t-t_i)} -$$

$$g\int_{t_i}^t d\tau a(0,\tau)e^{i\left(\beta\frac{L}{2}-\omega_m\right)\tau}e^{-\gamma(t-\tau)}\frac{(p+i\beta t)^{i\mu}}{(p+i\beta\tau)^{i\mu+1}}, \tag{B.16}$$

and for $\beta = 0$:

$$a^{(\beta=0)}(p,t) = \frac{1}{p}a(0,t) - |g|^2 N \int_{t_i}^t d\tau a(0,\tau)e^{i\omega_m(t-\tau)}e^{-\gamma(t-\tau)}\frac{1}{p^2}\exp\left[-\frac{|g|^2 N}{p}(t-\tau)\right] +$$

$$g^* N s(p,t_i)\frac{1}{p}\exp\left[-\frac{|g|^2 N}{p}(t-t_i)\right]e^{-\gamma(t-t_i)}e^{i\omega_m t}, \tag{B.17}$$

$$s^{(\beta=0)}(p,t) = s(p,t_i)\exp\left[-\frac{|g|^2 N}{p}(t-t_i)\right]e^{-\gamma(t-t_i)} - g\int_{t_i}^t d\tau a(0,\tau)e^{-i\omega_m\tau}e^{-\gamma(t-\tau)}\frac{1}{p}$$

$$\exp\left[-\frac{|g|^2 N}{p}(t-\tau)\right], \tag{B.18}$$

where $\mu = |g|^2 N/\beta$, $t \in [t_i,t_f]$.

B.2 Derivation of the exact analytical solution for GEM: Storage

The time and space evolution of the field and the collective coherence during storage is given by the inverse Laplace transformation of Eqs. (B.15) - (B.18) with $t_i = -T$ and $t_f = 0$, subjecting to the initial condition $s_s(z,-T) = 0$ and boundary condition $a_s(z = 0,t) = a_{\text{in}}(t)$. Here the arrival time t_{in} of $a_{\text{in}}(t)$ is smaller than zero, and the subscript "s" denotes the storage process. The spatial variable $z \in [0,L]$.

From Eqs. (B.15) and (B.16) we have the solution of a gradient absorption in Laplace domain

$$a_s^{(\beta\neq 0)}(p,t \leqslant 0) = \frac{1}{p}a_{\text{in}}(t) - |g|^2 N \int_{-T}^t d\tau a_{\text{in}}(\tau) \times$$

$$e^{-i\left(\beta\frac{L}{2}-\omega_m\right)(t-\tau)}e^{-\gamma(t-\tau)}\frac{p^{i\mu-1}}{[p-i\beta(t-\tau)]^{i\mu+1}}, \tag{B.19}$$

$$s_s^{(\beta\neq 0)}(p,t \leqslant 0) = -g\int_{-T}^t d\tau a_{\text{in}}(\tau)e^{i\left(\beta\frac{L}{2}-\omega_m\right)\tau}e^{-\gamma(t-\tau)}\frac{(p+i\beta t)^{i\mu}}{(p+i\beta\tau)^{i\mu+1}}. \tag{B.20}$$

Similar result can be obtained for a flat single-frequency absorption out of Eqs. (B.17) and

(B.18).

The following inverse Laplace transformation [240] will be used:

$$\mathcal{L}^{-1}\left\{p^{i\mu-1}\left[p-i\beta\left(t-\tau\right)\right]^{-i\mu-1}\right\}=z\,{}_1F_1(i\mu+1;2;i\beta\left(t-\tau\right)z)\,,\tag{B.21}$$

$$\mathcal{L}^{-1}\left\{(p+i\beta t)^{i\mu}\left(p+i\beta\tau\right)^{-i\mu-1}\right\}=e^{-i\beta tz}\,{}_1F_1(i\mu+1;1;i\beta\left(t-\tau\right)z)\,,\tag{B.22}$$

and

$$\mathcal{L}^{-1}\left\{\frac{1}{p^2}\exp\left[-\frac{|g|^2N\left(t-\tau\right)}{p}\right]\right\}=z\frac{J_1(2\sqrt{|g|^2N\left(t-\tau\right)z})}{\sqrt{|g|^2N\left(t-\tau\right)z}}\,,\tag{B.23}$$

$$\mathcal{L}^{-1}\left\{\frac{1}{p}\exp\left[-\frac{|g|^2N\left(t-\tau\right)}{p}\right]\right\}=J_0(2\sqrt{|g|^2N\left(t-\tau\right)z})\,,\tag{B.24}$$

where ${}_1F_1$ is the Kummer confluent hypergeometric function and J_ν is the νth order Bessel function. Substituting Eqs. (B.21), (B.22) back into Eqs. (B.19), (B.20), and Eqs. (B.23), (B.24) back into Eqs. (B.17), (B.18), and making use of $\mathcal{L}^{-1}\left\{p^{-1}\right\}=1$, we obtain the exact solution during storage process:

$$a_s^{(\beta\neq0)}(z,t\leqslant0)=a_{\text{in}}(t)-\mu\beta z\int_{-T}^t d\tau a_{\text{in}}(\tau)e^{-i\left(\beta\frac{L}{2}-\omega_m\right)(t-\tau)}e^{-\gamma(t-\tau)}\times$$

$$\qquad\qquad\qquad {}_1F_1(i\mu+1;2;i\beta z(t-\tau))\,,\tag{B.25}$$

$$s_s^{(\beta\neq0)}(z,t\leqslant0)=-ge^{-i\beta zt}\int_{-T}^t d\tau a_{\text{in}}(\tau)e^{i\left(\beta\frac{L}{2}-\omega_m\right)\tau}e^{-\gamma(t-\tau)}\,{}_1F_1(i\mu+1;1;i\beta z(t-\tau))\,,$$

$$\tag{B.26}$$

$$a_s^{(\beta=0)}(z,t\leqslant0)=a_{\text{in}}(t)-|g|^2Nz\int_{-T}^t d\tau a_{\text{in}}(\tau)e^{i\omega_m(t-\tau)}e^{-\gamma(t-\tau)}\frac{J_1(2\sqrt{|g|^2Nz(t-\tau)})}{\sqrt{|g|^2Nz(t-\tau)}}\,,$$

$$\tag{B.27}$$

$$s_s^{(\beta=0)}(z,t\leqslant0)=-g\int_{-T}^t d\tau a_{\text{in}}(\tau)e^{-i\omega_m\tau}e^{-\gamma(t-\tau)}J_0(2\sqrt{|g|^2Nz(t-\tau)})\,.\tag{B.28}$$
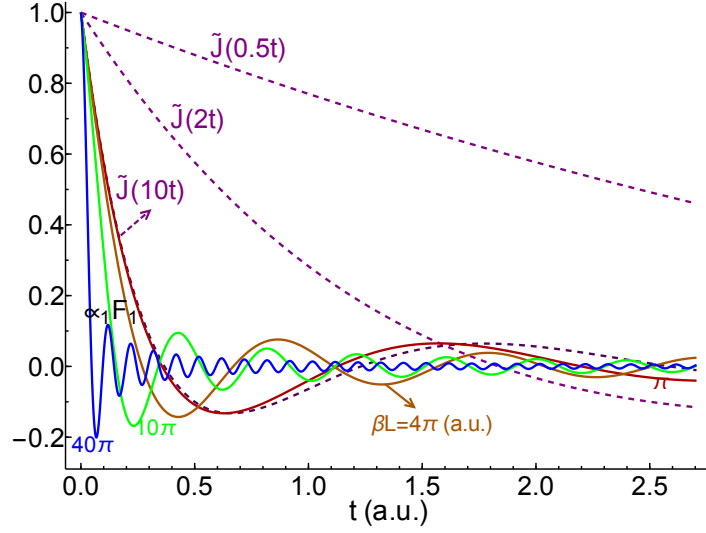
Figure B.1: The functions of $e^{-i\beta Lt/2} {}_1F_1(i\mu + 1; 2; i\beta Lt)$ (solid lines of various colors) and $\tilde{J}_1(|g|^2 NLt)$ (dashed lines of purple color), where $\tilde{J}_1(x) = J_1(2\sqrt{x})/\sqrt{x}$. The solid lines are plotted under $|g|^2 NL = 10$ a.u., among which the red, orange, green and blue colors represent $\beta L = \pi, 4\pi, 10\pi, 40\pi$ a.u. respectively.

Comparing Eqs. (B.25) and (B.27), it is seen that the difference between a gradient absorption and flat single-frequency absorption lies in $e^{-i\beta tL/2} {}_1F_1(i\mu + 1; 2; i\beta zt)$ and $\frac{J_1(2\sqrt{|g|^2 Nzt})}{\sqrt{|g|^2 Nzt}}$. In Fig. B.1 we plot these two functions for different parameters.

B.3   Derivation of the exact analytical solution for GEM: Retrieval

The exact solution of gradient echo is calculated based on Eqs. (B.15) and (B.16) in retrieval time window $t \in [t_i, t_f] = [0, T]$ with parameters β', g', N', μ', and ω'_m. The boundary condition is

$$a_r(z = 0, t) = 0, \tag{B.29}$$

where the subscript "r" denotes retrieval. In the usual GEM method, $s_r(z,0) = s_s(z,0)$. So from Eq. (B.20), we have

$$s_r(p,0) = s_s(p,0) = -g \int_{-T}^{0} d\tau a_{\text{in}}(\tau) e^{i(\beta \frac{L}{2} - \omega_m)\tau} e^{\gamma\tau} \frac{p^{i\mu}}{(p+i\beta\tau)^{i\mu+1}}. \tag{B.30}$$

Substituting the boundary and initial conditions (B.29) and (B.30) into Eqs. (B.15) and (B.16), we obtain the GEM echo and retrieval collective coherence in the Laplace domain:

$$a_r(p, t \geqslant 0)$$

$$= -gg'^* N' \int_{-T}^{0} d\tau a_{\text{in}}(\tau) e^{-i(\beta't - \beta\tau)\frac{L}{2}} e^{i(\omega_m' t - \omega_m \tau)} e^{-\gamma(t-\tau)} \frac{p^{i\mu'-1} (p - i\beta't)^{i(\mu-\mu')}}{[p - i(\beta't - \beta\tau)]^{i\mu+1}}, \tag{B.31}$$

$$s_r(p, t \geqslant 0) = -g \int_{-T}^{0} d\tau a_{\text{in}}(\tau) e^{i(\beta\frac{L}{2} - \omega_m)\tau} e^{-\gamma(t-\tau)} \frac{p^{i(\mu-\mu')} (p + i\beta't)^{i\mu'}}{(p + i\beta\tau)^{i\mu+1}}. \tag{B.32}$$

We will use the following inverse Laplace transformation [240]:

$$\mathfrak{L}^{-1} \left\{ \frac{p^{i\mu'-1} (p - i\beta't)^{i(\mu-\mu')}}{[p - i(\beta't - \beta\tau)]^{i\mu+1}} \right\} = z\Phi_2 \left(i\mu + 1, i\mu' - i\mu; 2; i(\beta't - \beta\tau)z, i\beta'tz \right), \tag{B.33}$$

and

$$\mathfrak{L}^{-1} \left\{ \frac{p^{i(\mu-\mu')} (p + i\beta't)^{i\mu'}}{(p + i\beta\tau)^{i\mu+1}} \right\} = \Phi_2 \left(i\mu + 1, -i\mu'; 1; -i\beta\tau z, -i\beta'tz \right), \tag{B.34}$$

where Φ_2 is the Humbert double hypergeometric series.

Substituting Eqs. (B.33) and (B.34) back to the inverse Laplace transformation of Eqs. (B.31) and (B.32), we obtain the exact analytical expression of the field and atomic

collective coherence during retrieval:

$$a_r(z,t \geqslant 0) = -gg'^*N'z \int_{-T}^{0} d\tau a_{\text{in}}(\tau) e^{-i(\beta' t - \beta \tau)\frac{L}{2}} e^{i(\omega'_m t - \omega_m \tau)} e^{-\gamma(t-\tau)} \times$$

$$\Phi_2 \left(i\mu + 1, i\mu' - i\mu; 2; i\left(\beta' t - \beta \tau\right) z, i\beta' zt\right), \tag{B.35}$$

$$s_r(z,t \geqslant 0) = -g \int_{-T}^{0} d\tau a_{\text{in}}(\tau) e^{i(\beta\frac{L}{2} - \omega_m)\tau} e^{-\gamma(t-\tau)} \Phi_2 \left(i\mu + 1, -i\mu'; 1; -i\beta z\tau, -i\beta' zt\right), \tag{B.36}$$

where $z \in [0, L]$, $t \in [0, T]$.

If $g' = g$, $N' = N$, $\beta' = \beta$, $\mu' = \mu$, and $\omega'_m = \omega_m$, we recover the storage solution. If $g' = g$, $N' = N$, $\beta' = -\beta$, and $\mu' = -\mu$, from Eqs. (B.35) and (B.36) we obtain the exact GEM solution:

$$a_r(z,t \geqslant 0) = -\mu\beta z \int_{-T}^{0} d\tau a_{\text{in}}(\tau) e^{i\beta\frac{L}{2}(t+\tau)} e^{i(\omega'_m t - \omega_m \tau)} e^{-\gamma(t-\tau)} \times$$

$$\Phi_2 \left(i\mu + 1, -2i\mu; 2; -i\beta z(t+\tau), -i\beta zt\right), \tag{B.37}$$

$$s_r(z,t \geqslant 0) = -g \int_{-T}^{0} d\tau a_{\text{in}}(\tau) e^{i(\beta\frac{L}{2} - \omega_m)\tau} e^{-\gamma(t-\tau)} \Phi_2 \left(i\mu + 1, i\mu; 1; -i\beta z\tau, i\beta zt\right), \tag{B.38}$$

where $z \in [0, L]$, $t \in [0, T]$. From this solution, the GEM output echo (i.e., at $z = L$) can be expanded into the following form by using Eq. (B.48):

$$a_{r,\text{out}}(t \geqslant 0) = -\mu\beta L \sum_{n=0}^{\infty} \frac{(-2i\mu)_n}{(n+1)!} \frac{(-i\beta Lt)^n}{n!} \int_{-T}^{0} d\tau a_{\text{in}}(\tau) e^{i\beta\frac{L}{2}(t+\tau)} e^{i(\omega'_m t - \omega_m \tau)} e^{-\gamma(t-\tau)}$$

$$\times {}_2F_1 \left(-n, i\mu + 1; 2i\mu + 1 - n; 1 + \frac{\tau}{t}\right). \tag{B.39}$$

B.4   Some properties for the Humbert double hypergeometric series Φ_2

It is seen from Eq. (B.35) that the GEM echo is mainly determined by Humbert double hypergeometric function Φ_2. Some of the remarks of this relatively complicated

special function can be found in recent studies [241--244]. The function $\Phi_2(\alpha, \alpha'; v; x, y)$

satisfies the following partial differential equation:

$$x\frac{\partial^2 \Phi_2}{\partial x^2} + y\frac{\partial^2 \Phi_2}{\partial x \partial y} + (v - x)\frac{\partial \Phi_2}{\partial x} - \alpha \Phi_2 = 0, \tag{B.40}$$

$$y\frac{\partial^2 \Phi_2}{\partial y^2} + x\frac{\partial^2 \Phi_2}{\partial x \partial y} + (v - y)\frac{\partial \Phi_2}{\partial y} - \alpha' \Phi_2 = 0. \tag{B.41}$$

It has an integral representation

$$\Phi_2(\alpha, \alpha'; v; x, y) = \frac{\Gamma(v)}{\Gamma(\alpha)\Gamma(\alpha')\Gamma(v - \alpha - \alpha')} \int_0^1 \int_0^1 d\xi d\eta e^{x\xi + y(1-\xi)\eta} \xi^{\alpha - 1} \eta^{\alpha' - 1} \times$$

$$(1 - \xi)^{v - \alpha - 1}(1 - \eta)^{v - \alpha - \alpha' - 1}. \tag{B.42}$$

Two useful relations in special cases between Φ_2 and Kummer confluent hypergeo-

metric function $_1F_1$ are:

$$\Phi_2(\alpha, v - \alpha; v; x, y) = e^y {}_1F_1(\alpha; v; x - y), \tag{B.43}$$

$$\Phi_2(\alpha, \alpha'; v; x, x) = {}_1F_1(\alpha + \alpha'; v; x). \tag{B.44}$$

The function $\Phi_2(\alpha, \alpha'; v; x, y)$ can also be defined through a double series as:

$$\Phi_2(\alpha, \alpha'; v; x, y) = \sum_{m,n=0}^{\infty} \frac{(\alpha)_m(\alpha')_n}{(v)_{m+n}m!n!}x^m y^n, \tag{B.45}$$

where $(\alpha)_m = \alpha(\alpha + 1)\cdots(\alpha + m - 1) = \Gamma(\alpha + m)/\Gamma(\alpha)$, $(\alpha)_0 = 1$. Another expansion

in terms of Gauss hypergeometric function $_2F_1$ is [243]

$$\Phi_2(\alpha, \alpha'; v; x, y) = \sum_{m=0}^{\infty} \frac{(\alpha)_m}{(v)_m} {}_2F_1\left(-m, \alpha'; 1 - \alpha - m; \frac{y}{x}\right) \frac{x^m}{m!}. \tag{B.46}$$

So in the case of usual gradient echo in Eq. (B.37),

$$\Phi_2(i\mu + 1, -2i\mu; 2; -i\beta z(t + \tau), -i\beta zt)$$

$$= \frac{1}{\Gamma(i\mu + 1)\Gamma(-2i\mu)} \sum_{m,n=0}^{\infty} \frac{\Gamma(i\mu + 1 + m)\Gamma(-2i\mu + n)}{(m + n + 1)!m!n!} (-i\beta zt)^n [-i\beta z(t + \tau)]^m \quad \text{(B.47)}$$

$$= \frac{1}{\Gamma(-2i\mu)} \sum_{m=0}^{\infty} \frac{\Gamma(-2i\mu + m)}{(m + 1)!} \frac{(-i\beta zt)^m}{m!} {}_2F_1\left(-m, i\mu + 1; 2i\mu + 1 - m; 1 + \frac{\tau}{t}\right). \quad \text{(B.48)}$$

Eq. (B.48) provides a series to Eq. (B.37) that illustrates how the gradient echo is constructed.

One should be careful when evaluating Φ_2 using expansions (B.47) and/or (B.48), since for larger argument βzT they become numerically unstable. Also it is useful to check Eqs. (B.47) and/or (B.48) with its special values of Φ_2 by, for example, the following cases:

$$\Phi_2 = \begin{cases} {}_1F_1(-2i\mu; 2; -i\beta zt), & \text{if } \tau = -t, \\ {}_1F_1(i\mu + 1; 2; -i\beta z\tau), & \text{if } t = 0, \\ {}_1F_1(-i\mu + 1; 2; -i\beta zt), & \text{if } \tau = 0. \end{cases}$$

Sometimes Φ_2 can be numerically evaluated more easily with inverse Laplace transformation algorithm [245, 246] directly from Eq. (B.31).

APPENDIX C

EVOLUTION EQUATIONS OF QUANTUM MEMORY BASED ON CONTROL FIELD DISCRETE SPATIAL CHIRP[*]

In this appendix[1], we derive the evolution equations for the quantum storage scheme based on control field discrete spatial chirp. Very similar methods can be used to derive the evolution equations for the quantum memories based on PMC in Chap. II and/or control field spatial chirp in Chap. III.

C.1 Hamiltonian of the system

First of all we write the signal field $E_s(\mathbf{r},t)$ and control field $E_c(\mathbf{r},t)$ in the laboratory frame F in SI unit as:

$$\mathbf{E}_s(\mathbf{r},t) = \hat{\epsilon}_s \frac{i}{n_{\mathrm{bg}}} \mathscr{E}_s \hat{a}(\mathbf{r},t) e^{i(\mathbf{k}_s \cdot \mathbf{r} - \varphi_{0s})} + H.c., \tag{C.1a}$$

$$\mathbf{E}_c(\mathbf{r},t) = \hat{\epsilon}_c E_0(\mathbf{r},t) e^{i[\mathbf{k}_c(\mathbf{r}) \cdot \mathbf{r} - \omega_c(\mathbf{r})t - \varphi_{0c}(\mathbf{r})]} + c.c., \tag{C.1b}$$

in which $\hat{\epsilon}_{s,c}$ are the polarization vectors of the signal and control fields [in the example of ^{87}Rb provided in Chap. V, $\hat{\epsilon}_s = \hat{\sigma}^+$, $\hat{\epsilon}_c = (0,0,1)$], $\mathscr{E}_s = \sqrt{\hbar \omega_s/(2\varepsilon_0 V)} \in \mathbb{R}$, $\mathscr{E}_c = \mathrm{Const} \in \mathbb{R}$, ε_0 is the vacuum permittivity, $\varphi_{0s} = \mathbf{k}_s \cdot \mathbf{r}_0 - \omega_s t_0$, $\varphi_{0c} = \mathbf{k}_c(\mathbf{r}_0) \cdot \mathbf{r}_0 - \omega_c(\mathbf{r}_0)t_0$, $k_c = n_{\mathrm{bg}}\omega_c/c$, $k_s = n\omega_s/c$. Here n is the refractive index taking into account

---

[*]The preprint of the related work "Quantum storage based on controllable frequency comb" by Xiwen Zhang, Alexey Kalachev, Philip Hemmer, and Olga Kocharovskaya is available on arXiv:1602.02322 (2016), and will be submitted to journal publication soon.

[1]Some notations in this appendix, such as the slowly varying part of the signal field $\tilde{a}(z,t)$, are different from that in the main text of Chaps. II - VI. The validity of these notations stay only in this appendix.

the atom-environment interaction (background) and the atom-atom Raman interaction: $n = n_{\text{bg}}n_{\text{int}}$, c is the speed of light in vacuum. The control field feels the background refractive index n_{bg}, while the signal field feels total one n. The expression of $\mathscr{E}_s$ is obtained following Ref. [177], which derives the quantization amplitude of a photon in a medium with refractive index n as $(i/n)\sqrt{\hbar\omega_s/(2\varepsilon_0 V)}$ upon the neglect of dispersion (assuming c/v_g is equal to n). Here n_{bg} is used in the quantization amplitude because we have in mind a quantized field under the background interaction, and the additional modification of the refractive index imposed by the Raman interaction, n_{int}, is thereafter calculated via treating Maxwell equation in a uniform, isotropic background, which is consistent with the field quantization.

The level scheme we are considering is shown in Fig. 5.1 (a). We define the one-photon frequency detuning as $\Delta = \omega_s - \omega_{21}$, and two-photon frequency detuning as

$$\delta(\mathbf{r},t) = \omega_s - \omega_c(\mathbf{r},t) - \omega_{31} - \frac{|\Omega_c(\mathbf{r},t)|^2}{(\omega_s - \omega_{21}) + i\gamma_{21}}, \qquad \text{(C.2)}$$

with its central value $\delta_0 = \omega_s - \omega_{c0} - \omega_{31}$, where $\omega_{c0} = \omega_c(\mathbf{r}=0)$, γ_{21} is the decoherence rate between the excited state $|2\rangle$ and ground state $|1\rangle$. In addition, the control field angular frequency distribution satisfies $\omega_c(\mathbf{r}) - \omega_{c0}(\mathbf{r}=0) = m(\mathbf{r})\delta\omega_c$, $m(\mathbf{r})$ is a position dependent integer. Since we consider an off-resonant interaction, γ_{21} will be neglected with respect to $\omega_s - \omega_{21}$.

In general, the atoms in the medium can move with finite speeds subjecting some velocity distributions. So we start from the distribution of an atom in its moving frame, and change to laboratory frame later on. The Hamiltonian of such a system in the atomic

moving frame F' then can be written as

$$\hat{H} = \hbar\omega_1 |1\rangle\langle 1| + \hbar\omega_2 |2\rangle\langle 2| + \hbar\omega_3(t) |3\rangle\langle 3| - e\mathbf{R}_{12} \cdot \mathbf{E}'_s(\mathbf{r}',t) - e\mathbf{R}_{23} \cdot \mathbf{E}'_c(\mathbf{r}',t), \quad \text{(C.3)}$$

where $\mathbf{R}_{ij}$ are the internal coordinates of the electronic transitions, $\mathbf{E}'_s$ and $\mathbf{E}'_c$ are the fields' variable names in the moving frame. From the relation between the laboratory frame F and moving frame F': $\mathbf{r} = \mathbf{r}' + \mathbf{v}t'$, $t = t'$, we have

$$\mathbf{E}_s(\mathbf{r},t) = \mathbf{E}_s(\mathbf{r}' + \mathbf{v}t',t') \triangleq \mathbf{E}'_s(\mathbf{r}',t';\mathbf{v}) = \hat{\epsilon}_s \frac{i}{n_{\text{bg}}} \mathscr{E}_s \hat{a}'(\mathbf{r}',t';\mathbf{v}) e^{i[\mathbf{k}_s \cdot (\mathbf{r}'+\mathbf{v}t')-\varphi_{0s}]} + H.c.,$$

$$\text{(C.4a)}$$

$$\mathbf{E}_c(\mathbf{r},t) = \mathbf{E}_c(\mathbf{r}' + \mathbf{v}t',t') \triangleq \mathbf{E}'_c(\mathbf{r}',t';\mathbf{v})$$

$$= \hat{\epsilon}_c E'_0(\mathbf{r}',t';\mathbf{v}) e^{i[\mathbf{k}_c[\mathbf{r}'+\mathbf{v}t']\cdot(\mathbf{r}'+\mathbf{v}t')-\omega_c(\mathbf{r}'+\mathbf{v}t')t'-\varphi_{0c}(\mathbf{r}'+\mathbf{v}t')]} + c.c., \quad \text{(C.4b)}$$

where $\mathbf{k}_c[\mathbf{r}' + \mathbf{v}t']$ denotes the time and space dependence of $\mathbf{k}_c$. Using

$$e\mathbf{r} \cdot \mathbf{E}'_s(\mathbf{r}',t';\mathbf{v}) \approx i\hbar\bar{g} |2\rangle\langle 1| \hat{a}'(\mathbf{r}',t';\mathbf{v}) e^{i[\mathbf{k}_s \cdot (\mathbf{r}'+\mathbf{v}t')-\varphi_{0s}]}$$

$$- i\hbar\bar{g}^* |1\rangle\langle 2| \hat{a}'^\dagger(\mathbf{r}',t';\mathbf{v}) e^{-i[\mathbf{k}_s \cdot (\mathbf{r}'+\mathbf{v}t')-\varphi_{0s}]}, \quad \text{(C.5a)}$$

$$e\mathbf{r} \cdot \mathbf{E}'_c(\mathbf{r}',t';\mathbf{v}) \approx \hbar\Omega'^*_c(\mathbf{r}',t';\mathbf{v}) |2\rangle\langle 3| e^{i[\mathbf{k}_c[\mathbf{r}'+\mathbf{v}t']\cdot(\mathbf{r}'+\mathbf{v}t')-\omega_c(\mathbf{r}'+\mathbf{v}t')t'-\varphi_{0c}(\mathbf{r}'+\mathbf{v}t')]}$$

$$+ \hbar\Omega'_c(\mathbf{r}',t';\mathbf{v}) |3\rangle\langle 2| e^{-i[\mathbf{k}_c[\mathbf{r}'+\mathbf{v}t']\cdot(\mathbf{r}'+\mathbf{v}t')-\omega_c(\mathbf{r}'+\mathbf{v}t')t'-\varphi_{0c}(\mathbf{r}'+\mathbf{v}t')]}, \quad \text{(C.5b)}$$

in which

$$\bar{g} = \frac{d_{21}\mathscr{E}_s}{n_{\text{bg}}\hbar} = \frac{e\langle 2|\mathbf{r}\cdot\varepsilon_s|1\rangle}{\hbar} \frac{1}{n_{\text{bg}}} \sqrt{\frac{\hbar\omega_s}{2\varepsilon_0 V}}, \quad \text{(C.6)}$$

$$\Omega'_c(\mathbf{r}',t';\mathbf{v}) = \frac{d_{32}E'^*_0(\mathbf{r}',t';\mathbf{v})}{\hbar}, \quad \text{(C.7)}$$

and $d_{21} = e\langle 2|\mathbf{R}_{12}\cdot\hat{\epsilon}_s|1\rangle$, $d_{23} = e\langle 2|\mathbf{R}_{23}\cdot\hat{\epsilon}_c|3\rangle$, and denoting $|m_j\rangle\langle n_j| = \hat{\sigma}^j_{mn}$, the Hamil-

tonian for jth atom in its moving frame is written into:

$$\hat{H}^j = \hbar\omega_{21}\hat{\sigma}_{22}^j(\mathbf{r}^{j\prime},t') + \hbar\omega_{31}\hat{\sigma}_{33}^j(\mathbf{r}^{j\prime},t') - i\hbar\bar{g}\hat{\sigma}_{21}^j(\mathbf{r}^{j\prime},t')\hat{a}\left(\mathbf{r}^j,t\right)e^{i\left(\mathbf{k}_s\cdot\mathbf{r}^j - \varphi_{0s}\right)} +$$

$$i\hbar\bar{g}^*\hat{\sigma}_{12}^j(\mathbf{r}^{j\prime},t')\hat{a}^\dagger\left(\mathbf{r}^j,t\right)e^{-i\left(\mathbf{k}_s\cdot\mathbf{r}^j - \varphi_{0s}\right)} - \hbar\Omega_c^*(\mathbf{r}^j,t)\hat{\sigma}_{23}^j(\mathbf{r}^{j\prime},t')e^{-i\omega_c(\mathbf{r}^j)t} \times$$

$$e^{i\mathbf{k}_c[\mathbf{r}^j]\cdot\mathbf{r}^j - i\varphi_{0c}(\mathbf{r}^j)} - \hbar\Omega_c(\mathbf{r}^j,t)\hat{\sigma}_{32}^j(\mathbf{r}^{j\prime},t')e^{i\omega_c(\mathbf{r}^j)t}e^{-i\mathbf{k}_c(\mathbf{r}^j)\cdot\mathbf{r}^j + i\varphi_{0c}(\mathbf{r}^j)}, \qquad (C.8)$$

where $\hat{a}(\mathbf{r}^j,t) = \hat{a}'(\mathbf{r}^{j\prime},t';\mathbf{v})$, and $\mathbf{r}^j = \mathbf{r}^{j\prime} + \mathbf{v}t'$ on the phase factors. Here $\omega_{mn} = \omega_m - \omega_n$

$(m,n = 1,2,3)$, and ω_1 is set to be zero. We use $\mathbf{r}$ (in laboratory frame F) and $\mathbf{r}'$ (in moving

frame F') to denote time-independent frame coordinates, and $\mathbf{r}^j$ and $\mathbf{r}^{j\prime}$ to denote specific

time-dependent atomic positions, where $\mathbf{r}^j = \mathbf{r}_0^j + \mathbf{v}^j t$ and $\mathbf{r}_0^j = \mathbf{r}^{j\prime}$.

C.2 Atomic equation

In the following we derive the equation for the atomic evolution. For convenience

the constant phase of the signal field propagating along $\hat{z}$ will be set to zero: $\varphi_{0s} = 0$. We

consider weak excitation and vacuum noise, where the fluctuation has no influence to the

system for quantum memory. From Heisenberg equation $\frac{\partial\hat{\sigma}_{mn}^j}{\partial t} = \frac{i}{\hbar}\left[\hat{H},\hat{\sigma}_{mn}^j\right]$, adding decay

terms by hand, one obtains the following equations in the moving frame F':

$$\frac{\partial\hat{\sigma}_{11}^j}{\partial t'} = \Gamma_{2\to1}\hat{\sigma}_{22}^j + \bar{g}\hat{\sigma}_{21}^j\hat{a}e^{ik_s z^j} + \bar{g}^*\hat{\sigma}_{12}^j\hat{a}^\dagger e^{-ik_s z^j}, \qquad (C.9a)$$

$$\frac{\partial\hat{\sigma}_{22}^j}{\partial t'} = -\Gamma_2\hat{\sigma}_{22}^j - \bar{g}\hat{\sigma}_{21}^j\hat{a}e^{ik_s z^j} - \bar{g}^*\hat{\sigma}_{12}^j\hat{a}^\dagger e^{-ik_s z^j} + i\Omega_c^*\hat{\sigma}_{23}^j e^{-i\omega_c(\mathbf{r}^j)t} \times$$

$$e^{i\mathbf{k}_c[\mathbf{r}^j]\cdot\mathbf{r}^j - i\varphi_{0c}(\mathbf{r}^j)} - i\Omega_c\hat{\sigma}_{32}^j e^{i\omega_c(\mathbf{r}^j)t}e^{-i\mathbf{k}_c[\mathbf{r}^j]\cdot\mathbf{r}^j + i\varphi_{0c}(\mathbf{r}^j)}, \qquad (C.9b)$$

$$\frac{\partial\hat{\sigma}_{33}^j}{\partial t'} = \Gamma_{2\to3}\hat{\sigma}_{22}^j - i\Omega_c^*\hat{\sigma}_{23}^j e^{-i\omega_c(\mathbf{r}^j)t}e^{i\mathbf{k}_c[\mathbf{r}^j]\cdot\mathbf{r}^j - i\varphi_{0c}(\mathbf{r}^j)} + i\Omega_c\hat{\sigma}_{32}^j e^{i\omega_c(\mathbf{r}^j)t}e^{-i\mathbf{k}_c[\mathbf{r}^j]\cdot\mathbf{r}^j + i\varphi_{0c}(\mathbf{r}^j)},$$

$$(C.9c)$$

173

$$\frac{\partial \hat{\sigma}_{13}^j}{\partial t'} = -\left[\gamma_{31} + i\omega_{31}(t')\right]\hat{\sigma}_{13}^j + \bar{g}\hat{\sigma}_{23}^j \hat{a} e^{ik_s z^j} + i\Omega_c \hat{\sigma}_{12}^j e^{i\omega_c(\mathbf{r}^j)t} e^{-i\mathbf{k}_c[\mathbf{r}^j]\cdot\mathbf{r}^j + i\varphi_{0c}(\mathbf{r}^j)}, \quad \text{(C.9d)}$$

$$\frac{\partial \hat{\sigma}_{12}^j}{\partial t'} = -\left(\gamma_{21} + i\omega_{21}\right)\hat{\sigma}_{12}^j + \bar{g}\left(\hat{\sigma}_{22}^j - \hat{\sigma}_{11}^j\right)\hat{a}\left(z^j, t\right)e^{ik_s z^j} +$$

$$i\Omega_c^* \hat{\sigma}_{13}^j e^{-i\omega_c(\mathbf{r}^j)t} e^{i\mathbf{k}_c[\mathbf{r}^j]\cdot\mathbf{r}^j - i\varphi_{0c}(\mathbf{r}^j)}, \quad \text{(C.9e)}$$

$$\frac{\partial \hat{\sigma}_{23}^j}{\partial t'} = -\left[\gamma_{23} - i\omega_{23}(t')\right]\hat{\sigma}_{23}^j + i\Omega_c\left(\hat{\sigma}_{22}^j - \hat{\sigma}_{33}^j\right)e^{i\omega_c(\mathbf{r}^j)t} e^{-i\mathbf{k}_c[\mathbf{r}^j]\cdot\mathbf{r}^j + i\varphi_{0c}(\mathbf{r}^j)} -$$

$$\bar{g}^* \hat{\sigma}_{13}^j \hat{a}^\dagger e^{-ik_s z^j}, \quad \text{(C.9f)}$$

in which $\hat{\sigma}_{mn}^j$ denotes $\hat{\sigma}_{mn}^j(\mathbf{r}^{j'}, t'; \mathbf{v}^j)$, $\mathbf{v}^j$ implicitly sits in $\mathbf{r}^j$ of the fields, $\hat{a}$ denotes $\hat{a}\left(z^j, t\right)$, Ω_c denotes $\Omega_c\left(\mathbf{r}^j, t\right)$, and we assume in a general case that level $|3\rangle$ is modulated in time [so that we have $\omega_{31}(t)$ and $\omega_{23}(t)$] to incorporate the discussions of quantum memory based on control field frequency chirp in Chap. II, $\Gamma_{i \to j}$ is the population decay rate from state $|i\rangle$ to $|j\rangle$, Γ_i is the total population loss rate for $|i\rangle$, $\gamma_{ij} = \gamma_{ji}$ is the decoherence rete between $|i\rangle$ and $|j\rangle$.

Let us define a collective atomic operator with respect to a constant velocity $\mathbf{v}_0$:

$$\frac{1}{N}\sum_j \int d\mathbf{v}^{j'} \hat{\sigma}_{mn}^j(\mathbf{r}^{j'}, t'; \mathbf{v}^j)\delta(\mathbf{r}' - \mathbf{r}^{j'})\delta(\mathbf{v}_0 - \mathbf{v}^{j'})$$

$$\approx \int d\mathbf{r}^{j'} \hat{\sigma}_{mn}(\mathbf{r}^{j'}, t'; \mathbf{v}_0)\delta(\mathbf{r}' - \mathbf{r}^{j'}) = \hat{\sigma}_{mn}(\mathbf{r}', t'; \mathbf{v}_0), \quad \text{(C.10)}$$

Here the summation of spacial variable is performed with respect to the moving frame variable $\mathbf{r}^{j'}$, which is equal to $\mathbf{r}_0^j$ (we assume each moving frame of different atoms has the same origin that overlaps with the corresponding laboratory frame origin). After similar

treatment to Eqs. (C.9a) - (C.9f), and using

$$\frac{\partial}{\partial z'} = \frac{\partial}{\partial z}, \tag{C.11a}$$

$$\frac{\partial}{\partial t'} = \frac{\partial}{\partial t} + \mathbf{v} \cdot \frac{\partial}{\partial \mathbf{r}}, \tag{C.11b}$$

the equations in the laboratory frame become

$$\left(\frac{\partial}{\partial t} + \mathbf{v}_0 \cdot \frac{\partial}{\partial \mathbf{r}}\right)\hat{\sigma}_{11}(\mathbf{r},t;\mathbf{v}_0) = \Gamma_{2\to 1}\hat{\sigma}_{22} + \bar{g}\hat{\sigma}_{21}\hat{a}e^{ik_s z} + \bar{g}^*\hat{\sigma}_{12}\hat{a}^\dagger e^{-ik_s z}, \tag{C.12a}$$

$$\left(\frac{\partial}{\partial t} + \mathbf{v}_0 \cdot \frac{\partial}{\partial \mathbf{r}}\right)\hat{\sigma}_{22}(\mathbf{r},t;\mathbf{v}_0) = -\Gamma_2\hat{\sigma}_{22} - \bar{g}\hat{\sigma}_{21}\hat{a}e^{ik_s z} - \bar{g}^*\hat{\sigma}_{12}\hat{a}^\dagger e^{-ik_s z} +$$

$$i\Omega_c^*\hat{\sigma}_{23}e^{-i\omega_c(\mathbf{r})t}e^{i\mathbf{k}_c[\mathbf{r}]\cdot\mathbf{r}-i\varphi_{0c}(\mathbf{r})} - i\Omega_c\hat{\sigma}_{32}e^{i\omega_c(\mathbf{r})t}e^{-i\mathbf{k}_c[\mathbf{r}]\cdot\mathbf{r}+i\varphi_{0c}(\mathbf{r})}, \tag{C.12b}$$

$$\left(\frac{\partial}{\partial t} + \mathbf{v}_0 \cdot \frac{\partial}{\partial \mathbf{r}}\right)\hat{\sigma}_{33}(\mathbf{r},t;\mathbf{v}_0) = \Gamma_{2\to 3}\hat{\sigma}_{22} - i\Omega_c^*\hat{\sigma}_{23}e^{-i\omega_c(\mathbf{r})t}e^{i\mathbf{k}_c[\mathbf{r}]\cdot\mathbf{r}-i\varphi_{0c}(\mathbf{r})} +$$

$$i\Omega_c\hat{\sigma}_{32}e^{i\omega_c(\mathbf{r})t}e^{-i\mathbf{k}_c[\mathbf{r}]\cdot\mathbf{r}+i\varphi_{0c}(\mathbf{r})}, \tag{C.12c}$$

$$\left(\frac{\partial}{\partial t} + \mathbf{v}_0 \cdot \frac{\partial}{\partial \mathbf{r}}\right)\hat{\sigma}_{13}(\mathbf{r},t;\mathbf{v}_0) = -\left[\gamma_{31} + i\omega_{31}(t')\right]\hat{\sigma}_{13} + \bar{g}\hat{\sigma}_{23}\hat{a}e^{ik_s z} +$$

$$i\Omega_c\hat{\sigma}_{12}e^{i\omega_c(\mathbf{r})t}e^{-i\mathbf{k}_c[\mathbf{r}]\cdot\mathbf{r}+i\varphi_{0c}(\mathbf{r})}, \tag{C.12d}$$

$$\left(\frac{\partial}{\partial t} + \mathbf{v}_0 \cdot \frac{\partial}{\partial \mathbf{r}}\right)\hat{\sigma}_{12}(\mathbf{r},t;\mathbf{v}_0) = -\left(\gamma_{21} + i\omega_{21}\right)\hat{\sigma}_{12} + \bar{g}\left(\hat{\sigma}_{22} - \hat{\sigma}_{11}\right)\hat{a}(z,t)e^{ik_s z} +$$

$$i\Omega_c^*\hat{\sigma}_{13}e^{-i\omega_c(\mathbf{r})t}e^{i\mathbf{k}_c[\mathbf{r}]\cdot\mathbf{r}-i\varphi_{0c}(\mathbf{r})}, \tag{C.12e}$$

$$\left(\frac{\partial}{\partial t} + \mathbf{v}_0 \cdot \frac{\partial}{\partial \mathbf{r}}\right)\hat{\sigma}_{23}(\mathbf{r},t;\mathbf{v}_0) = -\left[\gamma_{23} - i\omega_{23}(t')\right]\hat{\sigma}_{23} + i\Omega_c\left(\hat{\sigma}_{22} - \hat{\sigma}_{33}\right) \times$$

$$e^{i\omega_c(\mathbf{r})t}e^{-i\mathbf{k}_c[\mathbf{r}]\cdot\mathbf{r}+i\varphi_{0c}(\mathbf{r})} - \bar{g}^*\hat{\sigma}_{13}\hat{a}^\dagger e^{-ik_s z}, \tag{C.12f}$$

where $\hat{\sigma}_{mn}(\mathbf{r},t;\mathbf{v}_0)$ is the new variable name in the laboratory frame:

$$\hat{\sigma}_{mn}(\mathbf{r}',t';\mathbf{v}_0) = \hat{\sigma}_{mn}(\mathbf{r} - \mathbf{v}_0 t,t;\mathbf{v}_0) \underrightarrow{\text{re-denoted as}} \hat{\sigma}_{mn}(\mathbf{r},t;\mathbf{v}_0).$$

Defining the slow varying operators as

$$\hat{\sigma}_{12}\left(\mathbf{r},t;\mathbf{v}_0\right) = \tilde{\sigma}_{12}\left(\mathbf{r},t;\mathbf{v}_0\right)e^{-i\left(\omega_s t - \mathbf{k}_{12}\cdot\mathbf{r}\right)}, \tag{C.13a}$$

$$\hat{\sigma}_{23}\left(\mathbf{r},t;\mathbf{v}_0\right) = \tilde{\sigma}_{23}\left(\mathbf{r},t;\mathbf{v}_0\right)e^{i\left(\omega_c t - \mathbf{k}_{23}\cdot\mathbf{r}\right)}, \tag{C.13b}$$

$$\hat{\sigma}_{13}\left(\mathbf{r},t;\mathbf{v}_0\right) = \tilde{\sigma}_{13}\left(\mathbf{r},t;\mathbf{v}_0\right)e^{-i\left(\omega_s t - \omega_c t - \mathbf{k}_{13}\cdot\mathbf{r}\right)}, \tag{C.13c}$$

and

$$\hat{a}\left(z,t\right) = \tilde{a}\left(z,t\right)e^{-i\omega_s t}, \tag{C.14a}$$

$$\mathbf{E}_s\left(\mathbf{r},t\right) = \hat{\epsilon}_s \frac{i}{n_{\mathrm{bg}}}\mathcal{E}_s\tilde{a}\left(z,t\right)e^{-i\left(\omega_s t - \mathbf{k}_s\cdot\mathbf{r}\right)} + H.c., \tag{C.14b}$$

we can write down the new evolution equations for these operators. In these equations, the term $\mathbf{v}_0\cdot\left(\partial/\partial\mathbf{r}\right)$ can be neglected for slow motion of the atom, and the term $\mathbf{v}_0\cdot\mathbf{k}_{mn}$ (with $\mathbf{k}_{13} = \mathbf{k}_{12} - \mathbf{k}_{23}$) describing the Doppler effect can be incorporated into ω_s and ω_c. Without loss of generality, we can choose the arbitrary constant velocity $\mathbf{v}_0 = \mathbf{0}$. Since we are considering a weak excitation limit, we can take $\hat{\sigma}_{11} \approx 1$, $\hat{\sigma}_{22} \approx 0$, $\hat{\sigma}_{33} \approx 0$, $\tilde{\sigma}_{23} \approx 0$, $\partial\tilde{\sigma}_{12}/\partial t \approx 0$, then the equations become

$$\tilde{\sigma}_{12}\left(\mathbf{r},t;0\right) = \frac{-i\bar{g}}{\left(\omega_s - \omega_{21}\right) + i\gamma_{21}}\tilde{a}\left(z,t\right)e^{i\left(k_s z - \mathbf{k}_{12}\cdot\mathbf{r}\right)} -$$

$$\frac{\Omega_c^*\left(\mathbf{r},t\right)}{\left(\omega_s - \omega_{21}\right) + i\gamma_{21}}\tilde{\sigma}_{13}\left(\mathbf{r},t\right)e^{i\left(\mathbf{k}_{13}\cdot\mathbf{r} - \mathbf{k}_{12}\cdot\mathbf{r} + \mathbf{k}_c\left(\mathbf{r}\right)\cdot\mathbf{r}\right)}e^{-i\varphi_{0c}\left(\mathbf{r}\right)}, \tag{C.15a}$$

$$\frac{\partial}{\partial t}\tilde{\sigma}_{13}\left(\mathbf{r},t;0\right) = -\left\{\gamma_{31} - i\left[\omega_s - \omega_{31}\left(t\right) - \omega_c\left(\mathbf{r}\right)\right]\right\}\tilde{\sigma}_{13} +$$

$$i\Omega_c\tilde{\sigma}_{12}e^{-i\left(\mathbf{k}_{13}\cdot\mathbf{r} + \mathbf{k}_c\left(\mathbf{r}\right)\cdot\mathbf{r} - \mathbf{k}_{12}\cdot\mathbf{r}\right)}e^{i\varphi_{0c}\left(\mathbf{r}\right)}. \tag{C.15b}$$

Substituting Eq. (C.15a) into (C.15b), we have

$$\frac{\partial}{\partial t}\tilde{\sigma}_{13}(\mathbf{r},t;0) = -\left\{\gamma_{31} - i\left[\omega_s - \omega_{31} - \omega_c(\mathbf{r}) - \frac{|\Omega_c(\mathbf{r})|^2}{(\omega_s - \omega_{21}) + i\gamma_{21}}\right]\right\}\tilde{\sigma}_{13}$$
$$+ \frac{\Omega_c(\mathbf{r})\bar{g}}{(\omega_s - \omega_{21}) + i\gamma_{21}}\tilde{a}(z,t)e^{-i(\mathbf{k}_{13}\cdot\mathbf{r}+\mathbf{k}_c(\mathbf{r})\cdot\mathbf{r}-k_s z)}e^{i\varphi_{0c}(\mathbf{r})}, \tag{C.16}$$

where the temporal modulations on level $|3\rangle$ and control field amplitudes are dropped to focus on the discussion of quantum memory based on control field spatial chirp (where the atomic transition frequency ω_{31} and control field Rabi frequency Ω_c are time independent).

Recalling the definitions of one-photon detuning $\Delta = \omega_s - \omega_{21}$ and two-photon detuning δ in Eq. (C.2), we define the central two-photon detuning δ_0 and ac Stark shift induced in Raman interaction δ_{AC} as:

$$\delta_0 = \omega_s - \omega_{31} - \left[\omega_{c0} + \frac{|\Omega_c(\mathbf{r}=0)|^2}{\Delta + i\gamma_{21}}\right] \approx \omega_s - \omega_{31} - \left(\omega_{c0} + \frac{|\Omega_c(\mathbf{r}=0)|^2}{\Delta}\right), \tag{C.17}$$

$$\delta_{AC}(\mathbf{r}) = \frac{|\Omega_c(\mathbf{r})|^2}{\Delta + i\gamma_{21}} - \frac{|\Omega_c(\mathbf{r}=0)|^2}{\Delta + i\gamma_{21}} \approx \frac{|\Omega_c(\mathbf{r})|^2}{\Delta} - \frac{|\Omega_c(\mathbf{r}=0)|^2}{\Delta}, \tag{C.18}$$

where $\omega_{c0} = \omega_{c0}(\mathbf{r}=0)$, and the far off-resonant condition $\Delta \gg \zeta\gamma_{21}$ (with ζ denoting the collective broadening) is used. Then the two-photon detuning is written into

$$\delta(\mathbf{r}) = \delta_0 - [\omega_c(\mathbf{r}) - \omega_{c0}] - \delta_{AC}(\mathbf{r}). \tag{C.19}$$

Now we consider a control field propagating along $\hat{x}$ direction, so that Eqs. (C.15a) and (C.16) in far off-resonant Raman regime become

$$\tilde{\sigma}_{12}(\mathbf{r},t;0) = -\frac{i\bar{g}}{\Delta}\tilde{a}(z,t)e^{i(k_s z - \mathbf{k}_{12}\cdot\mathbf{r})} - \frac{\Omega_c^*(z)}{\Delta}\tilde{\sigma}_{13}(\mathbf{r},t)e^{i(\mathbf{k}_{13}\cdot\mathbf{r}-\mathbf{k}_{12}\cdot\mathbf{r}+k_c[z]x)}e^{-i\varphi_{0c}(\mathbf{r})},$$
$$\tag{C.20a}$$

$$\frac{\partial}{\partial t}\tilde{\sigma}_{13}(\mathbf{r},t;0) = -[\gamma_{31} - i\delta(z)]\tilde{\sigma}_{13} + \frac{\Omega_c(z)\bar{g}}{\Delta}\tilde{a}(z,t)e^{-i[\mathbf{k}_{13}\cdot\mathbf{r}+k_c[z]x-k_s z]}e^{i\varphi_{0c}(\mathbf{r})}, \tag{C.20b}$$

where $\bar{g} = d_{21}\mathcal{E}_s/(\hbar n_{bg}) = d_{21}\sqrt{\hbar\omega_s/(2\varepsilon_0 V)}/(\hbar n_{bg})$.

In the case of discrete spacial chirp, as mentioned before:

$$\omega_c(z) - \omega_{c0}(z=0) = m(z)\delta\omega_c, \tag{C.21}$$

$$m(z) = \sum_{m=-M_0}^{M_0} m\delta\omega_c(\Theta_-^m - \Theta_+^m) \tag{C.22}$$

in which $\delta\omega_c$ is the frequency spacing of the spacial chirp, $\Theta_{\mp}^m = \Theta(z - mL_0 \pm d/2)$, Θ is the Heaviside step function. If we choose ω_{c0} in such a way to make $\delta_0 = 0$, namely, $\omega_{c0} = \omega_s - |\Omega_c(z=0)|^2/\Delta - \omega_{31}$ where $\omega_s = \Delta + \omega_{21}$, then we obtain a two-photon detuning as follows:

$$\delta(z) = -\sum_{m=-M_0}^{M_0} m\delta\omega_c(\Theta_-^m - \Theta_+^m) - \delta_{AC}. \tag{C.23}$$

C.3   Field equation

The signal field evolvement is described by Maxwell equation, which is

$$\nabla \cdot \mathbf{D} = 0, \qquad \nabla \times \mathbf{E} = -\frac{\partial \mathbf{B}}{\partial t},$$
$$\nabla \cdot \mathbf{B} = 0, \qquad \nabla \times \mathbf{H} = \mathbf{J} + \frac{\partial \mathbf{D}}{\partial t}, \tag{C.24}$$

where $\mathbf{D} = \varepsilon_0\mathbf{E} + \mathbf{P}$, $\mathbf{B} = \mu_0\mathbf{H} + \mu_0\mathbf{M}$, $\mathbf{J} = \sigma\mathbf{E}$. Here let us assume the presence of a uniform, isotropic background, which modifies the constitutive equation as follows:

$$\mathbf{D} = \varepsilon_{bg}\mathbf{E} + \mathbf{P}, \qquad \mathbf{B} = \mu_{bg}\mathbf{H} + \mu_{bg}\mathbf{M}, \qquad \mathbf{J} = \sigma_{bg}\mathbf{E}, \tag{C.25}$$

where $\varepsilon_{bg} = \varepsilon_{bgr}\varepsilon_0$, $\mu_{bg} = \mu_{bgr}\mu_0$, $c^2 = 1/(\varepsilon_0\mu_0)$, μ_0 is the vacuum permeability, and functions ε_{bgr} and μ_{bgr} go to 1 as the background atoms number density N_{bg} approaches zero.

The propagation equation of optical fields is derived as follows. First, we have

$$\nabla \times (\nabla \times \mathbf{E}) = \nabla \times \left(-\frac{\partial \mathbf{B}}{\partial t} \right) = -\frac{\partial}{\partial t} \left(\mu_{\text{bg}} \nabla \times \mathbf{H} + \mu_{\text{bg}} \nabla \times \mathbf{M} \right)$$

$$= -\varepsilon_{\text{bg}} \mu_{\text{bg}} \frac{\partial^2}{\partial t^2} \mathbf{E} - \mu_{\text{bg}} \frac{\partial^2}{\partial t^2} \mathbf{P} - \mu_{\text{bg}} \sigma_{\text{bg}} \frac{\partial}{\partial t} \mathbf{E} - \mu_{\text{bg}} \frac{\partial}{\partial t} \nabla \times \mathbf{M}. \qquad (\text{C}.26)$$

By using $\nabla \times (\nabla \times \mathbf{E}) = \nabla (\nabla \cdot \mathbf{E}) - \nabla^2 \mathbf{E} = -\nabla^2 \mathbf{E}$, and further taking into account $\varepsilon_{\text{bg}} \mu_{\text{bg}} =$

$\varepsilon_{\text{bgr}} \mu_{\text{bgr}} \varepsilon_0 \mu_0 = n_{\text{bg}}^2 / c^2$, we obtain

$$\nabla^2 \mathbf{E} - \frac{n_{\text{bg}}^2}{c^2} \frac{\partial^2}{\partial t^2} \mathbf{E} - \mu_{\text{bg}} \sigma_{\text{bg}} \frac{\partial}{\partial t} \mathbf{E} = \mu_{\text{bg}} \frac{\partial^2}{\partial t^2} \mathbf{P} + \mu_{\text{bg}} \frac{\partial}{\partial t} \nabla \times \mathbf{M}. \qquad (\text{C}.27)$$

Assuming non-magnetic, non-conducting atoms in a non-magnetic, non-conducting background material, where $\sigma_{\text{bg}} = 0$, $\mu_{\text{bg}} = \mu_0$ and $\mathbf{M} = \mathbf{0}$, Eq. (C.27) becomes

$$\nabla^2 \mathbf{E} - \frac{n_{\text{bg}}^2}{c^2} \frac{\partial^2}{\partial t^2} \mathbf{E} = \mu_0 \frac{\partial^2}{\partial t^2} \mathbf{P} = \frac{1}{\varepsilon_0 c^2} \frac{\partial^2}{\partial t^2} \mathbf{P}. \qquad (\text{C}.28)$$

C.3.1 Polarization

From Eq. (C.20a), the single atom polarization operator can be written as

$$\hat{p}^j \left(\mathbf{r}^j, t; \mathbf{v}^j \right) = d_{12} \hat{\sigma}_{12}^j \left(\mathbf{r}^j, t; v^j \right) + d_{32} \hat{\sigma}_{32}^j \left(\mathbf{r}^j, t; v^j \right) + H.c.$$

$$\approx -\frac{i d_{12} \bar{g}}{\Delta + i \gamma_{21}} \tilde{a} \left(z^j, t; 0 \right) e^{-i \left(\omega_s t - k_s z^j \right)} e^{-i \mathbf{k}_{12} \cdot \mathbf{v}^j t} - \frac{d_{12} \Omega_c^*(z)}{\Delta + i \gamma_{21}} \times$$

$$\tilde{\sigma}_{13}^j \left(\mathbf{r}^j, t; 0 \right) e^{-i \omega_s t} e^{i \left(\mathbf{k}_{13} + \mathbf{k}_c [z^j] \right) \cdot \mathbf{r}^j} e^{-i \varphi_{0c}(\mathbf{r}^j)} e^{-i \mathbf{k}_{12} \cdot \mathbf{v}^j t} + H.c.. \qquad (\text{C}.29)$$

The macroscopic polarization can be obtained by averaging the single atom polarization operators:

$$\hat{P}(z,t) = \int f(\mathbf{v}^j) d\mathbf{v}^j \sum_j \hat{p} \left(\mathbf{r}_0^j, t; \mathbf{v}^j \right) \delta \left(\mathbf{r} - \left(\mathbf{r}_0^j + \mathbf{v}^j t \right) \right)$$

$$\approx N \int d\mathbf{r}_0^j \int d\mathbf{v}^j f(\mathbf{v}^j) \hat{p} \left(\mathbf{r}_0^j, t; \mathbf{v}^j \right) \delta \left(\mathbf{r} - \left(\mathbf{r}_0^j + \mathbf{v}^j t \right) \right)$$

$$= N \int d\mathbf{v}^j f(v^j) \hat{p} \left(\mathbf{r}, t; \mathbf{v}^j \right) = N \int d\mathbf{v} f(\mathbf{v}) \hat{p} \left(\mathbf{r}, t; \mathbf{v} \right) \qquad (\text{C}.30)$$

where we used $\sum_j \approx N \int d\mathbf{r}^j$, N is the number density of the atoms in the sample. The function f is the Maxwell distribution function:

$$f(v)dv = \sqrt{\frac{m}{2\pi k_B T}} \exp\left(-\frac{mv^2}{2k_B T}\right) dv, \tag{C.31}$$

which comes from a Boltzmann distribution of kinetic energy: $f(\varepsilon) \propto \exp\left[-\varepsilon/(k_B T)\right]$, $\varepsilon = mv^2/2$, $\Longrightarrow f_{\mathbf{p}} = (2\pi m k_B T)^{-3/2} \exp\left[-(p_x^2 + p_y^2 + p_z^2)/(2m k_B T)\right]$, $\Longrightarrow f_E dE = f_{\mathbf{p}} d\mathbf{p} = 2\sqrt{E/\pi}(k_B T)^{-3/2} \exp\left[-E/(k_B T)\right] dE$.

Since $\hat{\sigma}_{12}$ is excited by the signal field with carrier frequency ω_s, $\mathbf{k}_{12}$ should take the value of $\mathbf{k}_s$. Taking into account the integral of the velocity distribution:

$$\int d\mathbf{v} f(\mathbf{v}) e^{-i k_s v_z t} = \exp\left[-\frac{(k_s t)^2}{2m/(k_B T)}\right] = \exp\left(-\frac{t^2}{2t_d^2}\right), \tag{C.32a}$$

$$\int d\mathbf{v} f(\mathbf{v}) e^{-i[\mathbf{k}_{13} + \mathbf{k}_c(z)]\cdot\mathbf{v}t} = \exp\left(-\frac{t^2}{2t_d^2}\right), \tag{C.32b}$$

and the phase matching condition $\mathbf{k}_{13} + \mathbf{k}_c(z) = \mathbf{k}_s$, we have:

$$\hat{P}(z,t) = -\frac{iN d_{12}\bar{g} e^{-t^2/(2t_d^2)}}{\Delta + i\gamma_{21}} \tilde{a}(z,t) e^{-i(\omega_s t - k_s z)} - \frac{N d_{12}\Omega_c^*(z)}{\Delta + i\gamma_{21}} \tilde{\sigma}_{13}(\mathbf{r},t;0) \times$$

$$e^{-i\omega_s t} e^{-i\varphi_{0c}} e^{i[\mathbf{k}_{13} + \mathbf{k}_c(z)]\cdot\mathbf{r}} \exp\left(-\frac{t^2}{2t_d^2}\right) + H.c.. \tag{C.33}$$

where $t_d = 1/(\sqrt{k_B T/m} k_s)$ is the Doppler dephasing time constant. From the expression of t_d, we identify a dephasing velocity $v_s = \sqrt{k_B T/m}$. For $T = 100K$, $m = 58.4678u$, we have $v_s = 0.12$ m/s. During the $\Delta t \sim 100$ ns duration of the signal field, the corresponding distance is 12 nm, while the field propagates $c\Delta t = 30$ m and the medium length is $L \sim 1$ cm. So in such a case we are in the slow-motion regime. Here only the signal field dynamics is considered, so the dephasing is along the longitudinal direction $\hat{k}_s$. In general, the control field propagation direction could make arbitrary angle with respect to $\hat{k}_s$, leading to similar

transversal dephasing effect, which will be neglected for the sake of simplicity.

If we define

$$\hat{P}(z,t) = \tilde{P}(z,t)\,e^{-i(\omega_s t - k_s z)} + H.c.,\tag{C.34}$$

the slowly varying part of the positive rotating component of the medium polarization can

be written into

$$\tilde{P}(z,t) = -\frac{iNd_{12}\bar{g}e^{-t^2/(2t_d^2)}}{\Delta + i\gamma_{21}}\tilde{a}(z,t) -$$

$$\frac{Nd_{12}\Omega_c^*(z)}{\Delta + i\gamma_{21}}\tilde{\sigma}_{13}(\mathbf{r},t)\,e^{-i\varphi_{0c}}e^{i(\mathbf{k}_{13}+\mathbf{k}_c(z)-\mathbf{k}_s)\cdot\mathbf{r}}\exp\left(-\frac{t^2}{2t_d^2}\right).\tag{C.35}$$

C.3.2   Evolution equation of the signal field

We derive the field equation based on Eq. (C.28). Neglecting the transverse propaga-

tion of the signal field, one can replace ∇^2 by $\partial^2/\partial z^2$ (see relative discussions in Chaps. II

and III). Since the signal field is $\mathbf{E}_s(z,t) = \hat{\epsilon}_s(i/n_{\rm bg})\mathscr{E}_s\tilde{a}(z,t)e^{-i(\omega_s t - k_s z)} + H.c.$, Eq. (C.28)

gives

$$\left(\frac{\partial^2}{\partial z^2} - \frac{n_{\rm bg}^2}{c^2}\frac{\partial^2}{\partial t^2}\right)\hat{E}_s(z,t) = \left\{\frac{i}{n_{\rm bg}}\mathscr{E}_s\left(\frac{\partial^2}{\partial z^2} - \frac{n_{\rm bg}^2}{c^2}\frac{\partial^2}{\partial t^2}\right)\tilde{a}(z,t) + 2i\frac{i}{n_{\rm bg}}\mathscr{E}_s\times\right.$$

$$\left.\left(k_s\frac{\partial}{\partial z} + \frac{n_{\rm bg}^2\omega_s}{c^2}\frac{\partial}{\partial t}\right)\tilde{a}(z,t) + \frac{i}{n_{\rm bg}}\mathscr{E}_s\left[\left(\frac{n_{\rm bg}\omega_s}{c}\right)^2 - (k_s)^2\right]\tilde{a}(z,t)\right\}e^{-i(\omega_s t - k_s z)} + H.c.$$

$$= -\frac{1}{\varepsilon_0 c^2}\omega_s^2\tilde{P}(z,t)\,e^{-i(\omega_s t - k_s z)},\tag{C.36}$$

Neglecting the second order derivatives, and substituting in Eq. (C.35), one obtains

$$2i\frac{i}{n_{\text{bg}}}\mathscr{E}_s\left(k_s\frac{\partial}{\partial z}+\frac{n_{\text{bg}}^2\omega_s}{c^2}\frac{\partial}{\partial t}\right)\tilde{a}(z,t)+\frac{i}{n_{\text{bg}}}\mathscr{E}_s\left[\left(\frac{n_{\text{bg}}\omega_s}{c}\right)^2-(k_s)^2\right]\tilde{a}(z,t)=\frac{\omega_s^2}{\varepsilon_0 c^2}\times$$

$$\frac{iNd_{12}\bar{g}e^{-t^2/(2t_d^2)}}{\Delta+i\gamma_{21}}\tilde{a}(z,t)+\frac{\omega_s^2}{\varepsilon_0 c^2}\frac{Nd_{12}\Omega_c^*(z)}{\Delta+i\gamma_{21}}\tilde{\sigma}_{13}(\mathbf{r},t)e^{-i\varphi_{0c}}e^{i(\mathbf{k}_{13}+\mathbf{k}_c(z)-\mathbf{k}_s)\cdot\mathbf{r}}\exp\left(-\frac{t^2}{2t_d^2}\right).$$

$$\text{(C.37)}$$

Here we require the $\tilde{a}(z,t)$ terms on the left and right hand side of Eq. (C.37) to be canceled

by fixing k_s, which will be satisfied by a the following equation:

$$k_s=\frac{\omega_s}{c}n_{\text{bg}}\sqrt{1-\frac{N|d_{12}|^2e^{-t^2/(2t_d^2)}}{n_{\text{bg}}^2\varepsilon_0\hbar(\Delta+i\gamma_{21})}}=n_{\text{bg}}n_{\text{int}}\frac{\omega_s}{c}, \qquad \text{(C.38a)}$$

$$n_{\text{int}}=\sqrt{1-\frac{N|d_{12}|^2e^{-t^2/(2t_d^2)}}{n_{\text{bg}}^2\varepsilon_0\hbar(\Delta+i\gamma_{21})}}, \qquad \text{(C.38b)}$$

The refractive index n_{int} appears due to signal-medium interaction. After neglecting γ_{21}

with respect to Δ, the field equation then becomes

$$\left(\frac{\partial}{\partial z}+\frac{n_{\text{bg}}}{n_{\text{int}}c}\frac{\partial}{\partial t}\right)\tilde{a}(z,t)$$

$$=-\frac{\omega_s}{2\varepsilon_0 c\mathscr{E}_s n_{\text{int}}}\frac{Nd_{12}\Omega_c^*(z)}{\Delta}\tilde{\sigma}_{13}(\mathbf{r},t;0)e^{-i\varphi_{0c}}e^{i(\mathbf{k}_{13}+\mathbf{k}_c(z)-\mathbf{k}_s)\cdot\mathbf{r}}\exp\left(-\frac{t^2}{2t_d^2}\right). \qquad \text{(C.39)}$$

C.4 Atomic and field evolution equations

The full set of evolution equations is given by Eqs. (C.39) and (C.20b). Let us re-

define the collective atomic operator as

$$S(\mathbf{r},t)=\frac{\omega_s}{2\varepsilon_0 c\mathscr{E}_s n_{\text{int}}}\frac{Nd_{12}\Omega_c^*(z)}{\Delta}\tilde{\sigma}_{13}(\mathbf{r},t;0)e^{-i\varphi_{0c}}e^{i(\mathbf{k}_{13}+\mathbf{k}_c(z)-\mathbf{k}_s)\cdot\mathbf{r}}, \qquad \text{(C.40)}$$

so that Eqs. (C.39) and (C.20b) become

$$\left(\frac{\partial}{\partial z} + \frac{n_{\text{bg}}}{n_{\text{int}}c} \frac{\partial}{\partial t} \right) \tilde{a}(z,t) = -S(\mathbf{r},t) \exp\left(-\frac{t^2}{2t_d^2} \right), \tag{C.41a}$$

$$\frac{\partial}{\partial t} S(\mathbf{r},t) = -[\gamma_{31} - i\delta(z,t)] S(\mathbf{r},t) + \frac{\omega_s}{2\hbar\varepsilon_0 c n_{\text{bg}} n_{\text{int}}} \frac{N|d_{12}|^2 |\Omega_c(z)|^2}{\Delta^2} \tilde{a}(z,t). \tag{C.41b}$$

In the long-pulse regime, we neglect the $[n_{\text{bg}}/(n_{\text{int}}c)]\partial\tilde{a}/\partial t$ term. We can define a coupling

constant g as

$$g(z) = \sqrt{\frac{\omega_s}{2\hbar\varepsilon_0 c n_{\text{bg}} n_{\text{int}}}} \frac{d_{21}\Omega_c(z)}{\Delta}, \tag{C.42}$$

so that the evolution equations become:

$$\frac{\partial}{\partial z} \tilde{a}(z,t) = -S(z,t) \exp\left(-\frac{t^2}{2t_d^2} \right), \tag{C.43a}$$

$$\frac{\partial}{\partial t} S(z,t) = -[\gamma_{31} - i\delta(z)] S(z,t) + |g(z)|^2 N\tilde{a}(z,t), \tag{C.43b}$$

in which $\delta(z)$ is given by Eq. (C.23) with δ_{AC} given by Eq. (C.18).

In the estimation of control power, usually the intensity I is defined as $I = cn\varepsilon_0|E|^2/2$.

Since in our definition of E_c, the field E is equal to $2E_0$, we should calculate intensity,

control Rabi frequency ($\Omega_c = d_{32}E_0^*/\hbar$), and coupling constant using

$$I_c = 2cn\varepsilon_0|E_0|^2, \tag{C.44a}$$

$$\Omega_c = \frac{d_{32}}{\hbar} \sqrt{\frac{I_{\text{free}}}{2c\varepsilon_0}}, \tag{C.44b}$$

$$g = \sqrt{\frac{\omega_s}{2\hbar\varepsilon_0 c n_{\text{bg}} n_{\text{int}}}} \frac{d_{21}d_{32}}{\hbar\Delta} \sqrt{\frac{I_{\text{free}}}{2c\varepsilon_0}}, \tag{C.44c}$$

where I_{free} is the control intensity in free space.

APPENDIX D

ANALYTICAL SOLUTION OF THE ECHOES FROM A GRADIENT

FREQUENCY COMB[*]

In this appendix, we derive the analytical solution of Eqs. (V.4) - (V.5) (upon the neglect of Doppler dephasing) and Eqs. (VI.7) - (VI.8) in the gradient frequency comb regime.

In Fourier domain, Eqs. (VI.7) - (VI.8) or Eqs. (V.4) - (V.5) (for $t_d \to \infty$) can be solved to get the output field spectrum:

$$\mathcal{E}_{\text{out}}(\omega) \approx \mathcal{E}_{\text{in}}(\omega) \exp\left(-i|g|^2 Nd \sum_{m=-\infty}^{\infty} \frac{1}{\omega - m\beta\omega_0 + i\Gamma} \right), \qquad (\text{D.1})$$

where we extend M_0 to ∞. This extension is ensured by the finite bandwidth of the input signal $\mathcal{E}_{\text{in}}(\omega)$. Namely, in this work we always assume $2\pi/\Delta t \lesssim M\beta\omega_0$, which is also part of Eq. (VI.14) or Eq. (V.10). The real part of $\sum_{m=-\infty}^{\infty}(\omega - m\beta\omega_0 + i\Gamma)^{-1}$ is a periodic function. The imaginary part is not, but can be approximately treated as periodic for a high finesse comb. Under this condition, this summation term can be written into Fourier series, which is substituted back into Eq. (D.1) and leads to:

$$\mathcal{E}_{\text{out}}(\omega) \approx \mathcal{E}_{\text{in}}(\omega) \exp\left[-\frac{\pi|g|^2 Nd}{\beta\omega_0} \left(1 + 2\sum_{n=1}^{\infty} e^{-\frac{2\pi n}{\beta\omega_0}\Gamma} e^{i\frac{2\pi n}{\beta\omega_0}\omega} \right) \right]$$

$$= \mathcal{E}_{\text{in}}(\omega) e^{-\frac{\pi}{4}\zeta_{\text{eff}}^0} \prod_{n=1}^{\infty} \sum_{q=0}^{\infty} \left(-\frac{\pi}{2}\zeta_{\text{eff}}^0 e^{-\frac{\pi n}{\mathcal{F}}} \right)^q \frac{e^{inq\omega T_0}}{q!}, \qquad (\text{D.2})$$

where we define $\zeta_{\text{eff}}^0 = 4|g|^2 Nd/(\beta\omega_0)$, and used $T_0 = 2\pi/(\beta\omega_0)$ (or $\beta\omega_0$ replaced with

$\delta\omega_c$ in Chap. V). It is worth noting that in this derivation, the causality, which is built in through the fact $nq \geqslant 0$, is obtained out of calculation rather than being empirically imposed as a condition [58]. The leakage and the first echo signals are given by the first two terms in Eq. (D.2) with $n = 1$. The inverse Fourier transformation of these two terms gives the field in time and space domain:

$$\mathcal{E}_{\text{out}}(t) = e^{-\frac{\pi}{4}\zeta_{\text{eff}}^0}\mathcal{E}_{\text{in}}(t) - \frac{\pi\zeta_{\text{eff}}^0}{2}e^{-\frac{\pi\zeta_{\text{eff}}^0}{4}}e^{-\frac{\pi}{\mathcal{F}}}\mathcal{E}_{\text{in}}(t - T_0) + \text{Higher sequence GFC echoes.}$$

(D.3)

One can see from Eq. (D.2) that higher sequence GFC echoes will be important if ζ_{eff}^0 becomes large. If one takes a look at the whole sequence of echoes, for small or moderate optical thickness, the echo signals are not only attenuated exponentially as $e^{-\pi n/\mathcal{F}}$ due to the decoherence rate Γ, but also are phase modulated by $J_1\left(2\sqrt{\pi\xi_{\text{eff}}^0 n/2}\right)\bigg/\sqrt{\pi\xi_{\text{eff}}^0 n/2}$. For the leakage and first echo signal this coincides with (D.3). However this is not true if the individual effective optical thickness is large so that higher order interactions (re-emission and re-absorption among different targets) become significant. In such a case, Eq. (D.2) or (D.3) has to be used (under the condition $\mathcal{F} \gg 1$). Especially when ζ_{eff}^0 is large, higher sequence GFC echo can be stronger than lower ones, which might be useful for longer-time storage, although the efficiency usually is much smaller. In this dissertation we focus only on the first echo.

APPENDIX E

ANALYTICAL SOLUTION OF THE γ-RAY BEAM DEFLECTED BY A COHERENTLY VIBRATING NUCLEAR LATTICE[*]

Here we derive the analytical solution of Eqs. (VI.26) and (VI.27) in Chap. VI. These equations describe the dynamics of two coupled γ-ray waves with different propagation directions along Bragg angles in a vibrating Mössbauer nuclear lattice.

Equations (VI.26) and (VI.27) can be reduced to

$$\ddot{\Omega}_1 + i(\Delta + Q)\dot{\Omega}_1 + (\Omega_a^2 - \Delta Q)\Omega_1 + \Omega_a^2\Omega_2 = 0, \tag{E.1}$$

$$\ddot{\Omega}_2 + i(\Delta + Q)\dot{\Omega}_2 + (\Omega_a^2 - \Delta Q)\Omega_2 + \Omega_a^2\Omega_1 = 0, \tag{E.2}$$

where

$$Q(t) = \kappa v_d \cos(v_d t) \tag{E.3}$$

is a function describing the modulation produced by nuclear motion.

The initial conditions for Eqs. (E.1) and (E.2) are $\Omega_1(0) = A$, $\Omega_2(0) = 0$, and $\rho(0) = 0$. In order to satisfy the evolution equations, these initial conditions yield the relations: $\dot{\Omega}_1(0) = -i\Delta A$ and $\dot{\Omega}_2(0) = 0$.

Equations (E.1) and (E.2) have the following integral of motion

$$\Omega_1 = \Omega_2 + Ae^{-i\Delta t}. \tag{E.4}$$

Substituting Eq. (E.4) into Eq. (E.2) and introducing $\tilde{\Omega}_2$ according to

$$\Omega_2 = e^{-i\Delta t}\left(\tilde{\Omega}_2 - \frac{A}{2}\right) \tag{E.5}$$

we obtain the following equation for $\tilde{\Omega}_2$

$$\frac{d^2\tilde{\Omega}_2}{dt^2} + i(Q-\Delta)\frac{d\tilde{\Omega}_2}{dt} + 2\Omega_a^2\tilde{\Omega}_2 = 0 \tag{E.6}$$

which is an equation of parametric oscillator. Equation (E.6) has a solution in terms of special functions. However such solution is not very mathematically or physically insightful. Instead, we derive an approximate solution which clearly shows the physics behind parametric speed up of the energy transfer.

After introducing a function $u(t)$:

$$\frac{d\tilde{\Omega}_2}{dt} = e^{-i\int_0^t(Q-\Delta)dt'}u, \tag{E.7}$$

one can rewrite Eq. (E.6) as

$$\frac{du}{dt} = -2\Omega_a^2 e^{i\int_0^t(Q-\Delta)dt'}\tilde{\Omega}_2. \tag{E.8}$$

The exponential factor can be expended into the Fourier series as follows:

$$\exp\left\{i\int_0^t[Q(t')-\Delta]dt'\right\} = e^{-i\Delta t}e^{i\kappa\sin(\nu_d t)}$$

$$= e^{-i\Delta t}\left[J_0(\kappa) + 2iJ_1(\kappa)\sin(\nu_d t) + 2J_2(\kappa)\cos(2\nu_d t) + \ldots\right], \tag{E.9}$$

where $J_n(\kappa)$ are the nth order Bessel functions. We assume that ν_d is close to Δ while $\tilde{\Omega}_2$ and u are slowly varying functions of time on the scale $1/\nu_d$. Then in the Fourier expansion (E.9) one can keep only the slowly varying term and approximately write

$$e^{i\int_0^t(Q-\Delta)dt'} \approx J_1(\kappa)e^{i(\nu_d-\Delta)t}. \tag{E.10}$$

As a result, Eqs. (E.7) and (E.8) reduce to

$$\frac{d\tilde{\Omega}_2}{dt} = J_1(\kappa)e^{-i(\nu_d-\Delta)t}u, \tag{E.11}$$

$$\frac{du}{dt} = -2J_1(\kappa)\Omega_a^2 e^{i(\nu_d-\Delta)t}\tilde{\Omega}_2 \tag{E.12}$$

which can be solved analytically. Substituting this solution into Eqs. (E.4) and (E.5) we

finally obtain

$$\Omega_1 = \frac{Ae^{-i\Delta t}}{2}\left[\frac{\omega_+ e^{-i\omega_- t} - \omega_- e^{-i\omega_+ t}}{\sqrt{(\nu_d-\Delta)^2 + 8J_1^2(\kappa)\Omega_a^2}} + 1\right], \tag{E.13}$$

$$\Omega_2 = \frac{Ae^{-i\Delta t}}{2}\left[\frac{\omega_+ e^{-i\omega_- t} - \omega_- e^{-i\omega_+ t}}{\sqrt{(\nu_d-\Delta)^2 + 8J_1^2(\kappa)\Omega_a^2}} - 1\right], \tag{E.14}$$

where $\omega_\pm = \left[\nu_d - \Delta \pm \sqrt{(\nu_d-\Delta)^2 + 8J_1^2(\kappa)\Omega_a^2}\right]\Big/2$.

When the nuclear vibration frequency matches the γ photon's frequency detuning

with respect to the nuclear transition frequency, i.e., $\nu_d = \Delta$, we find the following solution

of Eqs. (VI.26) and (VI.27):

$$\Omega_1 = Ae^{-i\Delta t}\cos^2\left(\frac{J_1(\kappa)}{\sqrt{2}}\Omega_a t\right), \tag{E.15}$$

$$\Omega_2 = -Ae^{-i\Delta t}\sin^2\left(\frac{J_1(\kappa)}{\sqrt{2}}\Omega_a t\right). \tag{E.16}$$